NUMERICAL SIMULATION OF COASTAL EFFECTS ON OZONE
DISTRIBUTIONS IN TAMPA BAY, FLORIDA

BY

JUNNE-YIH ROBERT YEH

A DISSERTATION PRESENTED TO THE GRADUATE SCHOOL
OF THE UNIVERSITY OF FLORIDA IN PARTIAL FULFILLMENT
OF THE REQUIREMENTS FOR THE DEGREE OF
DOCTOR OF PHILOSOPHY

UNIVERSITY OF FLORIDA

1994

This dissertation is dedicated to my family members, especially to my wife Sheu-Mei.

ACKNOWLEDGEMENTS

TABLE OF CONTENTS

CHAPTERS

LIST OF TABLES

LIST OF FIGURES

NUMERICAL SIMULATION OF COASTAL EFFECTS ON OZONE
DISTRIBUTIONS IN TAMPA BAY, FLORIDA

By

JUNNE-YIH ROBERT YEH

April, 1994

During the period July 22-24, 1987, the Tampa Bay area in Florida experienced the worst exceedance of the ozone ambient air quality standard (AAQS) since 1980. A mesoscale meteorological model (MM4) was used to simulate the complex meteorological conditions existing for the peninsula. The meteorological data obtained from the MM4 simulations were incorporated into a photochemical model (STEM-II) to simulate chemical variables.

The model could predict the observed ozone concentrations at monitoring sites relatively well in terms of daytime ozone levels and peak ozone concentrations. The average peak prediction accuracy between daytime predicted and observed ozone levels during the episode for ozone data unpaired in time and site location (-13%), and the normalized bias (-14%) and error (26%) for data paired in time and space achieved the ozone model performance goals recommended by the California Air Research Board.

Back trajectory analyses suggested that emissions from coastal urban areas in southeast and southwest Florida contributed to the ozone exceedances in the Tampa Bay area. On the basis of forward trajectory analyses, the air masses containing peak ozone concentrations on July 23, 1987, in Hillsborough and Pinellas counties each contributed to excessive ozone levels in adjacent counties as a result of transport processes. On 24th July, peak ozone concentrations in Hillsborough county were transported over Pinellas County to the Gulf.

Results from these numerical model simulations suggested that VOC (Volatile Organic Compound) control alone is an appropriate strategy for meeting present and future O_3 compliance standards in the Tampa Bay area. Reduction in VOC emissions could have reduced maximum ozone levels to meet the ozone standard for the meteorological conditions existing on July 23, 1987, but could not have resolved the O_3 non-attainment problems existing on July 24, 1987. On the basis of emission reduction simulations, a statewide VOC reduction plan is recommended as a reasonable emission control strategy for the future.

CHAPTER 1
INTRODUCTION

1.1 Rationale

The state of Florida Department of Environmental Protection (DEP) has identified several urban areas in the state as having ozone (O_3) attainment difficulties. Forty-four exceedances (Chu, 1986) of the ozone ambient air quality standard (120 ppb) were recorded in three major metropolitan areas (Tampa, Jacksonville and Miami) from 1981 to 1986. Chu (1986) also suggested that ozone concentrations had obviously increased more in the Tampa Bay area within this period than in the other areas. The increases in monthly average ozone concentrations were from 5 to 8 ppb over these 6 years in the Tampa Bay area. The Air Quality Division of Pinellas County has carried out a study on the relationships among surface ozone concentrations, meteorological parameters and emissions in the Tampa Bay area. From a nine year (1980-1988) accumulation of ambient air quality data, a total of 42 exceedances were recorded for the area. Due to the rapid increase in population in the Tampa Bay area, the ozone attainment problem is expected to grow worse if there are no additional emission controls. At the same time, the expected greater abundance of ozone precursors and concomitant oxidants could be transported further downwind and lead to increased damage to crops, vegetation and forests in surrounding rural areas.

The largest industry in Florida is tourism; as a result motor vehicle emissions are considered to be the major anthropogenic source of ozone precursors-- oxides of nitrogen (NOx) and non-methane hydrocarbons (NMHC)-- in urban areas. Stationary point and area sources are estimated to have emitted only about 4% and 17% of total man-made

NMHC in the Tampa Bay area (Pinellas and Hillsborough counties.) Although two major power plant facilities contribute about 50% of the total NO_X emissions in this area, the NO_X concentrations are significantly diluted by dispersion when the plumes reach ground level. Mobile sources are estimated to have contributed more than 34% of the total NO_X emissions whereas the contribution of area sources was negligible. Thus, mobile sources should be the main concern in any ozone reduction strategy.

Other major factors that may lead to exceedances of the ozone National Ambient Air Quality Standard (NAAQS) are meteorological conditions and topography. The major urban areas experiencing ozone non-attainment in Florida are located in the coastal zone of either the Gulf of Mexico or the Atlantic Ocean. Coastal meteorological conditions (sea-land breezes) can have a great impact on the air quality in these urban areas. Synoptic scale weather patterns not only affect the formation of local flow patterns, but also can contribute to the deterioration of air quality. Chu (1986) found that 38 out of 44 ozone exceedances in urban areas of Florida were associated with a double-high weather pattern. The existence of high pressure systems can form subsidence inversions that limit the ability of pollutants to disperse vertically. Also, local flow patterns being induced by terrain form frequently under weak high pressure systems. For example, sea-land breezes are likely to be formed under such conditions, and contribute to the deterioration of air quality. The remaining ozone exceedance cases were related to stationary frontal patterns. The frontal inversions and the sinking air motion behind a cold front could contribute to violations of the ozone NAAQS.

According to the 1990 Clean Air Act Amendments (CAAA) section 181 (a), the Tampa Bay area is classified as one of the marginal ozone non-attainment areas, which experience ozone concentrations in the range from 120 to 138 ppb. The area was required to achieve attainment by November 15, 1993. To aid in reducing the average ozone level, an emission inspection program for motor vehicles was launched in Hillsborough and Pinellas counties in 1991. The Florida Department of Highway Safety

and Motor Vehicles estimates that VOC (Volatile Organic Compound) emissions were reduced by about 8% in the Tampa Bay area over the last three years. Since the inspection program began, no ozone exceedances have been observed in two consecutive years (1991 and 1992) in this area. The Tampa Bay area has an opportunity, therefore, to be reclassified as an attainment (urban) area, since there was no exceedance before the end of 1993. However, such a reduction may be partially or completely offset by an increase in population density and consequent increase in automobile density, similar to the Los Angeles metropolitan experience.

In spite of the rapidly growing population in this area, the ozone NAAQS has to be met continuously in the future. It is difficult to identify those factors which have brought about the improvement in ozone air quality in Tampa bay. It could partially be due to the implementation of the vehicle inspection program, or it could also be a result of the absence of meteorological conditions which are highly conducive to ozone episodes. To maintain ozone attainment status in the future, therefore, it is necessary to fully understand the specific influences of meteorology and pollutant emissions on the ozone non-attainment problem in this area.

Another important aspect of this study is to investigate the transport of ozone and its precursors from the Tampa Bay metropolitan area to its rural environs. It has been demonstrated that ozone has adverse effects not only on humans, but also on crops and vegetation. A significant impact can be expected on farm productivity in the surrounding area. Chassahowitzka National Wildlife Refuge, which is designated as a Class I Prevention of Significant Deterioration (PSD) area is located about 80 km north of Tampa Bay. Deterioration of the air quality over the refuge could result from transport of pollutants from the bay area. Although an increase in ozone levels is not the primary concern for this Class I area, the detrimental effects of ozone and copollutants on this protected fragile ecosystem cannot be ignored. Air quality related values of the refuge are to be protected under the Clear Air Act Amendments.

Under the influence of marine-land meteorology, the ozone generated in Tampa Bay can have an impact on surrounding rural areas in three different ways. A land breeze may push the ozone precursors out of the bay area into the Gulf and return them inland the next day with a sea breeze. Under the influence of synoptic scale winds, the polluted air mass can flow back to rural inland areas and cause elevated ozone levels after sunrise. If a surface inversion exists, the surface ozone can be quickly removed by reacting with nitric oxide (NO) emitted from the surface and by deposition to the ground after sunset. However, the ozone at high elevations can be transported out of the bay area, and then, mix down to ground surface after break-up of the surface inversion and growth of the mixing layer. After the passage of a sea breeze front, the downflow motion behind the sea breeze can contribute to a second ozone peak, which could be a higher ozone peak in downwind rural areas.

A Mesoscale Meteorological model, version 4 (MM4) and a transport and transformation model (Sulfate Transport Eulerian Model-II) were used to study ozone non-attainment situations in the Tampa Bay area. Since there were insufficient observations available to create meteorological data sets with reasonable spatial and temporal resolution, the MM4 meteorological model is used to provide the required input data for the STEM-II model. Subsequently, the STEM-II model is used to describe the transport and transformation of pollutants with the created meteorological data. There are three major advantages in using numerical simulations to study air pollution problems. First, numerical simulations allow for the examination of complex conditions simultaneously. Secondly, these models can be used as a predictive tool to estimate air quality for either meteorological or emission condition changes. Meteorological models are also considerably less expensive than setting up and operating a monitoring network. These advantages are very important in achieving the purposes of this research.

1.2 Characteristics of Coastal Meteorology and Air Quality

Meteorological processes in different time and space scales can have variable influences on the transport and diffusion of atmospheric pollutants. Macroscale dynamical processes could be larger than 2,000 km and last for a few days. A high or low pressure system is an example of a macroscale meteorological process. Microscale processes are confined to within a few kilometers and only occur for several minutes, such is the case for eddy turbulence. Mesoscale meteorological elements may extend a few hundred kilometers in space and exist from a few hours to a day. Sea-land breezes and mountain-valley circulations are typical cases of mesoscale processes.

Sea-land circulations are typical meteorological phenomena in coastal or lake-side areas. Since the heat capacities of ground surfaces are less than those of water bodies, ground surfaces are heated up more quickly by solar radiation and cool down more rapidly than water surfaces. On a calm and sunny day, a temperature decline is established from the land to the water surface. The expansion of air over a warm land surface causes a smaller vertical pressure gradient than over a cool water surface, therefore, higher pressure is found over the land at a constant upper level over both land and water surfaces. Consequently, the horizontal pressure gradient force produces an air flow from land to sea at higher altitude. The air flow generates a convergence that leads to an increase in pressure, and therefore, creates a subsiding flow to compensate for the departure from hydrostatic equilibrium over the water surface. The subsiding flow causes decreasing pressure from the water to the land surface, and creates an air flow from the water surface to land surface at lower elevations. Simultaneously the divergence being generated as the air flow from the land to the water surface at a high level, results in the pressure decrease. The generation of an uplifting air flow below the divergence is in response to the departure from hydrostatic equilibrium vertically. Ultimately, a sea breeze is formed. A land breeze is usually formed in the reverse way, because a water

surface is warmer than a land surface at night. A land breeze is usually weaker than a sea breeze, because solar energy is not available during the nighttime. From an air pollution point of view, researchers are more interested in sea breezes than land breezes. Two examples of typical sea breeze circulations for the Tampa Bay area are shown in Figure 1.1.

Simpson et al. (1977) compared the flow of a sea breeze to a gravity current head in a laboratory water tank. The gravity current head was created by a dense opposing flow above a moving floor with less dense fluid. They found that the instantaneous flow pattern (Figure 1.2) observed in water tank models is consistent with atmospheric data for a sea breeze. Both the gravity current head and the sea breeze show an uplifting at the front and a down draught at the rear that engulfs the denser air or fluid.

A sea breeze circulation will gradually increase in depth and horizontal extent, and advance slowly inland. At mid-latitudes, sea breezes tend to penetrate inland up to 50 km (Atkinson, 1981), but the inland penetration in the tropics could be more than 200 km (Wexler, 1946). The inland penetration of a sea breeze can be characterized by 1) a shift in the wind direction as observed for passage of a cold front; 2) a decrease in temperature; 3) an increase in relative humidity and 4) an uplifting zone at the front and a downdraught zone in the rear. The temperature decrease can be as large as 4.6 $^{\circ}$C in the tropics, and the humidity often rises by about 5 to 10% at the onset of a sea breeze. The uplifting velocity and downward velocity can be greater than 1 meter per second (m/s). Normally, cumulus clouds can be observed near the uplifting zone.

The prevailing large-scale wind (geostrophic wind) affects not only the formation of a sea breeze, but also its subsequent movement (Simpson et al., 1977). The influence of the synoptic wind has been demonstrated by Estoque (1962) and Pielke(1974) through model simulations. The onshore geostrophic wind ($\geq$ 5 m/s) tends to inhibit the formation of a sea breeze, because the advection suppresses the rise of temperature over land. The offshore prevailing wind can delay the formation time and reduce the distance
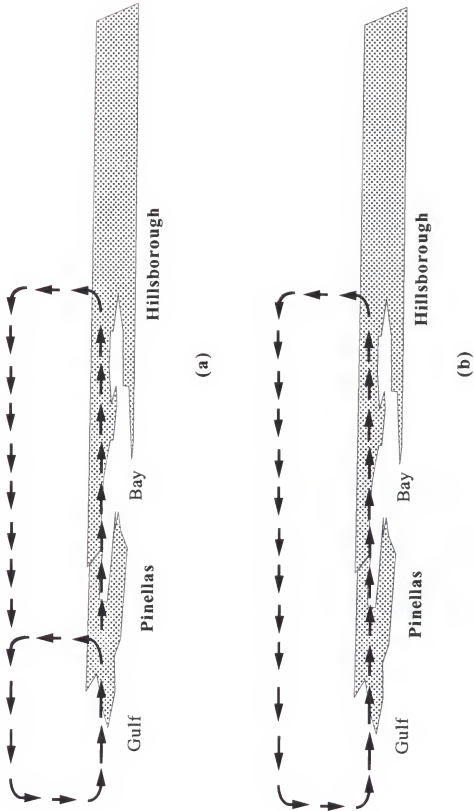
Figure 1.1. Typical sea breeze circulations (a) and (b) occurring in the Tampa Bay area.
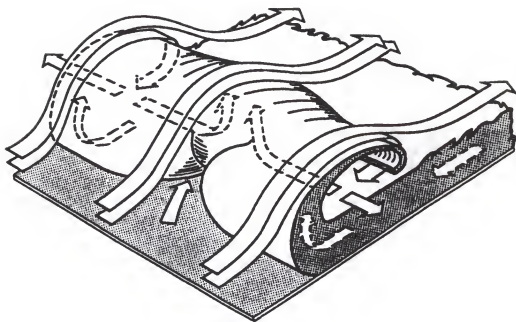
Figure 1.2. A schematic of gravity current flow. (Source: Simpson et al., 1977.)

of the sea breeze penetration. While the geostrophic wind is parallel to the shoreline with low pressure over the water, the effect is the same as the offshore prevailing wind. With low pressure over the land, the geostrophic wind blows in the opposite direction parallel to the shore line, and leads to an onshore effect on the formation of a sea breeze.

Sea breezes could influence the air quality in coastal and lake-side areas in two contrasting ways. They can relieve highly polluted urban areas by moving "clean" marine air into the area, and may prevent the effluent from a stack on the shore from reaching the ground (Atkinson, 1981). On the other hand, sea breezes can push back to the land polluted air that has drifted a short distance offshore during the previous night or the early morning, and therefore lead to a higher level of pollutants at the impacted area on the following day. This effect has been observed by Kauper (1960) in California, and Lyons and Olsson (1972) in Chicago. The closed circulation cells of sea breezes can also accumulate fresh pollutants and return them inland to increase the level of pollutants in inland areas. The latter adverse effect of sea breeze circulations has also been reported by Kauper (1960), Lyons and Olsson (1972), Young and Winchester (1980), and Bornstein and Thompson (1981). In metropolitan areas, the air flow retardation caused by friction on sea-breeze fronts could further increase concentrations in downwind areas (Bornstein and Thompson, 1981). In the morning, the growth of an internal boundary layer may fumigate the effluent (Figure 1.3) from a stack to the ground surface, if the plume is pushed inland by a sea breeze.

Ozone non-attainment problems have been studied for several decades in a number of coastal urban areas in the world, such as the Tokyo Basin in Japan, Athens in Greece, the Los Angeles Basin and the Great Lakes area in the U.S. Every coastal urban area has its own characteristic ozone problems, because of differences in coastal shore lines, synoptic weather systems, topographic structures and emissions of pollutants. For example, the concentrations of oxidants in an upper inversion could be as high as, or higher than those below the inversion in the downwind region of the Los Angeles Basin.
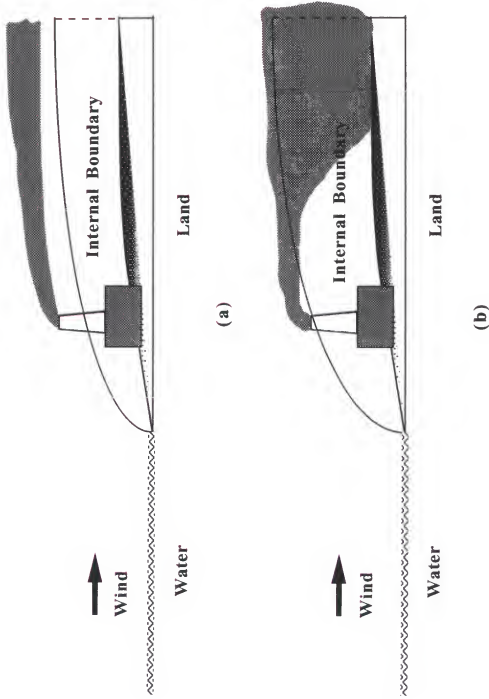
Figure 1.3. The internal boundary at the coastal zone. (a) In the early morning, the plume is above the internal boundary and (b) In the late moring, the internal boundary reaches the plume and causes fumigation.

This effect is caused by the upslope wind, which is induced by heated mountain slopes, carrying the oxidants into the inversion layer, and the pollutants spreading out horizontally back to the basin (Edinger, 1973). No similar phenomenon has been observed in the Great Lakes area. Over the Los Angeles Basin, a semi-permanent inversion hindering the vertical mixing of pollutants is frequently observed during high ozone days. This regular incident in the Los Angeles Basin has not been observed in the Tampa Bay area during local ozone episodes.

1.3 Ozone in the Troposphere

Photolysis is the key process in the formation of photooxidants. The photolysis rate K for a chemical compound, can be written as,

$$K_m = \int_{\lambda_1}^{\lambda_2} \sigma_m(\lambda, T) \phi_m(\lambda, T) I(\lambda) d\lambda \qquad (1.1)$$

where σ_m is the absorption cross section of a molecule m at wavelength λ and temperature T. ϕ_m is the quantum yield of the molecule m when it absorbs radiation of wavelength λ at temperature T. I is the actinic irradiation that depends not only on the wavelength, but also on the conditions of atmosphere and the location. In the troposphere, available wavelengths (λ) in the range from 280 to 730 nm may induce photochemical reactions.

The basic cycle of ozone formation in the troposphere starts with the photolysis of NO_2 (Seinfeld, 1986),

$$NO_2 + h\nu \rightarrow NO + O \qquad (1)$$

$$O + O_2 + M \rightarrow O_3 \qquad (2)$$

$$NO + O_3 \rightarrow NO_2 + O_2 \qquad (3)$$

where M is a third body that absorbs excess energy from 'nascent' ozone molecules. Reaction (2) is the only significant source of ozone in the troposphere. According to these basic reactions, the concentration ratio of NO_2/NO primarily determines the amount of ozone being generated. Nitrogen dioxide (NO_2) is generally less than 10% of the total oxides of nitrogen (NO_x) emissions from anthropogenic sources, and the only other major source of NO_2 is the oxidation of nitric oxide (NO) by ozone generated in this cycle. Apparently, the presence of NO and NO_2 is insufficient to produce the levels of ozone recorded in the troposphere.

Non-methane hydrocarbons (NMHCs) play an important role in supplying NO_2 through the catalyzed oxidation of NO. Basically, there are two main reaction paths that lead to the generation of NO_2. The first one is the chain reaction initiated by the reaction between VOCs and hydroxyl radicals (OH). The reactions of VOCs with OH generate free radicals. Subsequently, these free radicals produce peroxy radicals and/or hydroperoxy radicals (HO_2) due to the presence of oxygen. Consequently, NO is oxidized by HO_2 and/or peroxy radicals to produce NO_2. These catalytic chain reactions are important for most VOCs. For example, the chain reaction of propene and OH is initiated by addition of OH to either end of the double bond and, rearrangement into two types of hydroxyalkyl radicals (Atkinson, 1990),

$$CH_3CH=CH_2 + OH\bullet \quad \rightarrow \quad 0.35 \ CH_3CH(OH)CH_2\bullet \qquad (4a)$$

$$\rightarrow \quad 0.65 \ CH_3\overset{\bullet}{C}HCH_2(OH) \qquad (4b)$$

$$CH_3CH(OH)CH_2\bullet + O_2 \quad \rightarrow \quad CH_3CH(OH)CH_2O_2\bullet \qquad (5a)$$

$$CH_3\overset{\bullet}{C}HCH_2(OH) + O_2 \quad \rightarrow \quad CH_3CH\overset{\bullet}{O}_2CH_2(OH) \qquad (5b)$$

$$CH_3CH(OH)CH_2O_2\bullet + NO \quad \rightarrow \quad CH_3CHO + HO_2\bullet + \\ HCHO + NO_2 \qquad (6a)$$

$$CH_3CH\overset{\bullet}{O}_2CH_2(OH) + NO \quad \rightarrow \quad CH_3CHO + HCHO + \\ HO_2\bullet + NO_2 \qquad (6b)$$

$$HO_2\bullet + NO \quad\rightarrow\quad NO_2 + OH\bullet \tag{7}$$

The peroxy radicals subsequently produced react with NO to form NO_2.

The other path starts with the photolysis of certain VOCs, such as aldehydes, and ketones. Hydroperoxy radicals and peroxy radicals that lead to the oxidation of NO are also the products of this path. For formaldehyde, higher aldehydes, and acetone, this photolytic path is as important as their reactions with OH. The major termination step of these chain reactions (Finlayson-Pitts and Pitts, Jr., 1993) is the reaction of NO_2 and OH to form nitric acid (HNO_3). The photolysis of acetaldehyde (CH_3CHO) (Seinfeld, 1986) results in two initial processes. These two primary processes produce peroxy free radicals which react with NO to form NO_2,

$$
\begin{aligned}
CH_3CHO + h\upsilon \quad&\rightarrow\quad HCO\bullet + CH_3\bullet &(8a)\\
&\rightarrow\quad H\bullet + CH_3CO\bullet &(8b)\\[6pt]
CH_3\bullet + O_2 \quad&\rightarrow\quad CH_3O_2\bullet &(9a)\\
CH_3CO\bullet + O_2 \quad&\rightarrow\quad CH_3CO_3\bullet &(9b)\\[6pt]
CH_3O_2\bullet + NO + O_2 \quad&\rightarrow\quad NO_2 + HCHO + HO_2\bullet &(10a)\\
CH_3CO_3\bullet + NO \quad&\rightarrow\quad NO_2 + CH_3CO_2\bullet &(10b)
\end{aligned}
$$
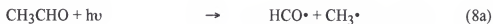
VOCs can also react with ozone but with much smaller reaction rates. Since the concentration of ozone is much higher than that of OH radicals in the atmosphere, NMHCs may also play an important role in reducing ozone concentrations. At night, the reaction of NO_2 and ozone becomes relatively significant in ozone reduction. The reaction forms the nitrate radical (NO_3) which may react with NMHCs, or may be removed by formation of nitric acid on wet surfaces (Finlayson-Pitts and Pitts, Jr., 1993).

Both methane and CO can generate ozone via reaction with OH forming HO_2, for example:

$$CO + OH\bullet \quad \rightarrow \quad CO_2 + H\bullet \quad \quad \text{(11 a)}$$
$$H\bullet + O_2 + M \quad \rightarrow \quad HO_2\bullet + M \quad \quad \text{(11 b)}$$

The reaction between methane and the OH radical is not similar to the propene example described above. In the former case a slower reaction occurs where the OH radical abstracts a hydrogen atom to produce a methyl radical ($CH_3\bullet$) and water. This mechanism is common to all alkanes. Due to its relatively low reactivity, however, methane does not play a significant role in urban and regional ozone pollution. On the other hand, high levels of CO can enhance O_3 production due to formation of hydroperoxy radicals in reaction (11b).

1.4 Sources of Ozone Precursors

High temperature combustion processes are the main sources of anthropogenic emissions of nitrogen oxides. The NO_x can be formed in combustion processes through the reaction between nitrogen (78%) and oxygen (21%) in the high temperature combustion air. Oxidation of organic nitrogen in fuels is another source of NO_x from combustion. Electric utility plant furnaces are the major stationary source of NO_x emissions in the United States. These furnaces are estimated to account for 35% (6.9 million metric tons)[1] from all man made sources in 1987. The other major anthropogenic source of nitrogen oxides is emissions from motor vehicles. The latter contributed about 43% (8.4 million metric tons)[1] of anthropogenic NO_x emissions in the U.S.

Nitrogen oxides can also be produced through lightning discharges in air and nitrification and/or denitrification processes by micro-organisms in soils (Payne, 1973). The NO_x generated from lightning is estimated to be about 6.6 million metric tons yr^{-1} (Chameides, 1986), and the same magnitude of NO_x is estimated to be generated from

---

[1] Technical Support Division national Air Data Branch. National air pollutant emission estimates, 1940-1987. EPA-450/4-88-022.

microbial activity in soils (Seinfeld, 1986). Florida has the highest frequency of lightning events in the U.S., thus lightning may be the major natural source of NO_x in the state. Kardono (1990) estimated a flux of $2.5E+10^{10}$ molecules·cm^{-2}·s^{-1} of NO from grassy soils in north central Florida, but showed that NO emissions from soils in wooded areas are negligible. The total grassy soils NO emission flux, however, is estimated to be about 1% of the maximum estimated anthropogenic emission rates in south Florida metropolitan areas.

A wide range of NMHC species are emitted from different kinds of anthropogenic sources. EPA[1] has reported that hydrocarbon emissions from industries and motor vehicles were about 8.4 million metric tons yr^{-1} and 6.0 million metric tons yr^{-1} respectively in the U.S. in 1987. Industrial emissions include incomplete fuel combustion, evaporation of organic compounds being used in industrial processes, and release from fuel and organic compound storage containers. Discharges from these industrial processes accounted for 98% (8.3 million metric tons yr^{-1}) of the total NMHC emitted from all industrial sources. The types of NMHC emitted from industries are process related.

Motor vehicle sources include emissions from exhaust pipes due to the incomplete combustion of gasoline, and evaporation of fuels from other parts of the vehicles. The emission from highway vehicles was about 78% (4.7 million metric tons yr^{-1}) of all transportation sources. Butane (C_4H_{10}) and pentane (C_5H_{12}) are the main alkane compounds being emitted from motor vehicles. Ethene (C_2H_4), propene (C_3H_6) and butene (C_4H_8) are the major alkene compounds in vehicle emissions. The primary aromatic species emitted from motor vehicles are benzene (C_6H_6), toluene (C_7H_8) and xylenes (C_8H_{10}). Stump et al. (1990) suggested that alkane and aromatic compounds account for more than 40% and 30%, respectively, of the total weight of NMHC emissions for various on-road conditions.

The major natural sources of NMHC are those due to activities in biomass, such as trees, grasses and crops. The main NMHC species of concern with biogenic origin are isoprene, α-pinene, β-pinene, and other mono-terpenes, because they are highly reactive and have significant emission rates. Lamb et al. (1987) estimated that the natural emission of NMHCs in the U.S. was 3.1 million metric tons yr^{-1}. Isoprene and α-pinene accounted for more than 60% of the total biogenic NMHCs. The emission strengths of biogenic NMHCs are not only biomass species dependent, but also are a function of temperature and/or solar radiation.

<u>1.5 Ozone Control Strategies</u>

Since complex chemical mechanisms are involved in ozone generation, it is difficult to apply an optimized control strategy. Historically, an ozone isopleth plot (Figure 1.4) has been used as a basis for applying control strategies. The isopleth plot shows relationships between maximum ozone concentrations and mixtures of NO_x and VOCs. The isopleth plot was a result of VOCs and NO_x mixtures being irradiated in photochemical chambers. Models have successfully simulated the chemical processes in these chambers. These models (Demerjian, 1985) use historical ambient concentration observations of NMHCs and oxides of nitrogen in the early morning and the resulting maximum ozone level for a worst case episodic day in a specific urban area to generate the isopleth. The isopleth is used as a basis for planning ozone reduction strategies in that particular urban area. This is the so called the Empirical Kinetic Modeling Approach (EKMA).

On the basis of these isopleths, the EKMA plot shows that VOC only control strategies could reduce ozone concentrations more effectively in low VOCs/NO_x ratio areas, such as urban areas. For example, the route from point D to E in Figure 1.4 (b) shows the effectiveness of VOC control in a low VOC/NO_x region. Any reduction of NO_x may initially have an adverse effect on the ozone air quality for low VOC/NOx ratio

17
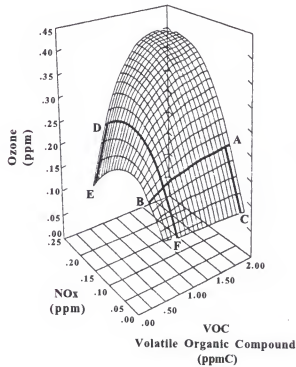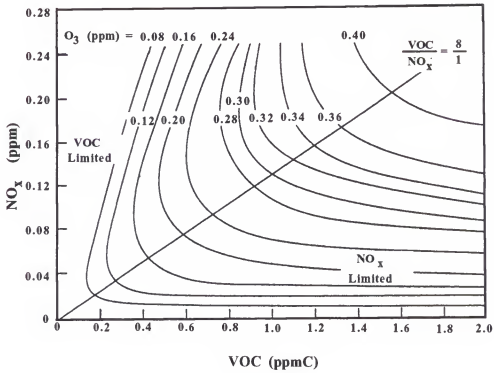
Figure 1.4. Ozone isopleth diagram (a) 2-D and (b) 3-D. The solid lines indicate O₃ concentrations in parts per million by volume(ppmv). (Source: Finlayson-Pitts and Pitts, Jr., 1993)

condition. The solid line from point D to F shows an increase of ozone in the early stages when NO_x is controlled.

It is not realistic however, to use the ozone isopleths as a basis for control strategies without detailed investigations of VOCs and NO_x levels within a region. Wolff and Korsog (1992) showed that there is no significant relationship between VOC/NO_x ratios and the maximum ozone concentrations as interpreted from chamber experiments. In the real atmosphere, deposition processes, existence of particulate matter, turbulence and variations in radiation are believed to be the primary causes of deviations from chamber studies. Another difficulty in applying the ozone isopleth method, is that the VOC/NO_x ratio at a monitoring site may not represent the ratio in a region.

The other approach in determining an optimal control strategy for ozone is to use air quality models. Model studies (Wolff and Korsog, 1992) have suggested that NOx reductions would cause deterioration in the ozone air quality in New York City, but NO_x reductions could lead to lower ozone concentrations in Atlanta. Milford et al. (1989) showed that different combinations of NO_x and VOC could reduce ozone in the Los Angeles basin more effectively in their model study. Air quality models have the capability to include the emission and meteorological characteristics of a region, therefore, they could be better tools to provide bases for optimal ozone control strategies.

1.6 Meteorological Models

Pearce (1955), Fisher (1959) and Estoque (1961) introduced two-dimensional non-linear models to describe the characteristics of a sea breeze. Pearce (1955) and Fisher (1959) used artificial heating mechanisms which ignored strong correlations among vertical heat transfer, exiting temperature and velocity fields (Estoque, 1961). Estoque (1961) treated the entire region as two stratification levels which have different characteristics in vertical eddy flux of momentum and heat. He successfully explained

several sea breeze phenomena, such as the formation of a sea breeze under the influence of geostrophic winds (Estoque, 1962).

Two-dimensional models neglect influences caused by the variation along the coastal line. In order to describe a complex coastal line, which is invariably the case, a three-dimensional model is required. Pielke (1974) developed a three-dimensional model to describe the sea breeze and thunderstorm occurrences in south Florida. A three-dimensional dynamic model developed at Pennsylvania State University (Anthes and Warner, 1978) could not only be used to describe the sea breeze, but also was able to simulate different meteorological conditions induced by terrain variations.

Meso-meteorological models are frequently used as tools to investigate the transport, diffusion and transformation of pollutants in complex terrains. They can predict three-dimensional flow fields, which dominate the advection and convection of pollutants. The horizontal and vertical eddy diffusivities produced by the models can be used to estimate the diffusion of pollutants. The temperature field is an important factor which affects the reactivities of pollutants. Such models can also predict cloud, rain and snow liquid water contents, which are important in scavenging and providing reaction sites for pollutants in the atmosphere. The models are especially useful in the case of sparse meteorological measurements, because most mesoscale meteorological conditions are primarily forced by the underlying terrain (Pielke et al, 1983).

1.7 Air Quality Models

Eulerian and Lagrangian approaches are the two basic ways to describe dispersion of pollutants in air quality models. Lagrangian methods focus on property changes and behavior of a representative fluid mass. The advantage of using the Lagrangian approach in an air quality model is that it is easier to trace the major sources that contribute to deteriorating air quality in a specific area. Conversely, the Lagrangian method cannot be applied to solve non-linear chemical reactions directly (Seinfeld, 1986). In addition,

Lagrangian methods are difficult to verify using measurement information, because they have limitations in resolving horizontal concentration fields (Demerjian, 1985). For example, the ELSTAR model is a multilayered Lagrangian model which can describe the history of an air mass. The Eulerian approach describes the behavior of a fluid mass in a fixed coordinate system. It does not have the disadvantages of the Lagrangian approach, but the Eulerian equations are not easily solved. The Regional Oxidant Model (ROM), Sulfate Transport Eulerian Model-II (STEM-II), and the Urban Airshed Model (UAM) are the best known Eulerian approach models. They are used quite extensively in air quality studies.

Lurmann et al. (1984) applied the ELSTAR Lagrangian model in studying the contribution of biogenic hydrocarbons (HC) to the ozone air quality in the Tampa/St. Petersburg area. They estimated that the total biogenic reactive hydrocarbon (RHC) emissions contributed from 31 to 44% to RHC levels along the air mass trajectories. Although biogenic RHCs contributed significant amounts to the total RHC emissions, the results of Lurmann et al. (1984) showed that the biogenic RHCs only contributed from 2 to 11 ppb or from 2 to 9% to the maximum O_3 concentrations. They suggested that the much faster reactions of biogenic RHCs with both OH and O_3 cause only small increments in O_3 levels in urban areas.

The governing equations for Eulerian air quality models basically consist of three parts which describe advection, diffusion and reactions of pollutants. Various physical processes or chemical mechanisms can be adapted to different applications on the basis of requirements determined by the users. The models require meteorological data, emission inventory data, initial conditions and boundary conditions as input data, therefore, the simulations should be supported by observation information. The following examples describe some of the applications of Eulerian air quality models.

Carmichael and Peters (1984) demonstrated the capabilities of the STEM-II model to simulate the interaction of emissions, deposition, chemical reactions and

transport of sulfur dioxide (SO_2) and sulfate (H_2SO_4) compounds. Since SO_2 is a primary pollutant, it is a source-dominated compound. Carmichael and Peters' (1984) results showed elevated SO_2 levels around major cities in the northeastern US. Elevated sulfate levels were predicted along the Atlantic coast, because of the prevailing westerly and southwesterly wind, lower deposition rates over the ocean surface, and higher SO_2 oxidation rates over the south eastern US.

Chemical reactions of pollutants incorporated into Eulerian models can involve single and multiple phases. Carmichael et al. (1986) have demonstrated the in-cloud removal of ammonia (NH_3), and in-cloud production of H_2SO_4 with the STEM-II model. They demonstrated the capabilities of their model in simulating multi-phase chemical reactions in the atmosphere.

Kitada et al. (1986a) discussed the dynamic and chemical characteristics of NO_2, nitrate (HNO_3), PAN, O_3, SO_2 and H_2SO_4 in a combined field of land/sea breeze and mountain/valley winds in Mikawa Bay, Japan. They performed simulations with different diurnal variation patterns and hypothetical emission rates, and with wind fields created by an objective method. They found that the combined fields of sea and valley winds could transport an NO_2-rich air mass into deep mountain sites. Since land and mountain circulations are weaker than sea and valley winds, they could not form a single circulation pattern. The weak land and mountain winds contributed to steady and moderate NO_2 levels found at a middle site. The peak concentrations of HNO_3 and sulfate moved inland with a velocity the same as that of the sea breeze fronts. Their conclusions demonstrated that the STEM-II Eulerian model can be used in complex meteorological and topographic conditions.

Dry deposition is an important process for the removal of pollutants from the atmosphere, and it is also believed to contribute to roughly half of the total acid deposition. Kitada et al. (1986b) incorporated a procedure into the STEM-II model that calculates dry deposition velocities from the aerodynamic, surface and residual

resistances, and evaluated the effects of dry deposition on pollutant concentrations within land- and sea-breeze circulations. On the basis of their results, dry deposition contributed 40% and 25% of the total removal for emitted NO_x and SO_2, respectively, over a 2 day period. The sea surface was responsible for only one fifth of the NO_x removal. The atmospheric removal of NO_x and SO_2 leads to an increase in hydrocarbon compounds, because less NO_x and SO_2 are available for chemical reactions.

The transport and formation of ozone are strongly influenced by the meteorological conditions and the composition of pollutants in the air masses. Chang et al. (1989) applied the STEM-II model to simulate the long term transport of ozone and its precursors in the early evening that contributed to high ozone concentrations (> 150 ppb) observed at Takasaki and Karuizawa Japan. These cities are located at large downwind distances (> 100 km) from the Tokyo metropolitan complex in Japan. Since the influences of local valley/mountain winds, synoptic on shore winds, and sea/land breezes are present, the characteristics of ozone concentrations in central Japan are very complex. Chang et al. (1989) found that the high concentrations of ozone might be a result of contributions from three chemically distinct air masses. These air masses originally came from the down flow of an aged air mass above the Fukaya region on the previous day, a polluted air mass which formed in the Tokyo area, and an air mass over the Sigami Bay.

Good quantitative agreement between the air quality model simulations and the observations can be obtained, if a detailed emission inventory and accurate meteorological data are available. Chang et al. (1990) evaluated their simulation results against observations of ozone, NO, NO_2 and hydrocarbon species in central Japan. Their simulations were supported with dense meteorology and air quality sites, and a detailed emission inventory, therefore, their results should agree with observations, both quantitatively and qualitatively. The surface ozone predictions showed a correlation coefficient of 0.88 over the simulation period. An average fractional difference (0.62) indicated that the difference between observations and predictions is more than a factor of

two, for ozone. This discrepancy could be due to the fact that the model had difficulties in predicting night time ozone. The model tended to overestimate the ozone at high ozone concentrations and underestimate low concentration areas. Their results, however, confirmed that the STEM-II model could perform accurately in predicting ozone levels in a complex area.

The future development of STEM-II models are oriented to employing diverse applications and to improving computing efficiency. The models will also be modified and developed to describe the behavior of pollutants and other natural factors in greater detail, such as incorporating chemical mechanisms of biogenic trace elements, cloud effects, solid phase chemical reactions, and stratosphere-troposphere exchange.. Expansion of the model capabilities leads to a decrease in performance rate of the model, and an increase the cost of the computer resource. In order to increase the performance rate and take advantage of the modern architecture of computer technology, the scheme of the STEM-II model maybe modified to utilize the vector and parallel architectural features more efficiently.

The basic assumption of this research is that the meteorological conditions existing during the worst ozone episode are the poorest conditions in terms of ozone attainment in the Tampa Bay area. If the ozone level can be reduced to below the ozone NAAQS by reducing either NO_x or NMHC emissions under these meteorological conditions, then the ozone NAAQS is likely to be met for a long time in the future in the Tampa Bay area. The ozone episode selected for this simulation study should meet the criteria and the assumptions given above. In chapter 2, the selected ozone episode will be described in detail to provide an understanding of the episode and the conditions that induced it to occur.

CHAPTER 2
REVIEW OF THE TAMPA BAY OZONE EPISODE

The ozone episode that was chosen to be studied lasted from July 22 to July 24, 1987. The highest ozone peak concentrations experienced in the Tampa Bay area from 1980 to 1990 occurred during this episodic period. Ozone air quality, the synoptic and local meteorological conditions, and the possibility of intrusion of stratospheric ozone are discussed in this chapter.

2.1 Ozone Air Quality

High ozone concentrations ($\geq$ 90 ppb) were found in five major urban and suburban areas of Florida (Table 2.1) within the period of July 22 to July 24 in 1987. Except for Orlando, these urban areas (Tampa, St. Petersburg, Jacksonville and Miami) are located either in the coastal zone of the Gulf or along the coast of the Atlantic Ocean. Also, Orlando is the only urban area where the observed ozone concentrations did not exceed the ozone ambient air quality standard ($\geq$ 120 ppb). Apparently the violation of the ozone ambient air quality standard (NAAQS) could be due in part to the enhancement of ozone generation and accumulation by sea-land circulation during this episode.

On July 22, 1987, a maximum concentration of 111 ppb was detected at a Tampa pump station site (Figure 2.1) in the Tampa suburban area. The following day, July 23, at all three monitoring sites (Tampa pump station, E.G. Simmons County Park and Davis Island) located in the Tampa suburban area maximum ozone concentrations were observed that were higher than the ozone NAAQS. On the same day, all the sites in St. Petersburg (Clearwater J.C. campus, Azalea Park and East Lake Tarpon) detected ozone concentrations that were only slightly less than the ozone NAAQS. Two of the

Table 2.1. Florida ozone air quality during a selected high ozone episode in Tampa Bay area.

	SITE	DATE	PERIOD*	MAX. (ppb)	TIME
Tampa	1	07/23/87	18:00-20:00	131	19:00
		07/24/87	12:00-16:00	171	14:00
	2	07/23/87	16:00-19:00	127	17:00
		07/24/87	11:00-16:00	113	14:00
	3	07/22/87	16:00-17:00	111	17:00
		07/23/87	15:00-19:00	142	17:00
		07/24/87	?????-16:00	156	14:00
St. Petersburg	1	07/23/87	15:00-19:00	116	17:00
	2	07/23/87	17:00-19:00	115	18:00
		07/24/87	12:00-17:00	142	14:00
	3	07/23/87	14:00-17:00	108	14:00
Orlando	1	07/23/87	13:00-19:00	113	14:00
	2	07/23/87	13:00-18:00	110	17:00
Jacksonville	1	07/23/87	?????-18:00	155	14:00
	2	07/23/87	13:00-18:00	>100	17:00
Miami	1	07/24/87	13:00-16:00	134	14:00

* Period of high ozone concentration ($\geq$ 90 ppb).

????? Missing data.

Site 1: E.G. Simmons County Park
Site 2: Davis Island
Site 3: Tampa pump station
Site 4: Clearwater J.C. campus
Site 5: Azalea Park
Site 6: East Lake Tarpon
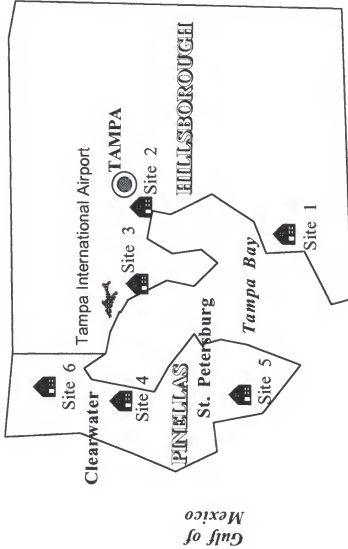
Figure 2.1. Locations of six ozone monitoring sites in Pinellas and Hillsborough counties.

three sites in Pinellas County are located within the suburban area, whereas the other is in a rural area. The rural area site (East Lake Tarpon) had the lowest maximum ozone concentrations (108 ppb) for Pinellas County. On July 24, 1987, ozone exceedances were observed at two of the three sites in Tampa. The exceedances were the highest observed in the episodic period. On the same day, one site (Azalea Park) in St. Petersburg recorded a maximum ozone concentration that exceeded the ozone NAAQS.

Both rural and suburban sites in Jacksonville detected high ozone concentrations on July 23, 1987. The suburban site experienced ozone exceedances. The maximum ozone concentrations at a rural site in Duval County could not be confirmed, because three hours of data are missing. An exceedance of the ozone NAAQS was also observed in Miami on July 24, 1987.

Transport of ozone and its precursors from regional metropolitan areas could contribute to the ozone episode in the Tampa Bay area, because both Jacksonville and Orlando are less than one-day transport distance from Tampa Bay. For example, the maximum ozone concentration recorded in Orlando was up to 5 hours earlier than those occurring in the Tampa and St. Petersburg regions. It is possible that the ozone and ozone precursors emitted and generated in the Orlando area were transported to Tampa Bay and contributed to the ozone episode on July 23 in the Tampa bay area. Therefore, it is necessary to consider the transport from other urban areas when the simulation domain is selected.

2.2 Meteorological Conditions

Synoptic weather systems and local thermally- induced circulations are the two primary factors that dominate the atmospheric transport and transformation of chemical species in coastal regions. This section describes and analyzes the synoptic weather patterns occurring during the recent ozone episode (from July 22, 1987, to July 24, 1987) in Tampa Bay. The region was selected for study on the basis of existing daily weather

maps. Vertical sounding data provide information about local elevated meteorological conditions that assist in the interpretation of the movement of pollutants within thermally induced circulations. In central Florida, Tampa International Airport (TIA) is the only vertical sounding station. Although the sounding information is limited to this location, it is essential for the analyses of local atmospheric stability and vertical distributions of horizontal wind flows. Also, meteorological analyses were carried out for the 20th and 21st of July, 1987, because a simulation will be run for these days preceding the episode to stabilize the chemical species for the initial conditions of the episode.

2.2.1 Synoptic Analyses

DATE: July 20 and 21, 1987

A broad surface high pressure system covered the eastern half of the United States. Three high pressure centers moved into the east coast of South Carolina, over Kentucky and Iowa by July 21, 1987. The former high pressure system generated a northeastern airflow in central Florida. An upper high covered the central and eastern U.S. continuously, so the upper air over Florida was dominated by eastern to southeastern airflow. Temperatures were in the range from mid-70s(^{o}F) to low-90s(^{o}F) in central Florida. Precipitation was reported all over Florida for these two days. The western part of the U.S. was mainly controlled by low pressure systems. A frontal system, originally at the border of eastern Canada and the U.S., on July 20 moved to the northeastern states of the U.S., and decreased in size by July 21, 1987.

DATE: July 22, 1987

At 12Z (7:00 AM Eastern Standard Time (EST)) the surface weather map showed a frontal system accompanying a low center in South Dakota (Figure 2.2). The frontal center was associated with a cold front extending to northern New Mexico and an occluded front extending to the north of the Great Lakes. A surface high center was formed on the east coast of Maine and it pushed a small frontal system from the continent
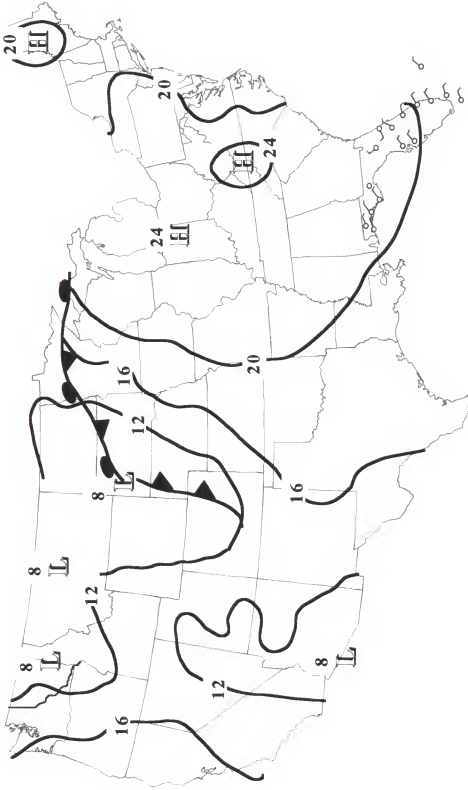
Figure 2.2. Surface weather map at 07:00 AM EST for July 22, 1987.

into the Atlantic Ocean. These frontal systems did not affect the weather in Florida. The eastern U.S. was still dominated by the same high pressure system and a northeastern surface airflow prevailed in central Florida. Scattered cirrus clouds covered less than seven-tenths of the sky and did not increase in central Florida. Precipitation was recorded at thirty-two percent of the observation stations in Florida. At 500 mb, the upper high continuously covered the eastern U.S., but the air flow shifted to the northeast in central Florida.

At 07:00 PM EST (Figure 2.3), the front center in South Dakota moved to North Dakota and another low center was formed at the front center. No significant change was observed in the eastern U.S. Northeastern and eastern winds still dominated the east and west coasts of Florida, but a southwestern wind, indicating a sea breeze, was observed in the panhandle area of Florida. The wind data suggested that there was no strong sea breeze along the west coast, except for the panhandle area. Fair weather cumulus clouds were observed in the Tampa area. The sounding data (Figure 2.4) showed differences between the airflow at 07:00 AM and that at 07:00 PM, which increased at higher elevation.

DATE: July 23, 1987

At 7:00 AM EST, the surface frontal system (Figure 2.5) in the mid-west moved north-eastward into Canada and the eastern U.S. was covered by the same high pressure system mentioned previously. A weak low pressure trough was formed near the east coast of Georgia and moved southward. The airflow in central Florida varied from northwest to southeast and the clouds observed were mostly cirrus-type. Precipitation was observed only in the northwest region of Florida. No significant change at the 500 mb surface was found. At 07:00 PM EST (Figure 2.6), the cloud cover increased on the west coast of Florida. Opposite air flows were observed on the east and west coasts of Florida, because of the influence of the local sea-land circulations. On the basis of the vertical sounding data (Figure 2.4) obtained at TIA, the wind was blowing from

Figure 2.3. Surface weather map at 07:00 PM EST for July 22, 1987.
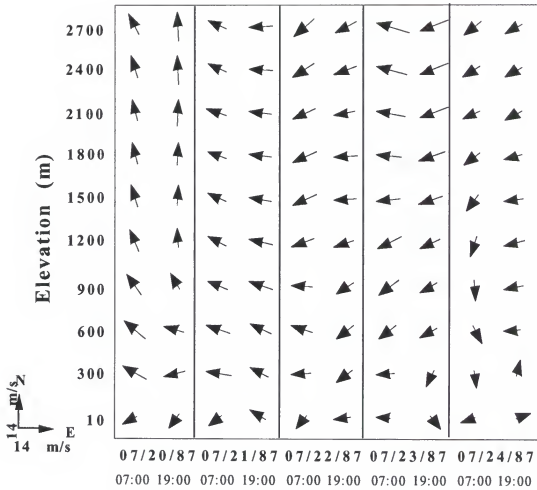
Figure 2.4.   Vertical sounding air flows at Tampa International Airport from 07/20/87 to 07/24/87.
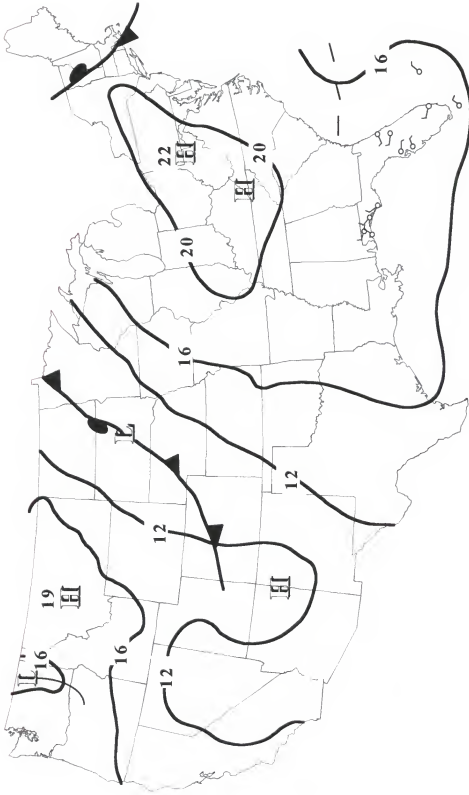
Figure 2.5. Surface weather map at 07:00 AM EST for July 23, 1987.
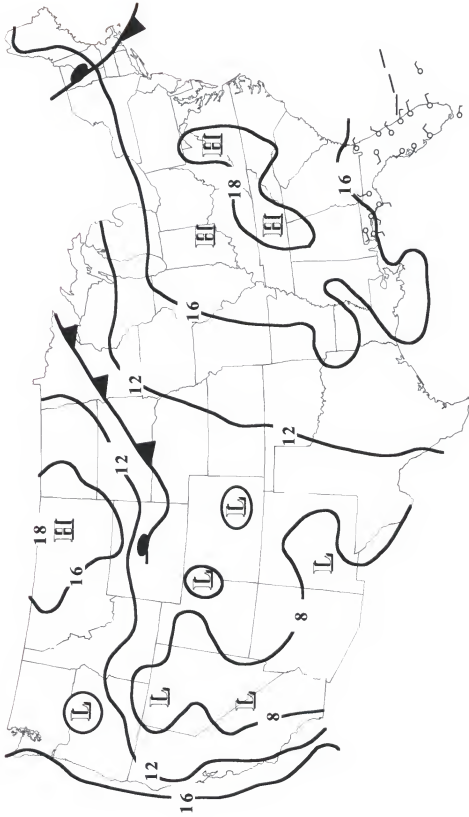
Figure 2.6. Surface weather map at 07:00 PM EST for July 23, 1987.

northwest to southeast at 07:00 PM. This air movement could be due to the Gulf type sea-land breeze. The return flow was found above an elevation of 300 meters.

DATE: July 24, 1987

At 7:00 AM EST, a series of occluded, cold and warm fronts (Figure 2.7) extended from Idaho to the east coast of Canada. Three low centers were associated with this frontal system. The weather patterns in the eastern U.S. were similar to those on July 23, 1987. The weak low pressure trough had already moved out beyond the continent and was now south of Miami. Again, north and northeast airflows prevailed in central Florida and the same weather patterns existed at the 500 mb elevation. At 7:00 PM (Figure 2.8), strong evidence of sea-land circulations in the coastal region of Florida was found. On the basis of the vertical sounding (Figure 2.4) and surface observations, the circulations could be identified as Bay type sea-land circulations. The return flow was higher than that of July 23, 1987; at about 450 meters elevation. Precipitation was observed in the northwest and northern regions of Florida. The cloud cover increased in Florida and remained dominated by cirrus clouds.

2.2.2 Vertical Sounding Analyses

The morning sounding (7:00 AM EST) on July 22, 1987 (Figure 2.9), indicated a surface inversion below 300 meters and a subsidence inversion between 1000 and 1200 meters. The atmosphere was relatively stable above the subsidence inversion and below the Cloud Condensation Level (CCL), as well as between the surface and subsidence inversion layers. The air above the subsidence inversion layer was extremely dry, which indicated the descent of dry air from upper elevations. Both the surface inversion and the subsidence inversion layers were absent in the afternoon sounding (Figure 2.10). The lower atmosphere appeared weakly stable to neutral in the afternoon sounding. The elevations of CCLs in both soundings, were higher than those of the maximum mixing heights (MMHs), so the development of clouds was suppressed on July 22, 1987.
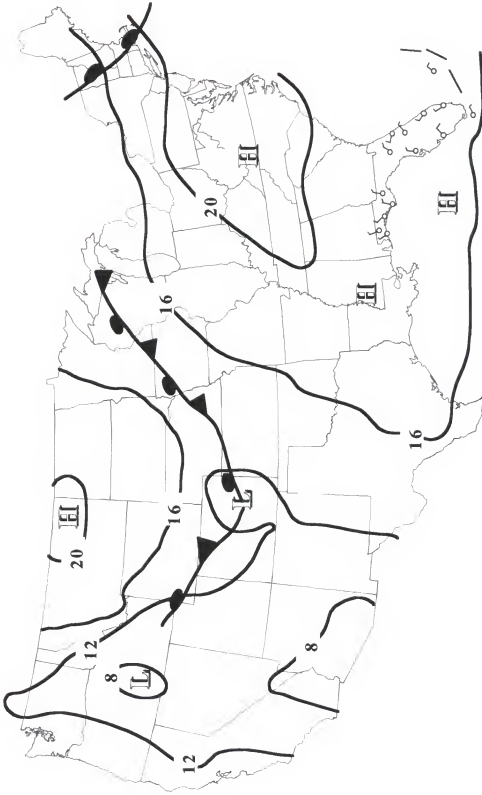
Figure 2.7. Surface weather map at 07:00 AM EST for July 24, 1987.
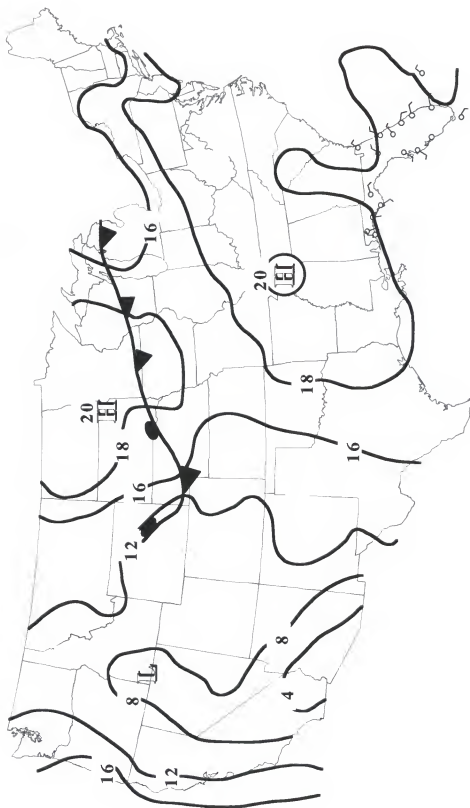
Figure 2.8. Surface weather map at 07:00 PM EST for July 24, 1987.
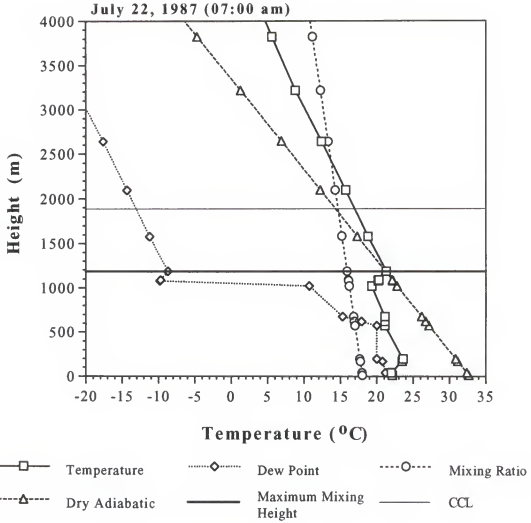
Figure 2.9. Vertical sounding temperature profiles and analysis for
Tampa International Airport at 07:00 AM on 07/22/87.
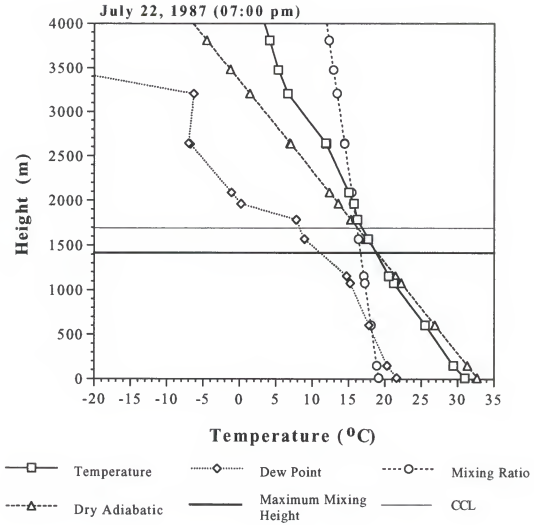
Figure 2.10. Vertical sounding temperature profiles and analysis for
Tampa International Airport at 07:00 PM on 07/22/87.

Because of radiation heating, the maximum mixing height increased from 1200 to 1600 meters in the afternoon.

A weak subsidence inversion was also found between 1000 and 1200 meters in the vertical soundings (Figure 2.11) at 07:00 (AM) on July 23, 1987. At the same time, inversion appeared below an elevation of 200 meters. The descending dry air from higher elevations caused the extremely low dew point temperature above the subsidence inversion layer. The surface inversion was removed by ground surface heating in the afternoon. Also, the subsidence inversion was eliminated. Since subsiding air existed at higher elevations, the layer above 1250 meters remained relatively stable in the afternoon sounding (Figure 2.12), which is why the MMH did not change from the morning to the afternoon sounding. CCLs were higher than MMHs in both soundings. The CCL in the morning was above 2000 meter elevation whereas the CCL in the evening was around the 1700 meter level. In both cases, the development of clouds was suppressed.

On July 24,1987 (Figure 2.13), the subsidence inversion disappeared in the upper air, but a surface inversion was present under 250 meters. The moisture increased above the surface layer, as compared to the sounding on July 23, 1987. The MMHs also increased to above 2000 meters. Both morning and afternoon soundings (Figure 2.14) showed higher MMHs than CCLs, so there was a chance for cumulus clouds to develop. Since the environmental temperature was lower than the air parcel temperature with a constant mixing ratio at CCL height, a trigger mechanism was required for a thunderstorm to develop. The thunderstorm, however, did not occur until July 25, 1987.

2.3 Influence of Stratospheric Ozone

The intrusion of ozone from the stratosphere can contribute to high ozone episodes in urban areas and elevated background levels in rural areas. On the basis of previous studies (Johnson and Viezee, 1981), ozone intrusion could extend down to 1.9 km above mean sea level, the top of the existing atmospheric boundary layer. Intruding
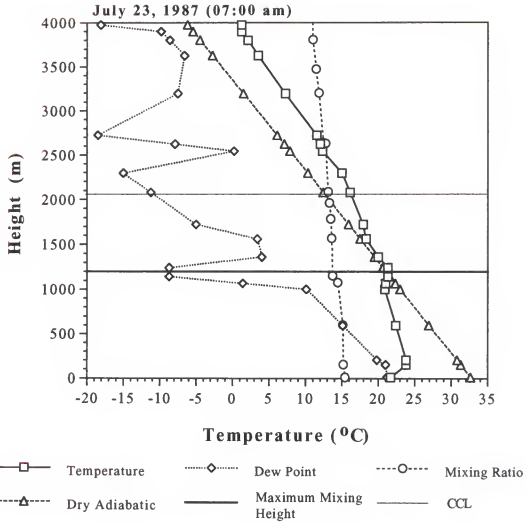
Figure 2.11. Vertical sounding temperature profiles and analysis for
Tampa International Airport at 07:00 AM on 07/23/87.
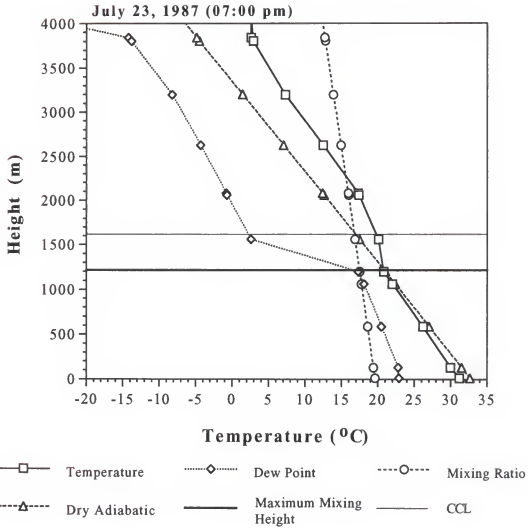
Figure 2.12. Vertical sounding temperature profiles and analysis for
Tampa International Airport at 07:00 PM on 07/23/87.
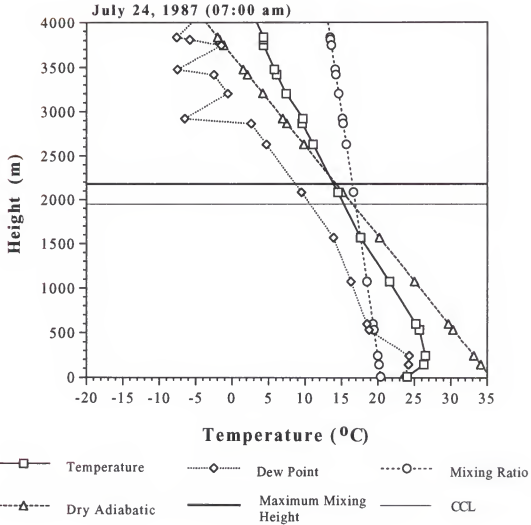
Figure 2.13. Vertical sounding temperature profiles and analysis for
Tampa International Airport at 07:00 AM on 07/24/87.

44
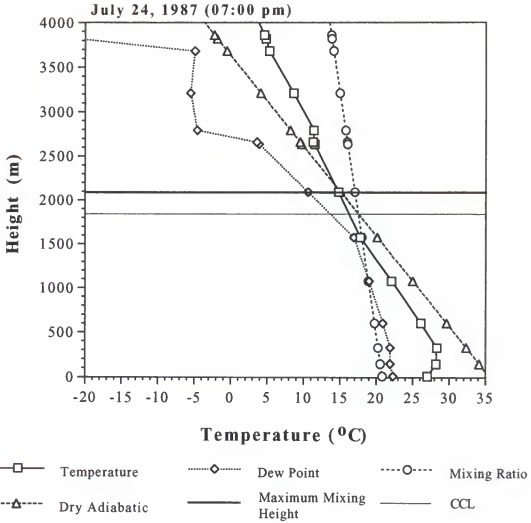
Figure 2.14. Vertical sounding temperature profiles and analysis for
Tampa International Airport at 07:00 PM on 07/24/87.

ozone could then be sequentially transported down to ground level by vertical mixing within the mixing layer, and down drafts within the frontal zone (Johnson and Viezee, 1981.)

In order to determine the effect of stratospheric ozone on the ozone episode being studied, several variables that indicate direct stratospheric intrusion, and meteorological conditions that can transport ozone at high elevation, were analyzed to determine the influence on ground level ozone concentrations. On the basis of suggestions by Meagher et al. (1987) and the observations of Johnson and Viezee (1981), these variables are: 1) the date of the episode; 2) the dew point temperatures at the top of the simulation domain; 3) the presence and the location of a 500 mb trough; 4) the presence of a cold front on or one day prior to the study period; and 5) the maximum mixing height during the study period. The probability of the influence of stratospheric ozone can only be judged from the factors listed above, because there were no direct observational data available for high elevation ozone.

On the basis of the surface weather maps and the sounding data at Tampa airport, convective mixing was the only mechanism that could transport intruded stratospheric ozone. No cold front passage in the episodic period was observed, so down drafts associated with a cold front did not exist. During the episode, the maximum mixing height varied from 1200 to 2200 meters in height. If there was any stratospheric ozone intrusion reaching the latter elevation, then mixing processes might have brought the ozone down to ground level. The next step was to examine the existence of ozone intrusion above the Tampa Bay area. Generally, stratospheric ozone intrusion is higher in the spring and fall than in the summer and winter. This cycle is associated with the seasonal variations of ozone concentration in the lower stratosphere and the incidence of tropopause folding (Johnson and Viezee, 1981). The episode being studied occurred in July, so a strong intrusion was not expected during this period. From the sounding data, it was found that the dew point temperatures above the top of the simulation domain did

not approach -40 °C, which would be indicative of intruded dry stratospheric air. On the 500 mb weather maps, the low pressure trough remained stationary over the west coast of the U.S. This trough was located more than 1300 km west of the Tampa Bay area, therefore, any ozone intrusion near the trough could not have reached the Tampa area. From the evidence presented above, it is concluded that there was only a small probability that stratospheric ozone affected ground level concentrations during the episode under investigation.

CHAPTER 3
MODEL DESCRIPTIONS

3.1 Mesoscale Meteorological Model Version 4[2]

3.1.1 General Description

The Mesoscale Meteorological Model Version 4 (MM4) is a suitable tool for predicting various types of meteorological conditions, such as frontal systems and sea-land circulations. The whole MM4 system (Figure 3.1) is a package of programs that pre-process the MM4 input, process the MM4 simulation and post-process the MM4 output. The simulations start with the TERRAIN program that performs three functions: 1) calculating the longitude and latitude for each grid point within the simulation domain; 2) accessing terrain heights and land-use characteristics from archived tapes; and 3) interpolating these data to the grid. The succeeding program is DATAGRID, which accesses global data from archived tapes and interpolates the data to the grid. The third program is RAWINS. It accesses upper-air, ship and surface data, and interpolates these data to the grids at each pressure elevation, thus providing a first guess at a prediction. In order to provide correct input data for the MM4, the first guess at pressure levels has to be interpolated to the model sigma levels. This work is done by GRIN. At the same time, GRIN is able to call on the graphic program to generate graphic outputs for both input of the MM4 and output from the MM4. The interpolated data sets are read by the MM4 main program for forecasting simulations. The output of the MM4 can be processed to calculate air parcel trajectories by the TRAJECTORY program.

---

[2] The description of the MM4 model is based on the NCAR TECHNICAL NOTE-Description of the Penn State/NCAR Mesoscale Model Version 4 (MM4).
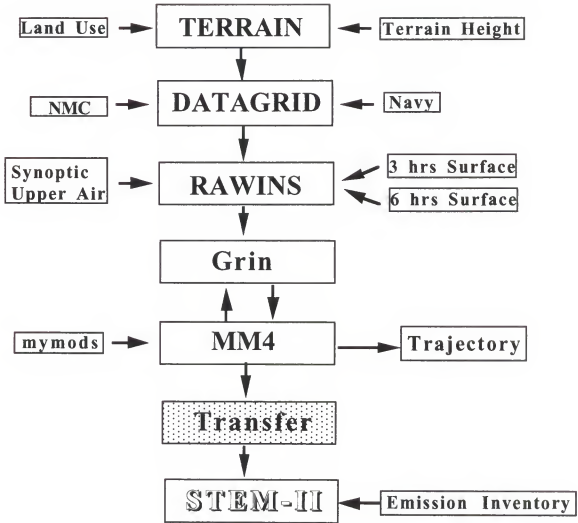
Figure 3.1. Schematic diagram of components of the Penn State/NCAR modeling system and STEM-II model.

MM4 output also provides a meteorological input for other models, such as acid deposition or photochemical models.

The "Arakawa B" grid (Figure 3.2) is used for the horizontal grid structure. The momentum variables (p^*u) and (p^*v) are calculated at circle points and all the other variables are computed at cross points. For the vertical grid structure (Figure 3.3), the vertical velocity is defined at the full-σ-levels and the rest of the variables are defined at the half-σ-levels.

3.1.2 Governing Equations

The fundamental equations being used to predict motion in the atmosphere are based upon three principles (Molton, 1979)-- conservation of energy, conservation of momentum, and conservation of mass. For a static atmosphere, the role of hydrostatic state is applied to the model. On the basis of these principles, the fundamental equations in the model are developed. Since a sigma coordinate system is used for the vertical coordinate, the equations are modified to sigma coordinates.

$$\sigma = \frac{p - p_t}{p_s - p_t} \qquad\qquad (3.1.1)$$

where

p = Pressure

p_s = Surface pressure

p_t = Pressure at the top of the model atmosphere

A map scale factor, m, is used to compensate for the effect of map projections. A choice among three map projections is available in the MM4 model system. They are the Polar
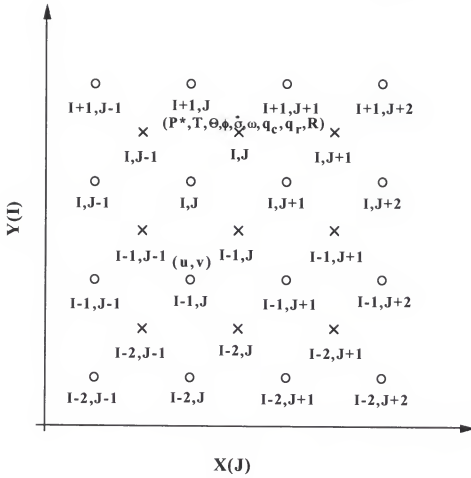
Figure 3.2.   Horizontal grid structure in the model. (Anthes et al. (1987)).
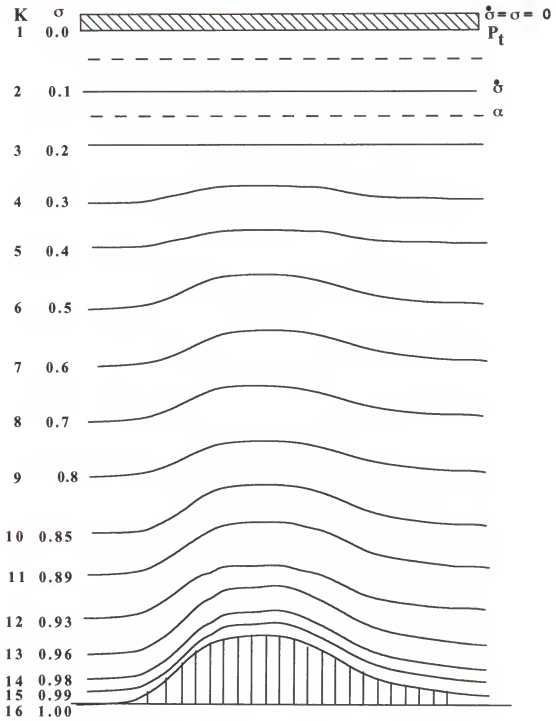
Figure 3.3. Vertical grid structure in the model.(Anthes et al. (1987)).

Stenographic map projection, the Lambert Conformal map projection and the Mercator projection. The Mercator projection is used in this study, because the study area is located in low latitudes.

The basic equations for conservation of momentum are the horizontal momentum equations. The equations of motion are

$$\frac{\partial p^* \overset{*}{u}}{\partial t} = -m^2 \left(\frac{\partial p^* \overset{*}{u}u/m}{\partial x} + \frac{\partial p^* \overset{*}{u}v/m}{\partial y} \right) - \frac{\partial p^* \overset{*}{u}\dot{\sigma}}{\partial \sigma}$$

$$- mp^* \left[\frac{RT_v}{(p^* + p_t/\sigma)} \frac{\partial p^*}{\partial x} + \frac{\partial \phi}{\partial x} \right] + fp^* v + F_{Hu} + F_{Vu} \qquad (3.1.2)$$

$$\frac{\partial p^* \overset{*}{v}}{\partial t} = -m^2 \left(\frac{\partial p^* \overset{*}{v}u/m}{\partial x} + \frac{\partial p^* \overset{*}{v}v/m}{\partial y} \right) - \frac{\partial p^* \overset{*}{v}\dot{\sigma}}{\partial \sigma}$$

$$- mp^* \left[\frac{RT_v}{(p^* + p_t/\sigma)} \frac{\partial p^*}{\partial y} + \frac{\partial \phi}{\partial y} \right] - fp^* u + F_{Hv} + F_{Vv} \qquad (3.1.3)$$

where

u	=	Eastward components of velocity
v	=	Northward components of velocity
p^*	=	$p_s - p_t$
$\dot{\sigma}$	=	Vertical velocity
ϕ	=	Geopotential
F_H	=	The effects of horizontal diffusion
F_V	=	The effects of vertical diffusion
T_v	=	Virtual temperature
f	=	The Coriolis parameter

R = The gas constant for dry air

m = Map scale factor (the ratio of distance on grid to actual distance on earth)

Based on conservation of mass, the continuity equation can be written as,

$$\frac{\partial p^*}{\partial t} = - m^2(\frac{\partial p^* u/m}{\partial x} + \frac{\partial p^* v/m}{\partial y}) - \frac{\partial p^* \dot{\sigma}}{\partial \sigma} \qquad (3.1.4)$$

so, the temporal variation of the surface pressure can be computed from,

$$\frac{\partial p^*}{\partial t} = - m^2 \int_0^1 (\frac{\partial p^* u/m}{\partial x} + \frac{\partial p^* v/m}{\partial y}) d\sigma \qquad (3.1.5)$$

The vertical integral result of Equation 3.1.4 is the vertical velocity at each sigma elevation.

$$\dot{\sigma} = - \frac{1}{p^*} \int_0^\sigma [\frac{\partial p^*}{\partial t} + m^2(\frac{\partial p^* u/m}{\partial x} + \frac{\partial p^* v/m}{\partial y})] d\sigma' \qquad (3.1.6)$$

On the basis of conservation of energy, the thermodynamic equation is given as,

$$\begin{aligned} \frac{\partial p^* T}{\partial t} = & -m^2(\frac{\partial p^* uT/m}{\partial x} + \frac{\partial p^* vT/m}{\partial y}) - \frac{\partial p^* T\dot{\sigma}}{\partial \sigma} \\ & + \frac{RT_v \omega}{c_{pm}(\sigma + p_t/p^*)} + \frac{p^* Q}{c_{pm}} + F_{HT} + F_{VT} \end{aligned} \qquad (3.1.7)$$

where

c_{pm} = The specific heat for moist air at constant p

$$[c_{pm} = c_p(1 + 0.8\ q_v)]$$

F_{HT} =   The effect of horizontal diffusion

F_{VT} =   The effect of vertical mixing and dry convective adjustment

q_v =   The mixing ratio of water vapor

Q =   Diabatic heating rate per unit mass

ω = $p^*\dot{\sigma} + \sigma(dp^*/dt)$ (3.1.8)

$$\frac{dp^*}{dt} = \frac{\partial p^*}{\partial t} + m(u\frac{\partial p^*}{\partial x} + v\frac{\partial p^*}{\partial y}) \qquad\qquad (3.1.9)$$

The hydrostatic equation is modified to include cloud and rain water effects and is written,

$$\frac{\partial \phi}{\partial \ln(\sigma + p_t/p^*)} = -RT_v[1 + \frac{q_c + q_r}{1 + q_v}]^{-1} \qquad\qquad (3.1.10)$$

where

q_c =   The mixing ratio of cloud water

q_r =   The mixing ratio of rain water

Equation 3.1.10 is used to compute the geopotential heights from the virtual temperature for a static atmosphere.

3.1.3 Data Interpolation

The Mesoscale Model Version 4 (MM4) was developed for forecasting different mesoscale weather systems. The standard output data do not completely meet the input requirements for the STEM-II model, so data manipulations and interpolations are necessary. Three major steps (Figure 3.4) are required to make the data suitable for input
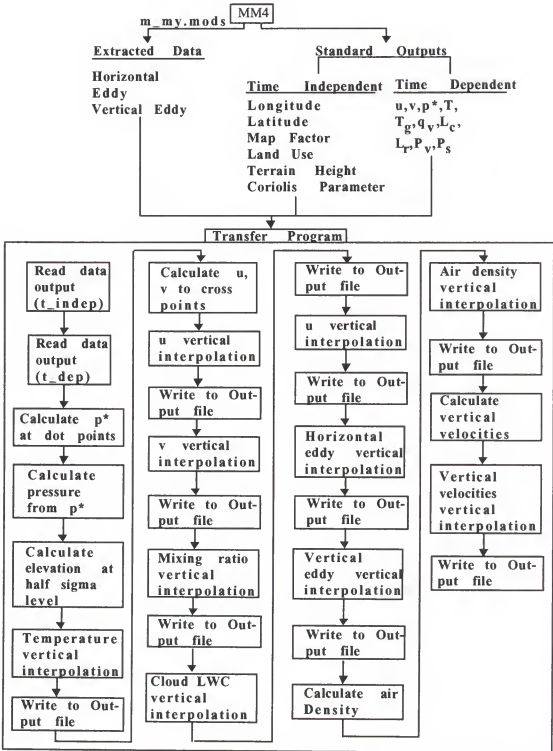
Figure 3.4   Schematic diagram of the flow chart of the transfer program.

to the STEM-II model. The first step is to obtain the required data sets which are not the standard output of the MM4. Second, vertical velocities are calculated on the basis of the MM4 outputs. At the end, the data for each variable are interpolated from a basis of the run of the sigma coordinate system to that of an elevation coordinate system.

The standard output of the MM4 includes horizontal wind speeds in x and y directions, temperatures, mixing ratios, cloud water contents, rain water contents, $P^*(=P_s - P_{top})$, ground temperatures, accumulated convective precipitation, and accumulated stable precipitation. In order to provide sufficient input data for the STEM-II model, horizontal eddy diffusivities, vertical eddy diffusivities, air densities and vertical velocities are required. Both horizontal and vertical eddy diffusivities are calculated in the MM4 source code and extracted by modified codes.

The density of air is calculated on the basis of the ideal gas law,

$$\rho = \frac{\left[(P_s - P_t)\sigma + P_t\right]}{RT} \tag{3.1.11}$$

Vertical velocities (omega) in pressure unit can be calculated from the combination of Equation 3.1.6 and Equation 3.1.8,

$$\omega = -\int_0^\sigma [\frac{\partial p^*}{\partial t} + m^2(\frac{\partial p^* u/m}{\partial x} + \frac{\partial p^* v/m}{\partial y})]d\sigma' + \sigma[\frac{\partial p^*}{\partial t} + m(u\frac{\partial p^*}{\partial x} + v\frac{\partial p^*}{\partial y})] \tag{3.1.12}$$

where

ω = the vertical velocity in pressure unit at each half sigma level (cb/s)

$\dfrac{\partial p^*}{\partial t}$ = the Pressure tendency (refer to Equation 3.1.5)

The first approximation relationship between omega and vertical velocity in elevation unit can be written as,

$$\omega \approx -\rho g w \qquad (3.1.13)$$

where

g = Gravity (m/s^2)

w = Vertical velocity in elevation units (m/s)

Based on the ideal gas law, the vertical velocity (m/s) at each half sigma level is,

$$w \approx -\omega RT/pg \qquad (3.1.14)$$

where the unit of p is center bar(cb).

The data set for each variable is interpolated from the sigma coordinate system to the elevation coordinate system by one of three methods. Before the interpolation, the elevation of a half sigma level at each grid point is calculated by using the hydrostatic equation,

$$Z_k^\sigma = Z_{k-1}^\sigma - \frac{RT}{g}\ln(\frac{p_k^\sigma}{p_{k-1}^\sigma}) \qquad (3.1.15)$$

where

Z_k^σ = Elevation at k level of sigma coordinate system

p_k^σ = Pressure at k level of sigma coordinate system

The first method is an objective analysis which vertically weights values by $(1/L^2)$. L is the distance between the elevation of a half sigma level (Z_k^σ) and a pre-determining elevation,

$$A_j = \frac{\sum(A_i/L_i^2)}{\sum(1/L_i^2)} \qquad (3.1.16)$$

where

A_j = Value of a variable at j elevation

A_i = Value of a variable at i half sigma level

L_i = Distance between j elevation and the elevation of i half sigma level

$(-600m \leq L_i \leq 600m)$

Another method is by linear interpolation. This is used when there is only one data point within the L_i range. This case occurs only at high elevations, so the linear interpolation is more suitable than the log linear interpolation. A power law is used to interpolate the horizontal wind velocity at the first layer (10 m). The power law is expressed as,

$$\frac{u}{u_1} = (\frac{z}{z_1})^p \qquad (3.1.17)$$

where p is a constant value (Sutton, 1953) that is determined by the difference between temperature at 400 ft and at 5 ft (Table 3.1).

3.2 STEM-II Model[3]

STEM-II is an episodic Eulerian acid deposition model which is capable of simulating transport, chemical and removal processes of atmospheric pollutants, and is capable of calculating the distributions of pollutants in the troposphere. A schematical

---

[3] The review of the STEM-II model is based on the STEM-II User's Guide-Documentation for Sulfur Transport Eulerian Model-2.

Table 3.1. The parameter p and the related temperature difference from 5 to 400 ft elevation.

ΔT (°F)	P	ΔT (°F)	P
< -2.25	0.145	2 to 4	0.44
-2.25 to -1.75	0.17	4 to 6	0.53
-1.75 to -0.5	0.25	6 to 8	0.63
-0.5 to 1.0	0.29	8 to 10	0.72
1.0 to 2.0	0.32	10 to 12	0.77

overview of this model is shown in Figure 3.5. The model requires input files of meteorological fields, initial conditions, boundary conditions and pollutant emissions. The central part of STEM-II consists of three basic components: 1) Transport module: describes the dispersion of pollutants in the atmosphere; 2) Chemical module: performs homogeneous, heterogeneous and liquid phase chemical reactions; and 3) Removal module: simulates dry deposition and wet removal processes, including rainout and washout. The outputs (Figure 3.5) of simulations provide spatial and temporal concentration distributions, dry deposition fluxes, advection flux through the boundary layer and concentrations in gas and liquid phases for every chemical species in the model.

3.2.1 Overview

The reaction mechanism of Atkinson et al. (1982) with updated reaction rates (Atkinson, 1990) was used for the gas phase chemical processes (APPENDIX A) in this
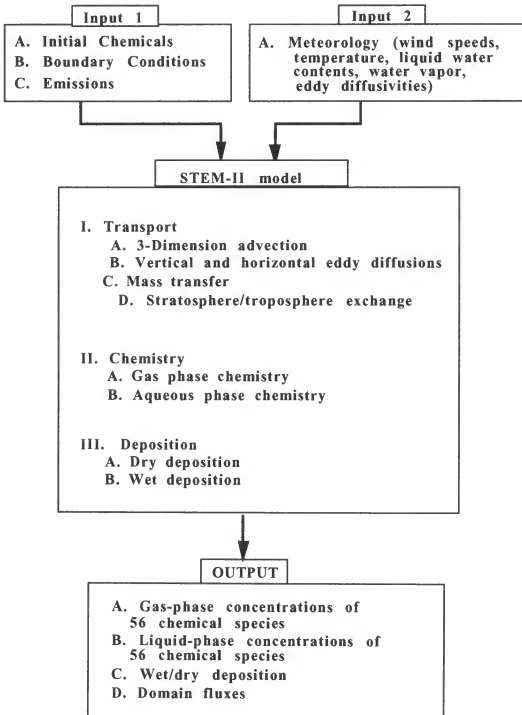
Figure 3.5.   Overview of STEM-II transport and transformation model.

specific version. The chemical species, 23 long-lived (Table 3.2) and 12 intermediate species (Table 3.3), are advected and they have to satisfy the non-linear partial differential equation,

$$\frac{\partial C_i}{\partial t} + \frac{\partial (U_j C_i)}{\partial X_j} = \frac{\partial [K_{jj}(\partial C_i/\partial X_j)]}{\partial X_j} + R_i + E_i + G_i \qquad (3.2.1)$$

$$i = 1,2,...,35$$

where

C_i = Concentrations of chemical species

U_j = Wind velocity components

K_{jj} = Eddy diffusivities

R_i = Rates of chemical reaction

G_i = Rates of mass transfer among phases

E_i = Rates of emissions

Twenty-one species are identified as short-lived species (Table 3.4) and assumed to be at steady state. They can be written as,

$$R_i(C_1, ---, C_{55}) = 0 \qquad i = 35,...,55 \qquad (3.2.2)$$

Based on the work of Chameides and Davis (1982), Chameides (1984), and Jacob (1986), 17 solution equilibria, 39 lumped species, and 16 ionic species are considered in liquid phase chemical processes. The liquid phase species satisfy the equation,

$$\frac{\partial}{\partial t}(S_m C_{im}) + \frac{\partial}{\partial X_j}(U_j - U_{sm})S_m C_{im} = \frac{\partial}{\partial X_j}[K_{jjm}C_{im}\frac{\partial S_m}{\partial X_j}] + R_{im}$$
$$+ G_{im} \qquad (3.2.3)$$

Table 3.2. Transport chemical species for the gas phase chemical processes in this specific STEM-II version.

	Formula	Name
1.	NO	Nitric oxide
2.	NO_2	Nitrogen dioxide
3.	HNO_3	Nitrate
4.	NH_3	Ammonia
5.	SO_2	Sulfur dioxide
6.	H_2SO_4	Sulfate
7.	O_3	Ozone
8.	C_3H_8	Propane
9.	C_nH_{2n+2} (n>3)	Alkane
10.	C_3H_6	Propene
11.	C_4H_8	Butene
12.	C_2H_4	Ethene
13.	C_6H_6	Benzene
14.	C_7H_7OH	Cresol
15.	C_7H_8	Toluene
16.	C_8H_{10}	Xylene
17.	$CH_3COC_2H_5$	Methyl Ethyl Ketone
18.	CH_3COCH_3	Dimethyl Ketone
19.	$CH_3CO_3NO_2$	Peroxyacetylnitrate (PAN)
20.	$C_2H_5CO_3NO_2$	Peroxypropionylnitrate (PPN)
21.	$RCOCH=CR'CO_3NO_2$	EL-NO_2
22.	C_9H_{12}	Propylbenzene
23.	CO	Carbon monoxide

Table 3.3.   Intermediate chemical species for the gas phase chemical processes in this specific STEM-II version.

	Formula	Name
1.	H_2O_2	Hydrogen peroxide
2.	HONO	Nitrous acid
3.	HCHO	Formaldehyde
4.	CH_3CHO	Acetaldehyde
5.	RCHO	(>C$_3$) Aldehyde
6.	ARCHO	Aromatic Aldehyde
7.	CH_3COCHO	Methylglyoxal
8.	CHOHC=CHCHO	Unsaturated dicarbonyl(DIAL)
9.	CHOCHO	Glyoxal
10.	CH_3COOH	Acetic Acid
11	HCOOH	Formic Acid
12	HCl	Hydrogen Chloride

Table 3.4. Radical chemical species for the gas phase chemical processes in this specific STEM-II version.

	Formula	Name
1.	N_2O_5	Dinitrogen Pentoxide
2.	HO_2NO_2	Pernitric Acid
3.	NO_3	Nitrate
4.	OH	Hydroxyl
5.	HO_2	Hydroperoxyl
6.	CH_3O_2	Methylperoxyl
7.	$C_2H_5O_2$	Ethylperoxyl
8.	CH_2O_2	Criegee biradical
9.	PO_2	Propylperoxyl
10.	AO_2	Higher Alkyl peroxyl
11.	ARO_2	Aromatic peroxyl
12.	XO_2	Methyl Ethyl Ketone peroxyl
13.	C_6H_5O	Phenyloxy (Phenoxy)
14.	$C_6H_5O_2$	Phenylperoxy (PhO$_2$)
15.	CH_3CO_3	Acelytperoxy
16.	RCO_3	Acylperoxy
17.	$ARCO_3$	Arylperoxy
18.	$RCOCH=CR'CO_3$	EL
19.	CH_3CHOO	Criegee biradical
20.	$CH_3C_6H_6(OH)O_2$	ADD
21.	$CH_3C_6H_5(OH)_2$	ADD2

$i = 1, 2, ..., 39$ $\qquad$ m = 1 for cloud

$\qquad\qquad\qquad\qquad\qquad\qquad\qquad$ m = 2 for rain

$\qquad\qquad\qquad\qquad\qquad\qquad\qquad$ m = 3 for snow

The initial and boundary conditions for these equations are,

I.C. $\qquad$ At $\quad$ t = 0 $\qquad$ $C_i(X, t=0) = C_i^0(X)$ $\qquad$ (3.2.4)

B.C. $\qquad$ i) $\quad$ For inflow (i.e. $\mathbf{n} \cdot \mathbf{U} < 0$)

$\qquad\qquad\qquad$ $\mathbf{n} \cdot (UC_{i,b} - K\nabla C_i) = F_e$ $\qquad$ (3.2.5)

$\qquad$ ii) $\quad$ For outflow (i.e. $\mathbf{n} \cdot \mathbf{U} \geq 0$)

$\qquad\qquad\qquad$ $-\mathbf{n} \cdot K\nabla C_i = 0$ $\qquad$ (3.2.6)

$\qquad$ iii) $\quad$ At the surface

$\qquad\qquad\qquad$ $\mathbf{n}_h \cdot (UC_i - K\nabla C_i) = Q_i - V_{g}C_i$ $\qquad$ (3.2.7)

where

$\qquad$ $\mathbf{n}$ $\quad$ = $\quad$ Outward unit vector normal to the boundary

$\qquad$ $\mathbf{n}_h$ $\quad$ = $\quad$ Inward unit vector normal to the earth's surface

$\qquad$ $\mathbf{U}$ $\quad$ = $\quad$ Velocity vector

$\qquad$ K $\quad$ = $\quad$ Eddy diffusivity

$\qquad$ Q_i $\quad$ = $\quad$ Surface emission

$\qquad$ V_{gi} $\quad$ = $\quad$ Dry deposition velocity

$\qquad$ F_e $\quad$ = $\quad$ Prescribed flux out of the boundary

$\qquad$ Clouds have strong effects on the solar flux values which control some primary chemical reactions in the atmosphere. The empirical correlation relating photon flux to cloud cover suggested by Kaiser and Hill (1976) is employed and written as,

$$F = F_c(1-0.55C^{1.75})$$
(3.2.8)

where F_c is the photon flux for a clear sky and C is the cloud cover fraction. The constant 0.55 is a proper value for cumulus clouds which are often observed along the coastal lines. The average cloud cover (C) was assumed 0.5.

3.2.2 Transport Algorithm

After reading input files the simulation starts with solving the advection and diffusion parts of the equations (3.2.1) and (3.2.3). These nonlinear equations are solved numerically, and the solutions should satisfy the initial and boundary conditions, described in equations (3.2.4) through (3.2.7). Based on Yanenko's (1971) work, these multi-dimensional equations are divided into time-dependent one-dimensional problems which are solved sequentially (X, Y and Z) by the Finite Element Method for each fractional time step. This procedure is the Locally One-Dimensional-Finite-Element Method. For example, the split equations for the gas phase are given by,

$$\frac{\partial C_i}{\partial t} + L_x C_i = 0$$
$$\frac{\partial C_i}{\partial t} + L_y C_i = 0$$
$$\frac{\partial C_i}{\partial t} + L_z C_i = 0$$
$$\frac{\partial C_i}{\partial t} = R_i + G_i$$
(3.2.9)

where

$$L_x C_i = \frac{\partial}{\partial x}(u C_i) - \frac{\partial}{\partial x}[K_{xx}(\frac{\partial C_i}{\partial x})]$$
$$L_y C_i = \frac{\partial}{\partial y}(v C_i) - \frac{\partial}{\partial y}[K_{yy}(\frac{\partial C_i}{\partial y})]$$

$$L \mathcal{C}_i = \frac{\partial}{\partial z}(wC_i) - \frac{\partial}{\partial z}[K_z(\frac{\partial C_i}{\partial z})]$$

Different time steps are applied for transport of corresponding phases. The transport time step for gas and cloud phases are identical and should be determined by users. Those for rain and snow phases are computed on the basis of the Courant Number, which is a function of the sum of the vertical wind velocity, the falling velocity, the distance of the vertical grid point, and the time step. The one-dimensional transport equations are solved using a Crank-Nicolson Galerkin approximation which assumes every variable is a linear combination of the values of that variable and those for the basic functions. Then, a tri-diagonal matrix can be established and solved by using the Thomas Algorithm.

3.2.3 Chemistry Algorithm

The characteristic times of the three different processes (gas phase reaction, aqueous phase reaction and mass transfer between phases) are spread over a wide range, so different time steps are normally assigned to gas phase and aqueous phase reactions. A modification of the Semi-Implicit Euler Method proposed by Preussner and Brand (1981) is introduced to integrate the chemistry and mass transfer terms and to eliminate the numerical difficulties of time step problems. Equation 3.2.9 can be further split into,

$$\frac{dC_i}{dt} = P_i - D_i C_i \tag{3.2.11}$$

where P_i and D_i represent chemical production and destruction terms, respectively. During the period of a time step, P_i and D_i are also considered as constant and all other concentrations are considered as constant. Analytical integration of equation (3.2.11) over a time step is given by,

$$C_i^{n+1} = \frac{P_i^n}{D_i^n} - \left\{ \frac{P_i^n}{D_i^n} - C_i^n \right\} \exp(-D_i^n \Delta t) \tag{3.2.12}$$

where C_i^n is the concentration of species i at time step n and C_i^{n+1} is the concentration of species i at the following time step. The numerical solution to equation 3.2.12 tends to reach an equilibrium value when D_i is large (Equation 3.2.13 a). A significant error in numerical calculation will arise as D_i becomes small, so the solution is modified as equation 3.2.13 (b). To make the calculation more efficient, equation 3.2.13 (c) is introduced (Odman et al., 1992) as the $\Delta t * D_i^n$ term is in the range from 0.085 to 0.01.

i) If $10 < \Delta t * D_i^n$, $\qquad C_i^{n+1} = \frac{P_i^n}{D_i^n}$ $\qquad\qquad\qquad\qquad$ (3.2.13 a)

ii) If $\Delta t * D_i^n < 0.01$, $\quad C_i^{n+1} = C_i^n (1 - \Delta t * D_i^n) + P_i^n * \Delta t$

$\qquad\qquad\qquad\qquad\qquad\qquad\qquad\qquad\qquad\qquad\qquad\qquad$ (3.2.13 b)

iii) If $0.01 < \Delta t * D_i^n \leq 0.085$

$$C_i^{n+1} = (C_i^n * (2/D_i^n - \Delta t) + 2 * P_i^n * \Delta t / D_i^n)/(2/D_i^n + \Delta t)$$

$\qquad\qquad\qquad\qquad\qquad\qquad\qquad\qquad\qquad\qquad\qquad\qquad$ (3.2.13 c)

iii) If $0.085 \leq \Delta t * D_i^n \leq 10$,

$$C_i^{n+1} = \frac{P_i^n}{D_i^n} + \left\{ C_i^n - \frac{P_i^n}{D_i^n} \right\} \exp(-D_i^n \Delta t) \tag{3.2.13 d}$$

The equation (3.2.13 a) introduces an error of $4.5 \times 10^{-3}\%$ when it is compared to the exponential term $(-D_i^n \Delta t)$ of the original solution (Equation 3.2.13 d). The same magnitude of error $(5.0 \times 10^{-3}\%)$ is also obtained for both equations 3.2.13 b and 3.2.13 c in this scheme.

3.2.4 Data Analyses

      To evaluate the performance of simulations, the predicted concentrations are compared to the observation data. Since only surface measurements are available, the comparisons are performed solely on concentrations at the surface. The predicted values are interpolated to the locations of the observation sites by,

$$C_p^k = \frac{\Sigma \, [C_{ij}/(R_{ij}^k)^2]}{\Sigma \, [1/(R_{ij}^k)^2]}$$

(3.2.14)

where

    C_p^k = Predicted concentration at the site k

    C_{ij} = Predicted concentration at the grid i,j

    R_{ij}^k = Distance between the site k and the grid i,j ($R_{ij}^k \leq R_o$)

The influence radius (R_o) is limited to 45 km for the coarse domain simulations and 15 km for the fine domain simulations.

   Mean error (ME) and root of mean square (RMS) are applied to present the differences between the predicted and observed concentrations. Both ME and RMS are calculated for each site over one simulation period (24 hours), and each hour over total sites (6 sites). The ME can be written as,

$$\text{Mean Error} = \frac{\sum_{1}^{N} C_r}{N}$$

(3.2.15)

where

    C_r = C_o - C_p (Residual concentration)

C_p = Predicted concentrations

C_o = Observed concentrations

N = Total pairs of predicted and observed concentrations

and the RMS is written as,

$$RMS = \sqrt{\frac{\sum_{1}^{N}(C_p)^2}{N}}$$ (3.2.16)

The mean error (ME) can indicate whether the simulations under or over-estimate the concentration at each hour and at each site. The root of mean square (RMS) provides the information that represent the deviations of predicted concentrations from observed ones. The average fractional difference (AFD) weighing predicted and observed concentrations equally (Shim and Carmichael, 1991) is expressed as,

$$AFD = \sqrt{\frac{1}{N}\sum_{1}^{N}(\frac{C_o - C_p}{C_o + C_p})^2}$$ (3.2.17)

It indicates the factor between the predictions and observations.

Systematic bias (SB) and gross error (GE) are two widely used statistic parameters suggested by Tesche (1988). They are defined as,

$$SB = \frac{1}{N}\sum_{1}^{N}\frac{(C_p - C_o)}{C_o}$$ (3.2.18)

$$GE = \frac{1}{N}\sum_{1}^{N}\frac{|C_p - C_o|}{C_o}$$ (3.2.19)

Correlation between predicted and observed concentrations can be calculated by,

$$COR = \frac{\sum_{1}^{N}[(C_p - \overline{C}_p)(C_o - \overline{C}_o)]/N}{\sqrt{[\sum_{1}^{N}(C_p - \overline{C}_p)^2 \sum_{1}^{N}(C_o - \overline{C}_o)^2]/N^2}} \qquad (3.2.20)$$

COR = Correlation between predicted and observed concentrations

$\overline{C}_p$ = Average predicted concentrations

$\overline{C}_o$ = Average observed concentrations

The correlation between predicted and observed concentrations can verify the ability of the model in predicting the variations of observed concentrations. The linear regression analysis shows the mathematical relationship between predictions and observations. The linear regression analysis consists of slope and intercept values which can be calculated by,

$$LSQ = \frac{\sum_{1}^{N}[(C_p - \overline{C}_p)(C_o - \overline{C}_o)]/N}{\sum_{1}^{N}(C_o - \overline{C}_o)^2/N} \qquad (3.2.21)$$

$$INT = \overline{C}_p - LSQ*\overline{C}_o \qquad (3.2.22)$$

where

LSQ = Least square (the slope of the regression)

INT = Intercept of the regression line

The peak prediction accuracy (PPA) is defined as the ratio of the difference between peak predicted concentration and the peak observed concentration, to the peak observed value,

$$PPA = \frac{C_p^p - C_o^p}{C_o^p} \qquad (3.2.23)$$

where

C_p^p = Predicted peak concentration

C_o^p = Observed peak concentration

A peak time difference (Δt^k) is defined as,

$$\Delta t^k = T_o^k - T_p^k \qquad (3.2.24)$$

where

T_o^k = Time when observing maximum concentration at site k

T_p^k = Time when predicting maximum concentration at site k

It shows the capability of the model to predict the occurrence of a peak concentration.

CHAPTER 4
MODEL SIMULATIONS

4.1 Simulation Domains

Numerical simulations of meteorological data during the episodic period begin with the generation of grid latitude-longitude, terrain elevation and land use categories. Expanded, coarse and nested domains (Figure 4.1 (a)) were selected, because there were insufficient observations in Florida and over the Gulf and Atlantic Ocean. An expanded domain and a coarse domain have the same grid size, which is 30 km. A nested domain has a grid size of 10 km, which is the smallest grid size suggested by the NCAR consultant. The expanded domain covers 2.05 million km^2 more area than the coarse domain in order to obtain additional data for better simulations, but the simulations were only performed on coarse and nested domains. In order to achieve better simulation results and flexibility of data usage, both coarse and nested domains are larger than the domains that were used in the pollutant transport and transformation simulations. The coarse and nested grid sizes for transport and transformation simulations were the same as those used in meteorological simulations.

It is very important to cover return flows of a sea-land circulation within the simulation domains of the pollutant transport and transformation model STEM-II. A coarse domain simulation is used first in order to provide boundary information for the simulations in the Tampa Bay area. Back trajectory analysis is required to determine the coarse domains. Back trajectory analysis is also used to locate the air masses that might contribute to the ozone exceedance in the Tampa Bay area during the episode.
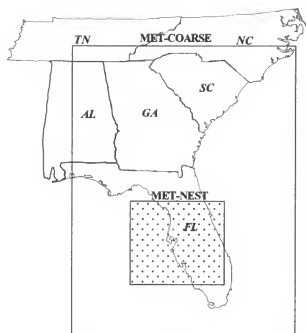
(a)

(b)

Figure 4.1. Coarse and nested domains of (a) meteorological
simulations and (b) transport and transformation
simulations.

Back trajectory calculations were started at four grid points in the Tampa Bay area. The first group of back trajectories began at 14:00 hr on July 24, 1987, when the highest O_3 concentration occurred in the Tampa Bay area, and ended at 01:00 hr on 07/22/87. The second group of back trajectories began at 17:00 hr on July 23, 1987, when the highest concentration occurred in Tampa bay area, and ended at 01:00 hr on 07/22/87. Air masses were released at 1010 mb pressure surface, and the trajectories were calculated every 10 minutes with predicted wind fields. On the basis of these back trajectory analyses, the coarse domain (Figure 4.1 (b)) for the STEM-II model simulations was chosen. The coarse domain not only covers the return flows, but also contains air masses that could contribute to the ozone episode in the Tampa Bay area. The results of back trajectory analyses will also be discussed later in the chapter.

Florida has relative flat topography. The terrain heights (Figure 4.2) within the domain are less than 50 m. The Gulf of Mexico is a shallow water surface which is located to the west of the Florida peninsula. The Atlantic Ocean is a relatively deep water area which is situated on the east coast of Florida. Land elevations along both coasts are close to sea level. Since the coast line in the Tampa bay area is relatively irregular, two-dimensional simulations are not suitable.

4.2 Meteorological Simulations

The meteorological conditions existing from July 20-24, 1987 were simulated by the MM4 model. In order to minimize numerical errors, each simulation was limited to 53 hours, which can cover two days at a time. The time steps for meteorological simulations depend on the grid size that is used in the simulations. The appropriate time step can be determined by,

$$\Delta t = 1.5 \Delta X \qquad (4.1)$$
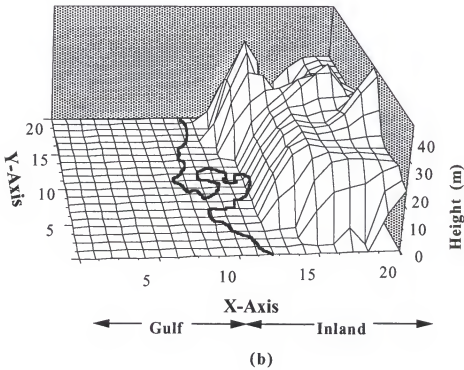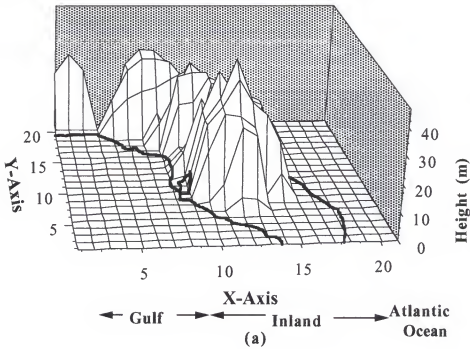
Figure 4.2. Topographic heights of (a) coarse domain and (b) nested domain for STEM-II simulations. The thick solid lines represent the coast line.

where

Δt = Time step (second)

ΔX = Grid size (kilometer)

A time step of forty-five seconds was used in the coarse simulations and a fifteen-second time step was used in the nested simulations.

The expanded domain covers a maximum of 156 twelve-hour surface meteorological stations. Two observations (07:00 hr and 19:00 hr EST) were recorded each day. Also, a maximum of 83 three-hour and a maximum of 117 six-hour surface analyses were included. Nineteen upper air stations are available in the expanded domain.

In the initial step (DATAGRID) of the MM4 simulation system, winds, temperatures, geopotential heights, moisture, and heights at 12 mandatory pressure levels (1000, 850, 750, 500, 400, 300, 250, 200, 150, 100, 70 and 50 mb), and also sea level pressure, and surface temperatures from National Meteorological Center (NMC) forecasting data set were interpolated to each grid in the expanded domain. A U.S. Navy data set was selected to provide sea surface temperatures at each grid point over water surface. This expanded domain data set was interpolated successively to additional pressure levels (950, 900, 800, 750 and 650 mb) which are assigned to improve resolution in the lower atmosphere.

An objective analysis scheme is performed with the observation data, which were qualitatively checked (Gill, 1992) through the following processors: 1) buddy check: comparison of groups of observations with neighbors, and 2) criterial difference check: comparison of observational data to the first generated data set. As a result, the first guess data were generated with adequate quality controls. The criterial differences between the first generated data at the locations of observations and the observations are assigned as 10 m/s, 13°C and 6 mb for wind speed, temperature and sea level pressures,

respectively. The acceptable criteria are relatively large, because of the intention to obtain as many observational data as possible. The first guess data set was interpolated from pressure elevations to σ coordinates, thus, the initial and boundary conditions for the meteorological simulations were created.

The results of the simulations were compared with objective analyses from observational data for wind speed(m/s), mixing ratio (g/Kg), temperature ($^\circ$C) and surface pressure (mb). The results of comparisons (Figure 4.3) were represented by the root of mean square differences and the mean error. The wind speed showed the greatest discrepancy between the simulations and the objective analyses. Goodin et. al. (1980) suggested that objective analyses generally underestimate the true wind speed, and the discrepancy may be up to 2.8 m/s. Smaller differences between observations and simulations would be obtained, if they were corrected for such underestimation. The model overestimated the wind speeds, the mixing ratios and the temperatures, but it underestimated the surface pressures.

Lack of sufficient observational data on large water surfaces could lead to great discrepancies between the simulations and the objective analyses. Florida is surrounded by the Atlantic Ocean and the Gulf of Mexico, and the number of observations on those water surfaces are significantly less than observations over land. Larger discrepancies were expected when the simulation domain covered a large portion of water surface.

The objective analyses themselves are interpolated from observation data, so the accuracy of the analyses over large water areas would be questionable. Therefore, using the objective analyses to judge the simulations is controversial for this case.

4.3 Emission Inventory

Preparing a comprehensive emission inventory is a tremendous amount of work that may take one to two years for several persons to prepare. It involves obtaining various data resources, running specific emission models and geographic arrangements.
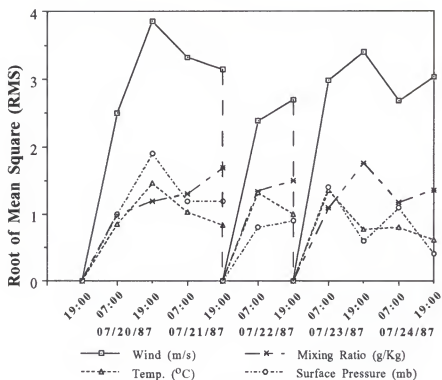
(a)
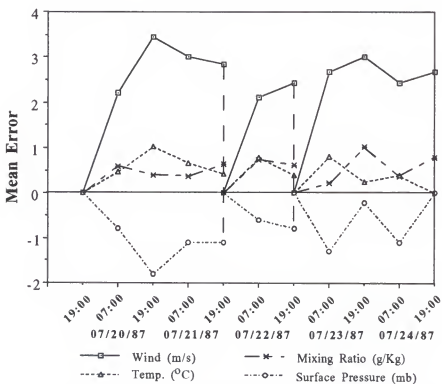
(b)

Figure 4.3. (a) Roots of mean squares, and (b) mean errors of wind speed,
mixing ratio, temperature and surface pressure as compared to
objective analyses.

In this research, simplified and reasonable processes were used to produce good emission data for the model inputs from existing inventories.

Emission sources were roughly classified into mobile, point and area sources in the model. The point sources are industrial emission sites, and the area sources include biogenic, industrial and residential sources. Although the emission sources can be classified into much more detailed categories, such an effort is beyond the scope of this project. This section describes the procedures for preparing mobile, area and point sources for the model inputs.

4.3.1 Emission Inventory for Mobile Sources

Emissions from mobile sources are the primary sources of air pollution in Florida, because tourism is the largest industry in the state. The Environmental Protection Agency (EPA) has required state agencies to report the total emissions of mobile sources in non-attainment counties and their neighboring counties within the state. The post-1987 total emission inventory of mobile sources for eleven counties in the state of Florida were reported by Florida Department of Environmental Regulation. They were Broward, Clay, Dade, Duval, Hernando, Hillsborough, Nassau, Pasco, Palm Beach, Pinellas, and St. Johns counties. Emission inventories were calculated from the EPA MOBILE4 model. Based on these reported values, the emissions from mobile sources for the rest of the counties and cities in the state are estimated.

Mobile sources are roughly classified into highway vehicles and non-highway vehicles. The highway vehicles include classifications such as: LDGV, LDDV, LDGT1, LDGT2, LDDT, HDGV, HDDV, and MC. Non-highway vehicles include train, aircraft, marine vessels and others. The emissions from highway vehicles is the primary source of mobile source emissions in the state. Emissions from highway vehicles are in the range from 66% to 93% of the total VOC mobile emissions (88% average), 68% to 85% of the

total mobile NO_X emissions (78% average), and 53% to 94% of the total mobile CO emissions (87% average).

Emissions from highway vehicles are strongly correlated (Figure 4.4) with the populations of counties. The population of each county and its major cities in 1987 are available from the Florida Statistical Abstract 1988. The population was estimated from the census counts in 1980. Figure 4.4 shows the regressions between emissions of VOC, NOx and CO, and population density. On the basis of the regressions, the emissions of highway mobile vehicles per person in other counties can be estimated. On the basis of the population of each city, the city emission rates can also be estimated. The population outside of the cities and in a county are assumed to be evenly distributed within the county. Therefore, the mobile emission in each grid point can be calculated by:

$$EM_m = \frac{(CO_m*(GR-\sum_1^n(CI_{an}))+\sum_1^n(CI_{an}*CI_{mn}))}{GR} \quad (4.2)$$

where

EM_m = Source strength within a grid for specie m.

CO_m = Source strength of the specie m for unincorporated population in the county within the grid.

GR = The grid area.

CI_{an} = Area of the city n in the grid.

CI_{mn} = Source strength of the pollutant m for the city n in the grid.

Railroad emissions for county areas calculated on the basis of lengths of railroad. The correlations (Figure 4.5) between the lengths of railroads and emission rates of reported counties are relatively low, but it is the proper way to estimate the railroad
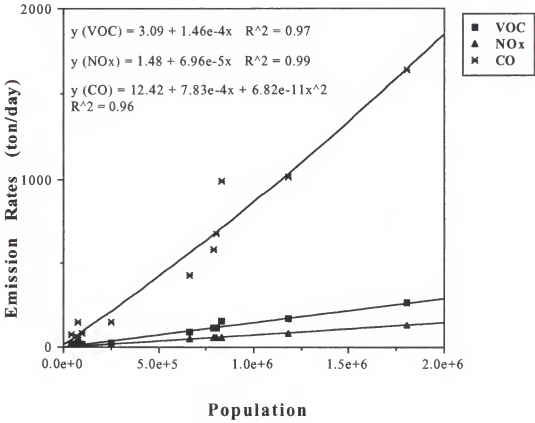
Figure 4.4. Regressions and variability for highway vehicle emission rates of volatile organic compounds, nitrogen oxides and carbon monoxide with population density in Florida counties.
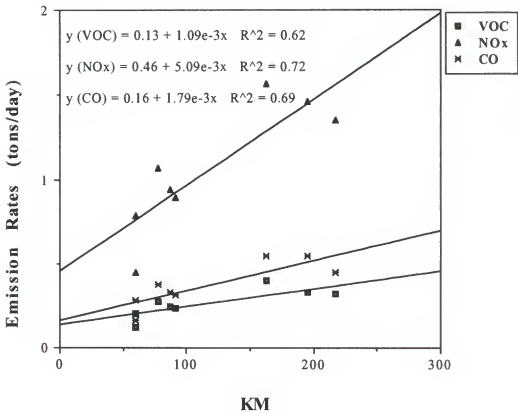
Figure 4.5. Regressions and variability for railroad emission rates of volatile organic compounds, nitrogen oxide and carbon monoxide with length of railroad in Florida counties.

emission rates. The length of the railroads within each grid cell were estimated, and the emission rates in every grid were calculated on the basis of the regression analysis.

The calculation of regressions (Figure 4.6) for aircraft emission rates is based on the number of aircraft operations at each airport. The emission rates were added to the grids where the corresponding airports are located. The other and marine vessel mobile sources (Figures 4.7 and 4.8) are treated in the same way as highway mobile sources.

The fingerprints listed in Table 4.1 are used to categorize the NO_x and VOCs into single or grouped species as adapted for the chemical mechanisms in the model. The VOCs fingerprints are interpolated from a study (Lonneman et al., 1986) of the Lincoln Tunnel mobile vehicle emissions in New York. The sum of the VOCs fractions (Table 4.1) are not equal to one, because some of the VOCs were unknown species.

4.3.2 Point Sources and Area Sources

A point source emissions inventory provided by the Florida Department of Environmental Protection (DEP) was used for the simulations. The facility emission report provides latitude and longitude, and emission rates of pollutants (tons/year) for large emission facilities in 1987. The master report has detailed information, including stack and gas properties, for each emission source in each facility.

On the basis of latitude and longitude of the facilities, each reported facility is assigned to a corresponding grid point. The effective stack height for each elevated point source in a facility is estimated by the Holland formula,

$$H = h + \frac{V_s D_s}{U_t}[1.5 + 2.68\text{E-}03{*}P_t{*}D_s(\frac{T_s - T_t}{T_s})] \qquad (4.3)$$

where

$\qquad$ h $\quad$ = $\quad$ Height of the stack

$\qquad$ V_s = $\quad$ Exhaust velocity of plume
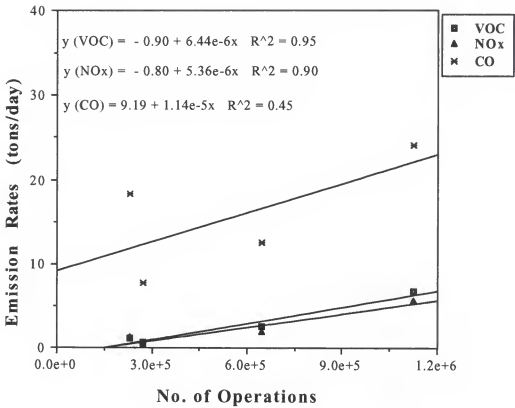
Figure 4.6. Regressions and variability for aircraft emission rates of volatile organic compounds, nitrogen oxides and carbon monoxide with number of aircraft operations in Florida counties.
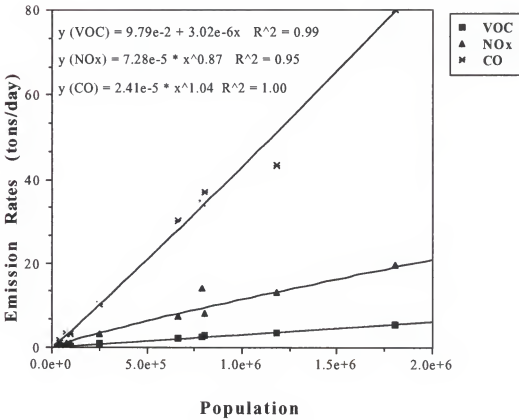
Figure 4.7. Regressions and variability for other mobile emission rates of volatile organic compounds, nitrogen oxides and carbon monoxide with population density in Florida counties.
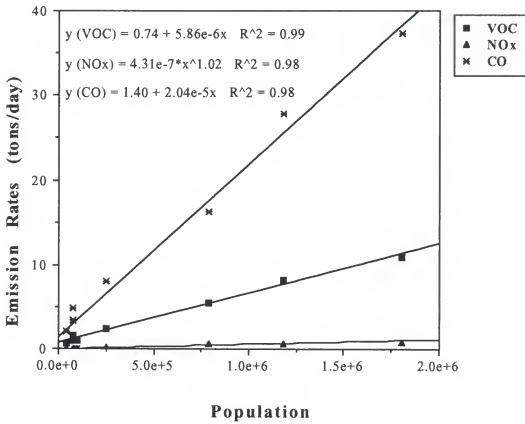
Figure 4.8.   Regressions and variability for marine vessels emission rates of
volatile organic compounds, nitrogen oxides and carbon monoxide
with population density in Florida counties.

Table 4.1.   Fingerprints of NO_x and VOCs for (I) mobile, and (II) point and area source emissions.

Group	Species	Weight Ratio I	Weight Ratio II
NO_x	NO	0.907	0.965
	NO_2	0.093	0.035
VOCs	Propane		0.006
	Alkane	0.198	0.862
	Propene	0.036	0.006
	Butene	0.067	0.022
	Ethene	0.129	0.015
	Benzene	0.061	0.003
	Cresol		0.002
	Toluene	0.114	0.015
	Xylene	0.065	0.010
	MEK		0.016
	CH_3OCH_3		0.016
	HCHO	0.037	0.022
	CH_3CHO	0.005	0.0002
	ARCHO		0.0004
	CH_3COOH	0.004	0.004

D_s = Stack diameter

U_s = Average wind speed at time t

P_t = Average pressure at time t

T_s = Stack effluent temperature

T_t = Average temperature at time t

The average wind speeds and temperatures over a whole domain at each hour were used to estimate the hourly effective stack height for each stack. The minimum effective stack height over a day was used as a basis to allocate the emissions to the corresponding elevated grid.

The NAPAP area source emission inventory (1987 baseline) was used to allocate area source emissions. The NAPAP area source database includes VOC, NO_x, CO and SO_2 emission rates (tons/year), and VOC overall control efficiency for each source on a county basis. The mobile vehicle, railroad, aircraft and marine vessel emissions in the NAPAP area emission inventory were removed, because they were calculated independently. On the basis of EPA recommendation, one of the methods to allocate county-level area sources to sub-county regions involve the use of spatial surrogate indicators. The detailed land use distribution data required to use the surrogating method could not be accessed, so a simplified method was used to manipulate the area source data.

On the basis of NAPAP area source categories[4] and the EPA[5] spatial allocation factor surrogates for area source categories, the area sources can be roughly classified into two groups. Categories such as forest wildfires, structural fires, agricultural field burning and other managed burning sources were ignored. One group utilized the

---

[4] Regional Interim Emission Inventories (1987-1991), Volume I: Development Methodologies. EPA-454/R-93-021a.
[5] Procedures for the Preparation of Emission Inventories for Carbon Monoxide and Precursors of Ozone, Volume II: Emission Inventory Requirements for Photochemical Air Quality Simulation Models. EPA-450/4-91-014.

population as a surrogate indicator, and the other employed urban land use as the surrogate indicator. The area source emissions were calculated with Equation 4.3, if the population is the surrogate indicator. The area source emissions were calculated by,

$$EM_m = \frac{\sum_1^n (CI_{an} * CI_{mn})}{GR} \qquad (4.4)$$

if urban land use is the surrogate indicator.

The total emissions of anthropogenic VOCs, NO_2 and NO for the coarse and fine grid systems being used in the simulations are shown in Figure 4.9 and Figure 4.10. Two large power plant facilities contributed a large amount of NO_x to the Tampa Bay area.

4.3.3 Biogenic Sources

Preparation of the biogenic source emission inventory was based on the work of Zimmerman (1978). He measured emissions of VOCs for 32 different land-use categories in the Tampa Bay area in the 1970s. Since detailed land-use data are not readily accessible, only land use data obtained from the NCAR data set were used. The latter data set contained 13 land-use indices only, therefore, similar types of land-use categories from Zimmerman's measurements were grouped according to the NCAR land use indices.

Since there were no chemical mechanisms involving isoprene in the version of STEM-II model used, isoprene emissions were allocated to propene with a multiplier factor of 3. Total emissions of biogenic VOCs (Figure 4.11) in the Tampa Bay area were estimated to be about 1.6E+6 moles/day. Anthropogenic emissions of VOCs were estimated to be about 2.9E+6 moles/day. Thus, the estimated biogenic sources accounted for about 36% of the total VOCs emissions in the Tampa Bay area. On the basis of the Hillsborough County annual 1990 report of baseline emissions inventory, biogenic emissions were estimated to be about 34% in Hillsborough County. The overall estimate
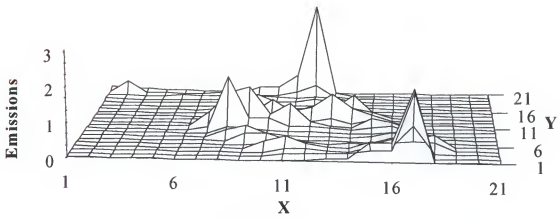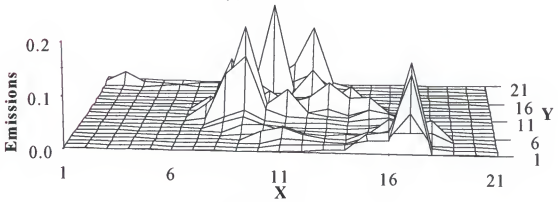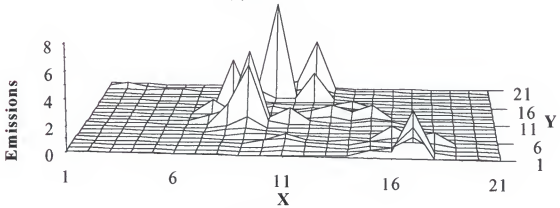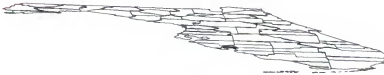
Figure 4.9. Anthropogenic emissions inventory over the coarse domain. (Unit: x10^{-6} moles/day)
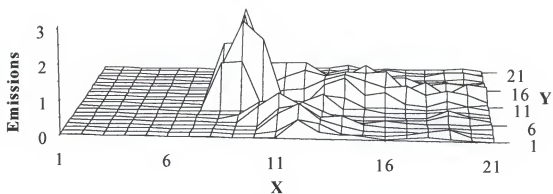
(a) VOC
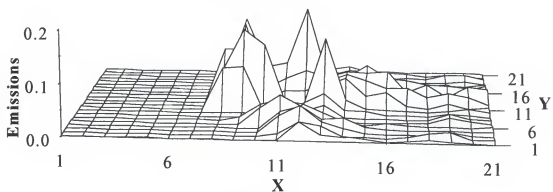
(b) NO2
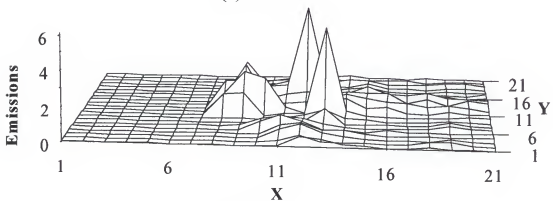
(c) NO

Figure 4.10. Anthropogenic emissions inventory over the fine domain. (Unit: x10^{-5} moles/day)
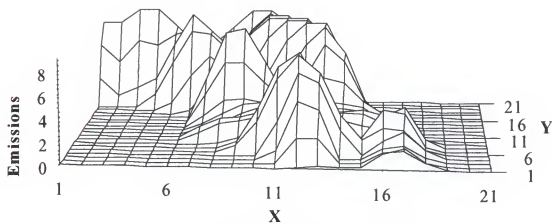
(a) Coarse
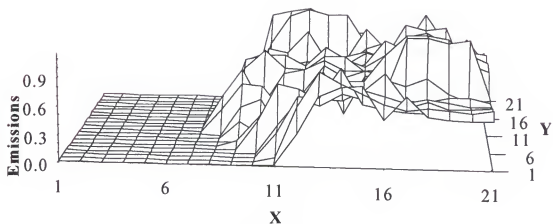
(b) Fine

Figure 4.11. Biogenic emissions inventory over the coarse and fine domains. (Unit: $\times 10^{-5}$ moles/day)

of biogenic emissions, therefore, seems reasonable and agrees with that proposed by Hillsborough County.

<center>4.4 STEM-II Simulations</center>

The STEM-II model requires 1) meteorological data: air densities, temperatures, relative humidities, U, V and W wind fields, horizontal eddies, vertical eddies, and cloud liquid water contents; 2) air quality data: initial concentrations, boundary conditions, point, area, and biogenic source emissions: 3) topography data: latitude and longitude, and terrain heights; and 4) dry deposition data. A total of seventeen to eighteen data files were used for a single-day simulation. Total input files for the simulations in this research account for about 430 megabytes of memory, just for the base case (1987) study.

4.4.1 Initial, Boundary, and Dry Depositions

Three sides of the coarse domain boundaries are over water, including the Atlantic Ocean and the Gulf of Mexico. No air quality observation data were available over these water bodies. In order to determine the proper boundary conditions for the coarse domain simulations, two sets of boundary conditions (Table 4.2) were tested. The BOUND I set (Hong and Carmichael, 1986) represents moderately polluted conditions, and the BOUND II set (Brost et al., 1989) characterizes relatively clean marine environments. Two sets of dry deposition data were also evaluated. The first set of dry deposition data (DRY I) contains identical dry deposition velocities for each chemical specie over water and land surfaces. The other set (DRY II) has different dry deposition velocities over the two types of surfaces. Dry deposition velocities in both data sets vary diurnally, and the diurnal variation was assumed to be identical for every specie. The dry deposition velocities over water surface were also assumed to be one fifth of those over land surface.

Four case studies (Table 4.3) were designed to aid in the determination of the proper data sets for simulations. The BOUND I set was used as the initial conditions for

Table 4.2.   The initial and boundary conditions from the surface to the top of the domain used in the simulations.

SPECIE	BOUND I (ppb)	BOUND II (ppb)
NO	7.5E+00 ~ 1.3E-04	2.0E-03 ~ 6.0E-03
NO_2	2.5E+00 ~ 4.2E-05	6.0E-03 ~ 1.8E-02
HNO_3	1.0E+00 ~ 1.0E+00	3.0E-02 ~ 6.0E-02
NH_3	5.0E+00 ~ 8.4E-05	5.0E-01 ~ 2.7E-01
SO_2	6.0E+00 ~ 1.0E-04	1.0E-02 ~ 1.0E-02
H_2SO_4	2.0E+00 ~ 2.0E+00	0.0E+00 ~ 0.0E+00
O_3	3.0E+01 ~ 3.0E+01	2.0E+01 ~ 3.1E+01
C_3H_8	1.7E+01 ~ 2.9E-04	1.0E+01 ~ 1.0E+01
$C_nH_{2n+2}(n>3)$	2.3E+01 ~ 3.8E-04	5.0E-01 ~ 5.0E-01
C_3H_6	7.0E-01 ~ 1.2E-05	1.0E-01 ~ 3.7E-02
C_4H_8	3.0E-01 ~ 5.1E-06	1.0E-01 ~ 3.7E-02
C_2H_4	2.1E+00 ~ 3.5E-05	2.0E-01 ~ 7.4E-02
C_6H_6	5.0E-01 ~ 8.4E-06	3.0E-02 ~ 1.1E-02
C_7H_8	5.0E-01 ~ 8.4E-06	3.0E-02 ~ 1.1E-02
C_8H_{10}	2.5E-01 ~ 4.2E-06	3.0E-02 ~ 1.1E-02
CO	2.8E+02 ~ 2.8E+02	1.2E+02 ~ 1.2E+02
H_2O_2	1.0E+00 ~ 1.0E+00	2.0E+00 ~ 1.5E+00
HONO	5.0E-01 ~ 5.0E-01	1.0E-02 ~ 3.7E-03
HCHO	2.0E+00 ~ 3.0E-04	2.0E-02 ~ 2.0E-02
CH_3CHO, RCHO, ARCHO	3.3E-01 ~ 5.0E-05	1.0E-02 ~ 1.0E-02
HCl	5.0E-01 ~ 5.0E-01	0.0E+00 ~ 0.0E+00

Table 4.3. Boundary conditions and dry deposition data test.

CASE	BOUND I	BOUND II	DRY I	DRY II
I*	√			√
II		√	√	
III	√		√	
IV†	√			√

* The concentrations of chemical species at the boundary were used as new boundary conditons after the first hour simulations.
† The boundary conditions are constant throughout the simulations.

all cases. Chemical species are assumed to be stablized after two days of simulation (July 20, and July 21, 1987). The results on July 22, 1987 for the designed cases were evaluated by peak performances and correlations coefficients. Figure 4.12(a) shows that a better peak prediction was achieved for Case I. If the values for dry deposition velocities over land were used, the average ozone peak could be 25 ppb lower than for Case I. Correlation coefficients between predicted and observed ozone concentrations are shown in Figure 4.12(b). The correlation coefficients for Case I were higher than those for the other cases at sites in Hillsborough County. The correlation coefficients for Case I were similar to those for Case II on the average in Pinellas County, but the Case II simulation shows a very low peak O_3 value. As a result, Case I appears to be the best choice for this study.

4.4.2 Simulations

The STEM-II model simulations were limited by available CPU time and accessible memory on the IBM ES9000 mainframe computer at the Northeast Regional Data Center (NERDC). Source codes were modified to adapt the vectorization structure of the mainframe computer, in order to improve the efficient use of CPU time. The
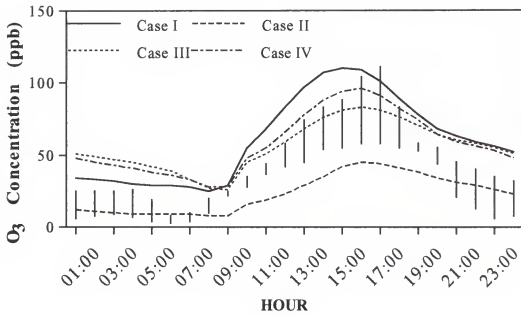
(a)
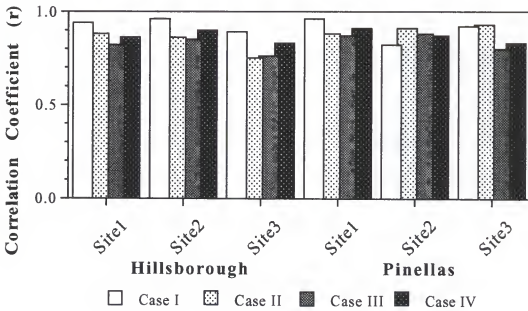
(b)

Figure 4.12. Comparisons of four simulation cases for the coarse domain on
July 22, 1987, (a) observed ozone range vs. predicted average, and (b)
correlation coefficients at observation sites in the Tampa Bay area.

vectorization is more effective for repeating calculation loops. The chemical mechanisms scheme can not be vectored, since the calculation routine for each species' concentration depends on the concentration of the previous time step. The chemical scheme utilizes a major portion of CPU time, therefore, the model could not take advantage of vectorization efficiently.

Carbon monoxide can be an essential pollutant that contributes to the generation of ozone in urban areas, since large amount of CO are emitted from mobile sources. The emissions of CO, and the variations of CO concentrations were not considered in the original STEM-II model codes. The model has been modified to include the contributions of CO emissions in the reactions. The only CO destruction term in the chemical mechanisms included in the model is the reaction with OH.

All the meteorological data were read on an hourly basis during the simulations. The emissions data were read at the beginning of a simulation, and then, were calculated to create diurnal variations on the basis of hourly contribution factors. The boundary conditions for the fine domain were interpolated while the simulations were performed over the coarse domain. Due to the limitations of accessible computer permanent storage memory, boundary conditions were only available every two hours for the fine domain study. Therefore, the boundary conditions were read every two hours, but they did not remain constant within the two-hour period. In order to take the emissions at the boundary into account, calculated concentrations in the fine domain case were used as boundary conditions at each transport step within every two hour period. The concentrations at the end of the 24 hour coarse grid simulation were interpolated to the fine grid, and then were used as initial conditions for the fine grid simulations.

The emissions inventory for each source was read and calculated for diurnal variations. The area, mobile, and biogenic sources (unit: molecules/cm^2) were divided by 100 which is the conversion factor from centimeters to meters, so that the units can be matched with those of point sources (unit: molecules/cm^3) in numerical calculations.

This factor had been overlooked when the program code was modified, therefore, a great deal of time was spent in locating this mistake.

Grid sizes used in the meteorological data simulations were also used in the STEM-II model simulations. The vertical extension of the coarse domain was from the surface to an elevation of 3000 meters which included the estimated maximum mixing heights during the ozone episodes. The elevation at the top of the fine domain was 2000 meter. Time steps for the coarse and fine domain simulations were 15 and 10 minutes, respectively. Time steps for the gas phase chemical reactions (Figure 4.13) were decided by the diurnal variation of radiation. A 12 second time step was used during sunset and dawn. The 30 and 60 second time steps were used for day time and at night, respectively.

Effects of existing cloud were assumed to influence the intensity of solar radiation. Liquid-phase and multi-phase chemical reactions and physical processes were ignored. The suggested time step for liquid phase reactions is 5 second, therefore, these calculations could consume a great deal of CPU time. If the liquid water content (LWC) at a grid point was greater than 10^{-4} kg/m^3 that is LWC of non-precipitating maritime cumulus over Gulf of Mexico near Houston suggested by Ryan et al. (1972), then the cloud would have an effect on solar radiation.

The concentrations of ozone from the output of the STEM-II model simulations are calculated as hourly averages. The results are discussed in the following chapter.
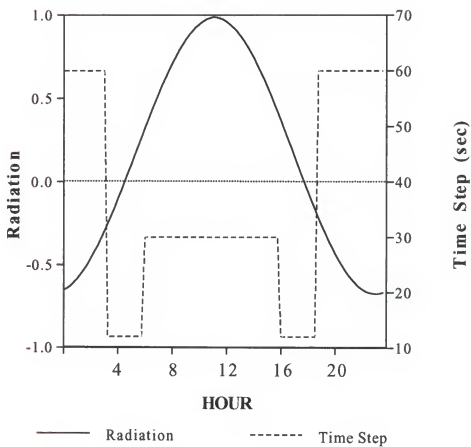
Figure 4.13. Diurnal variation of solar radiation and time steps for the gas phase chemical reactions.

CHAPTER 5
RESULTS AND DISCUSSION

In this chapter the results, in terms of the proposed objectives, are described and discussed. At the beginning of the chapter, predicted ozone concentrations are compared with observations at the sites during the ozone episode in the Tampa Bay area. Surface flow fields, X-Z vertical flow fields, and ozone isopleths from model simulations are described for the Tampa Bay area. The capabilities of the model to simulate the ozone episode are evaluated by methods described in Chapter 3.

Results of trajectory analyses for the episode are discussed. Forecasting of ozone changes for the year 2000 are described for the same meteorological conditions existing on episodic days in 1987. A secondary spring ozone episode was selected and evaluated to verify the capabilities of the model in predicting ozone episodes associated with the approach of a cold front system. Finally, current control strategies are evaluated on the basis of ambient VOCs/NO_x ratios, and necessary reductions in VOCs and/or NO_x emissions are proposed.

5.1 Evaluation of Simulated Ozone Distributions on July 22, 1987

In the early morning (03:00 hr) of July 22, 1987, a prevailing easterly air flow was predicted within the domain. Predicted ozone concentrations were below 30 ppb in the Tampa Bay area. Generally, ozone concentrations over the Gulf surface waters (Figure 5.1 (a)) were projected to be higher than those inland, because there were no NO sources in the Gulf to titrate out the ozone. Since more ozone was removed by stronger NO emissions in the Tampa Bay area and the land-based air mass was transported by easterly winds, ozone concentrations to the west of Tampa Bay over the Gulf were lower than
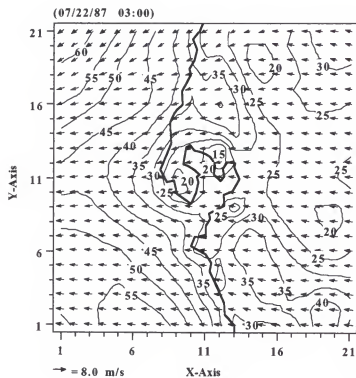
(a)
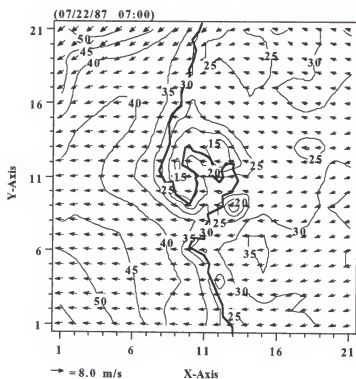
(b)

Figure 5.1. Surface flow fields and isopleths of ozone concentrations at (a) 03:00 hr, and (b) 07:00 hr, on July 22, 1987.

those in either the northwest or southwest domain regions. Ozone concentrations were higher at higher elevations (Figure 5.2 (a)) over the land surface, but were nearly constant from the surface to about 200 meters elevation over the water surface. Ozone concentrations were less than 19 ppb at 10 km inland.

At 07:00 hr, the easterly wind still predominated over the entire domain. The predicted wind directions were consistent with meteorological observations. Ozone concentrations around the Tampa Bay area (Figure 5.1 (b)) fell to less than 20 ppb, due to strong NO_x emissions from early morning high density traffic. Vertical motion had not been initiated over the land surface, therefore, the vertical X-Z ozone distributions (Figure 5.2 (b)) were similar to those at 03:00 hr. Since the intensity of pollutant emissions increased over the St. Petersburg area, the horizontal ozone concentration gradient became stronger at the Gulf coast.

The wind changed from the east to the northeast over the land surface at 11:00 hr. The increase in ozone concentrations within the Tampa Bay area (Figure 5.3 (a)) was less than that in the surrounding area. The pollutant-rich air mass contributed by morning traffic was transported into the Gulf, hence, the ozone concentrations increased faster over the water surface off the west coast of Tampa Bay. Strong NO_x emissions from the two utilities plants kept the ozone concentrations low (< 40 ppb) in the surrounding area around the bay in Hillsborough County. Vertical mixing became stronger over the land surface, so that, the distributions of ozone concentrations (Figure 5.4 (a)) was more evenly distributed below an elevation of 250 m. Stronger horizontal ozone gradients could be observed for the interfaces between land and water.

At 15:00 hr, sea breezes were predicted along the Gulf coast. The land surface was still dominated by northeast winds (Figure 5.3 (b)), but north to northwest winds prevailed close to the Gulf coast over the water surface. A maximum concentration (160 ppb) of ozone was predicted to the south of Tampa bay over the water surface. Generally, the primary area of interest around Tampa Bay in Hillsborough County lay

(07/22/87 03:00)

(07/22/87 07:00)

Figure 5.2. X-Z cross section flow fields and isopleths of ozone concentrations at (a) 03:00 hr, and (b) 07:00 hr, on July 22, 1987.

Figure 5.3. Surface flow fields and isopleths of ozone concentrations at (a) 11:00 hr, and (b) 15:00 hr, on July 22, 1987.

Figure 5.4. X-Z cross section flow fields and isopleths of ozone concentrations at (a) 11:00 hr, and (b) 15:00 hr, on July 22, 1987.

between the ozone isopleths for 60 and 100 ppb O_3. Stronger uplifting flows (Figure 5.4 (b)) at the sea breeze front carried the polluted air to higher elevations and created a maximum ozone (> 140 ppb) concentration at an elevation of 900 m, just behind the front on the water side.

The increase in NO_x emissions during the afternoon heavy traffic hours titrated out the ozone rapidly in the Tampa Bay area at 19:00 hr. Ozone concentrations decreased down to less than 70 ppb (Figure 5.5 (a)) in that area. Easterly winds still dominated most of the land surface, and matched the meteorological observations very well. A peak ozone center (>200 ppb) was transported from the northwest boundary over the Gulf water surface. Figure 5.6 (a) indicates that the uplifting flow at the sea breeze front was still strong. The peak ozone center located at 900 m elevation at 15:00 hr was split into two peaks. One part was transported to the west and the other part moved to a higher elevation. The down flow at the rear end of the sea breeze front maintained higher ozone concentrations just behind the sea breeze front, while the ozone levels decreased to less than 30 ppb on the other side of the front over Pinellas County.

At 23:00 hr, the land breeze was established over almost the entire domain (Figure 5.5 (b)), and the convergent zone over the Gulf coast vanished. A high ozone center (> 90 ppb) which was transported from the northern boundary approached the Tampa Bay area, and O_3 levels decreased slowly due to low night time emissions of NO_x. Weaker uplifting flows were extended up to 1800 m elevation (Figure 5.6 (b)). A positive gradient in vertical ozone levels was predicted over the land surface, and was similar to that predicted in the early morning.

Figure 5.7 shows predicted and observed ozone concentrations at each of the monitoring sites. The observation data at site 1 were questionable, because the recorded ozone concentrations remained constant for 9 hours. The model predicted that the peak O_3 concentrations would occur about 0 to 3 hours earlier than those observed. Half of the monitoring sites had peak prediction accuracies (PPAs) of 0.0%, -10.8%, and -14.4%

(a)
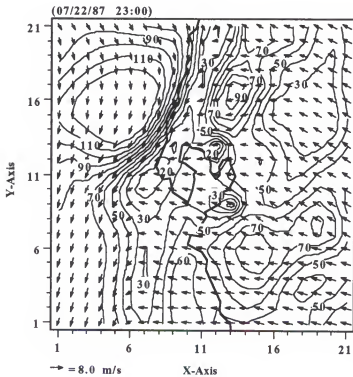
(b)

Figure 5.5. Surface flow fields and isopleths of ozone concentrations at (a) 19:00 hr, and (b) 23:00 hr, on July 22, 1987.

Figure 5.6. X-Z cross section flow fields and isopleths of ozone concentrations
at (a) 19:00 hr, and (b) 23:00 hr, on July 22, 1987.

Figure 5.7. Comparisons of predicted and observed hourly ozone concentrations at each of the monitoring sites in the Tampa Bay area on July 22, 1987.

when they were unpaired in time and paired by site. These sites provided PPAs in the range ±20%, which is the model performance goal recommended by the California Air Resources Board (CARB). The peak prediction accuracy unpaired in time and sites was only -1.8%, but that for data unpaired in time and space was 44%.

Table 5.1 shows the results of statistical calculations which were used to evaluate model performance. The smallest (11 ppb) value for root of mean square difference (RMS) was obtained at site 4. It indicated that the predicted ozone levels were closest to the observed values at site 4. Generally, the model overestimated ozone concentrations at all sites, since the mean errors (ME) were negative. Half of the sites (sites 1, 4, and 5) had average fractional differences less than 0.33, which corresponded to a factor of two difference between predicted and observed ozone levels. The higher AFD values (> 0.4) at the other three sites were apparently due to higher predicted nighttime values. Even small differences between predicted and observed ozone concentrations could lead to high AFD values, since the observed nighttime ozone levels normally are low.

Table 5.1. Statistical evaluation of model performance for O_3 predictions on July 22, 1987.

Statistics*	Site 1	Site 2	Site 3	Site 4	Site 5	Site 6
RMS (ppb)	23	24	18	11	17	26
ME (ppb)	-12	-23	-12	-5	-4	-19
AFD (24 hrs)	0.24	0.47	0.43	0.24	0.23	0.42
AFD (day)	0.20	0.19	0.12	0.13	0.21	0.23
AFD (night)	0.25	0.58	0.61	0.28	0.21	0.47
Correlation	0.81	0.97	0.92	0.91	0.69	0.82

* Statistical terms were defined in Chapter 3.

The correlation coefficients (r) were relatively high (> 0.8), except for site 5. The latter discrepancy could be due to the fact that predicted ozone levels increased slightly after 21:00 hr, but the increase was not observed at the monitoring site.

Figure 5.8 shows the frequency (%) of residual ozone in pre-determined categories. The data suggested that the model more frequently over-predicted than under-predicted ozone concentrations for the July 22, 1987 case. Generally, the model tended to over-predict (Figure 5.9) when the O_3 concentrations were lower than 70 ppb. The average predicted ozone concentrations at the sites were higher than the maximum observed ozone concentrations (Figure 5.10) for each hour before 15:00 hr, and within the range of observed levels after 15:00 hr. The correlation coefficient (r) between predicted and observed ozone concentrations (Figure 5.11) for all sites was 0.79. A slope of 0.84 and an intercept of 17 ppb was deduced from linear regression analyses.

5.2 Evaluation of Simulated Ozone Distributions on July 23, 1987

Southeasterly surface wind predominated in the southern half of the domain (Figure 5.12 (a)), while easterly surface winds were predicted for most of the northern half of the domain at 03:00 hr on July 23, 1987. Pinellas and a small part of Hillsborough County had ozone concentrations less than 30 ppb. The rest of Hillsborough County would experience relatively high ozone levels, due to the influence of a high ozone (> 60 ppb) center, and low nighttime NO emissions. Figure 13 (a) indicates that a maximum ozone (> 70 ppb) level was predicted at about 700 m above the ground surface, and higher ozone concentrations should be observed when compared to those at 03:00 hr on the previous day.

At 07:00 hr, the predicted surface flows shifted mainly to the south and southeast (Figure 12 (b)), which approximately agreed with the observed wind (southeast wind) at Tampa. Both Pinellas and Hillsborough counties were in the area experiencing ozone concentrations less than 35 ppb. The major suburban area of Tampa experienced ozone

Figure 5.8.   Frequency (%) of residual ozone values on July 22, 1987.

Figure 5.9.   Distribution of residual ozone concentrations as a function of observed ozone concentrations on July 22, 1987.

Figure 5.10. Range of observed and mean of predicted hourly averaged ozone levels at monitoring sites on July 22, 1987.

Figure 5.11. Linear regression analysis of predicted and observed ozone levels on July 22, 1987.
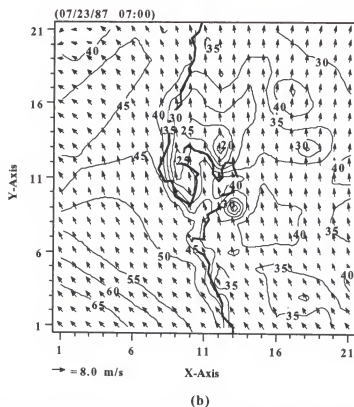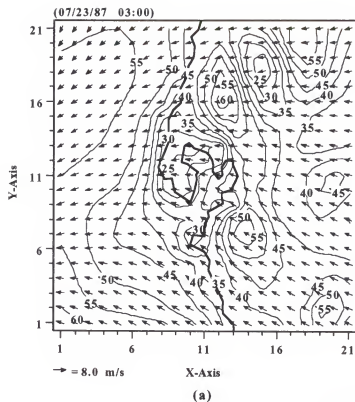
Figure 5.12. Surface flow fields and isopleths of ozone concentrations at (a) 03:00 hr, and (b) 07:00 hr, on July 23, 1987.
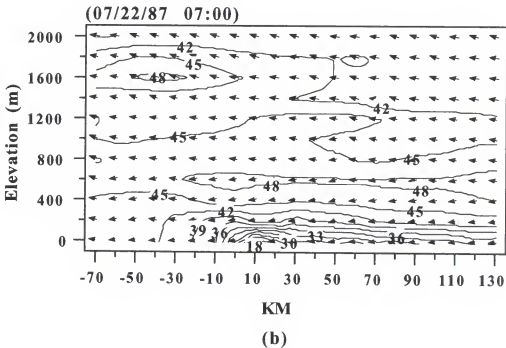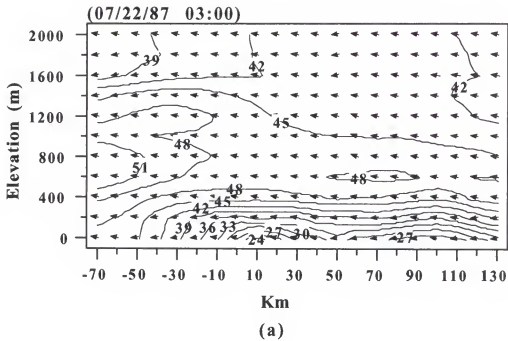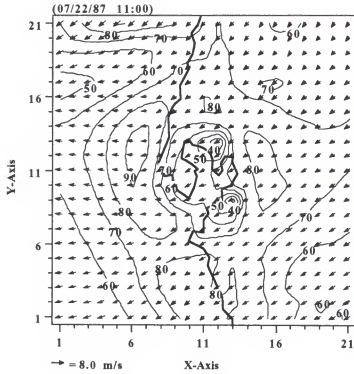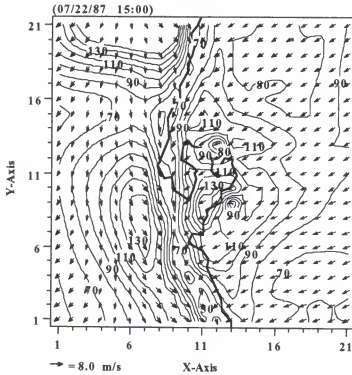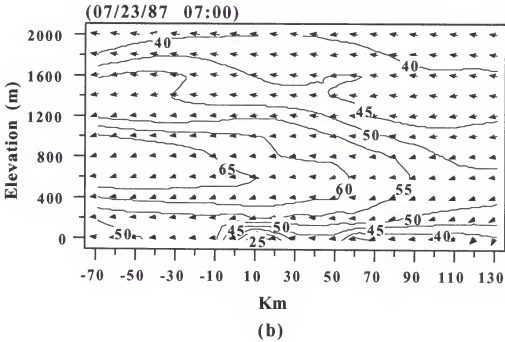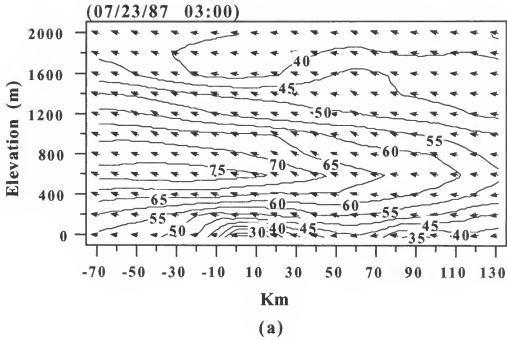
Figure 5.13. X-Z cross section flow fields and isopleths of ozone concentrations at (a) 03:00 hr, and (b) 07:00 hr, on July 23, 1987.

levels lower than 25 ppb. Increased emissions in Pinellas County created a stronger horizontal ozone concentration gradient (Figure 13 (b)) at the shores of the Gulf and the bay.

The winds over the Gulf (Figure 14 (a)) did not change too much when compared to those at 07:00 hr, but winds close to the coast and over the land surface in the northern half of the domain had obviously altered. A sea breeze type of convergence was predicted along the coastal area in Pinellas County. Two low ozone centers with strong horizontal ozone gradients existed close to Tampa Bay, because of the strong NO_x point source emissions. In contrast to the ozone isopleths at the same time on the previous day, the highest ozone center over the Gulf was to the north instead of to the west of Pinellas County. The highest ozone center (> 100 ppb) over the land surface existed to the northwest of Tampa bay. The sea breeze front was predicted at 10 km inland over Pinellas County. The vertical lifting force at the sea breeze front (Figure 15 (a)) raised the highly polluted air to one of the higher ozone centers (> 95 ppb) at an elevation of 400 m at the front. The other high ozone center (> 95 ppb) was just behind the sea breeze front, since the recirculation of sea breeze accumulated the pollutants and no NO_x emissions were present over the water surface. A wave-like motion was predicted in front of the sea breeze front over the land side. Due to stronger vertical mixing, ozone concentrations were consistently distributed vertically below an elevation of 200 m.

At 15:00 hr, sea breezes developed along the whole coastal zone in the domain (Figure 14 (b)), and the front moved 20 km further inland in the Tampa bay area. The highest ozone center (> 150 ppb) was predicted to the northeast of the Tampa urban center. The second highest ozone center (> 140 ppb) was predicted at the east shore of the Tampa bay. Stagnant air in front of the sea breeze over the land surface could be the reason why these peak ozone concentrations were formed. Vertical flows became stronger and the zone of the sea breeze front was expanded. A constant vertical ozone profile (Figure 5.15 (b)) could exist up to an elevation of 800 m at the sea breeze front.

Figure 5.14. Surface flow fields and isopleths of ozone concentrations at (a) 11:00 hr, and (b) 15:00 hr, on July 23, 1987.
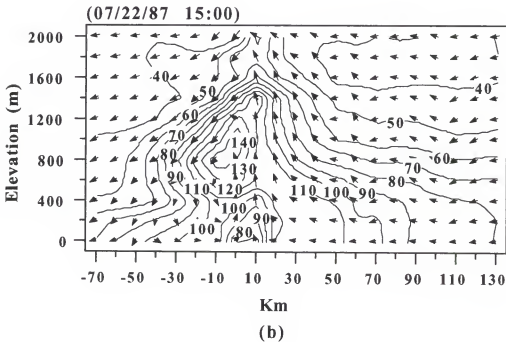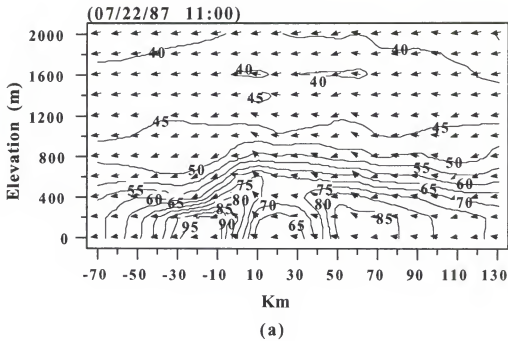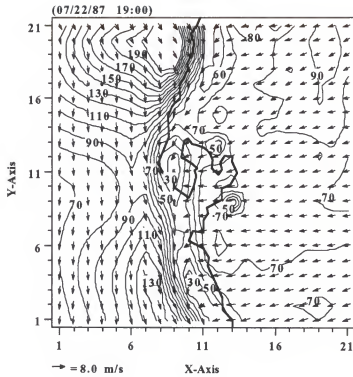
Figure 5.15. X-Z cross section flow fields and isopleths of ozone concentrations
at (a) 11:00 hr, and (b) 15:00 hr, on July 23, 1987.

Three high ozone centers (> 150 ppb) were predicted behind the sea breeze front at an elevation above 1000 m. A relatively low ozone center (> 130 ppb) was predicted 200 m above the ground at the front edge of the sea breeze front.

Four hours later, the sea breeze front moved 20 km further inland (Figure 5.16 (a)) and reached the east shore of Tampa bay. The air flows behind the sea breeze front were dominated by north-northwest to northwest winds, which were consistent with the observations. Ozone concentrations were titrated very rapidly behind the sea breeze front at two locations where there were strong NO_x emissions. Pinellas County was covered by an air mass with relatively high ozone concentrations (~ 70 ppb). One of the highest ozone centers (> 110 ppb) was located to the east of the Tampa urban area. Another high ozone concentration center (> 120 ppb) was transported from the north boundary of the domain by northwesterly winds. The downflows behind the sea breeze front (Figure 5.17 (a)) transported high ozone air masses further away from land. The highest ozone center (> 150 ppb) was predicted at 1200 m elevation. This elevated high ozone concentration center did not reach the ground surface, since the downflows behind the sea breeze front were not strong enough.

The sea breeze front moved faster and reached the east boundary of the domain (Figure 5.16 (b)) at 23:00 hr. The region with a relatively high ozone (> 70 ppb) level was transported into Pinellas County from the Gulf. The winds at the northeastern boundary of the domain were shifted to the north and brought down a high ozone center (> 120 ppb). The intensity of the uplifting flow decreased (Figure 5.17 (b)), and the high ozone center, which originated at 1200 m elevation, was transported out of the west boundary of the domain.

Figure 5.18 shows the predicted and observed ozone concentrations at each of the monitoring sites. The model predicted peak ozone concentrations would occur about 1 to 6 hour earlier than those observed. Two thirds of the monitoring sites had peak prediction accuracies of -11.5%, -1.6%, -10.3 and -1.9% with unpaired data in time and

Figure 5.16. Surface flow fields and isopleths of ozone concentrations at (a) 19:00 hr, and (b) 23:00 hr, on July 23, 1987.
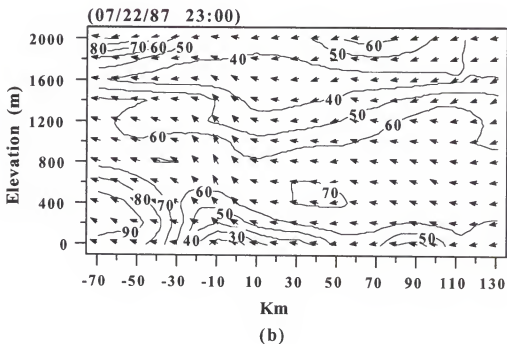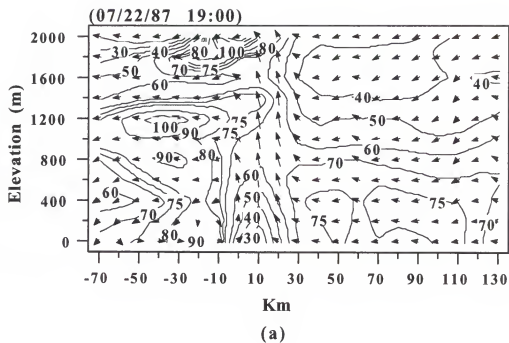
Figure 5.17. X-Z cross section flow fields and isopleths of ozone concentrations at (a) 19:00 hr, and (b) 23:00 hr, on July 23, 1987.
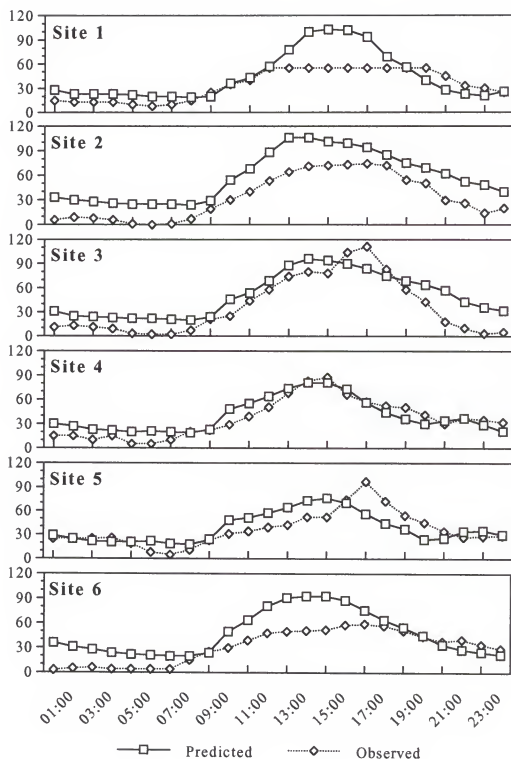
Figure 5.18. Comparisons of predicted and observed hourly ozone concentrations at each of the monitoring sites in the Tampa Bay area on July 23, 1987.

paired by sites, which agreed with the performance goal recommended by the California ARB. The peak prediction accuracy with data unpaired in time and sites was only -12.0%, and that with data unpaired in time and space was 4.9%.

Table 5.2 shows the results of statistical calculations which were used to evaluate the model performance. The smallest (27 ppb) root of mean square difference (RMS) value was obtained at site 5. It indicated that predicted ozone levels were closer to the observed ones at site 5. On the average, the model overestimated the ozone concentrations at every site. Only one site (site 5) had average fractional differences less than 0.33 which is a factor of two between predicted and observed ozone levels. The higher AFD values (> 0.4) at sites 1, 2, and 6 were due to higher night time values. Sites 3 and 4 also had relatively high AFD values during the day time. The correlation coefficients (r) were relatively low (< 0.65). The low correlation coefficients were due to large gaps between the predicted and observed peak times, as a result, the predicted ozone

Table 5.2. Statistical evaluation of model performance for O_3 predictions on July 23, 1987.

Statistics*	Site 1	Site 2	Site 3	Site 4	Site 5	Site 6
RMS (ppb)	42	35	42	34	27	29
ME (ppb)	0	-10	-3	-11	-7	-10
AFD (24 hrs)	0.36	0.49	0.52	0.42	0.28	0.36
AFD (day)	0.33	0.31	0.41	0.34	0.26	0.27
AFD (night)	0.40	0.56	0.54	0.43	0.26	0.39
Correlation	0.14	0.53	0.36	0.54	0.50	0.63

started to decrease as the observed ozone concentrations were increasing. The complex meteorological conditions existing for the passage of a sea breeze front on July 23, 1987 were not accurately simulated by the model, therefore, the ozone simulations were not as successful as those for the July 22, 1987 case.

Figure 5.19 shows the frequency (%) of residual ozone in pre-determined categories. The data suggested that the model more frequently over-predicted rather than under-predicted ozone concentrations for the July 23, 1987 case. Generally, the model tended to over-predict (Figure 5.20) when the observed ozone concentrations were lower than 60 ppb, and underpredict concentrations at levels higher than 60 ppb. Figure 5.21 indicates that the model overpredicted ozone concentrations in the morning and underpredicted observed values in the afternoon. The correlation coefficient between predicted and observed ozone concentrations (Figure 5.22) for all sites was only 0.43. A slope of 0.31 and an intercept of 40 ppb were deduced from linear regression analyses.

5.3 Evaluation of Simulated Ozone Distributions on July 24, 1987

The predicted air flows (Figure 5.23 (a)) formed a counterclockwise type of circulation over the domain, due to the influence of the passage of a weak low pressure trough. A high ozone center (> 200 ppb) was transported from the north boundary of the domain toward the Tampa Bay area by north winds at 03:00 hr, the source of the ozone center was unknown. Transport of the high ozone center led to an unexpected increase in predicted ozone levels in the early morning for the Tampa Bay area. Uplifting flows still existed above 400 m elevation over the land surface (Figure 5.24 (a)), meanwhile, downward flows were predicted over the Gulf. The vertical cross section plot was totally different from that of the previous day. There were not any obvious horizontal ozone concentration gradients over the interface between land and water. These unique results could only be explained by the interference of the low pressure trough within a broad high pressure system.
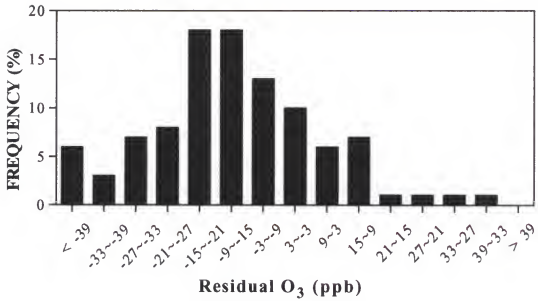
Figure 5.19. Frequency (%) of residual ozone values on July 23, 1987.
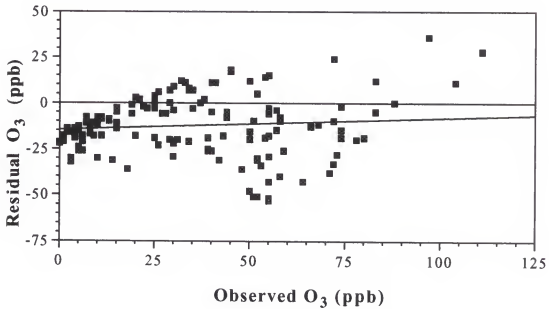

Figure 5.20. Distribution of residual ozone concentrations as a function of observed ozone concentrations on July 23, 1987.
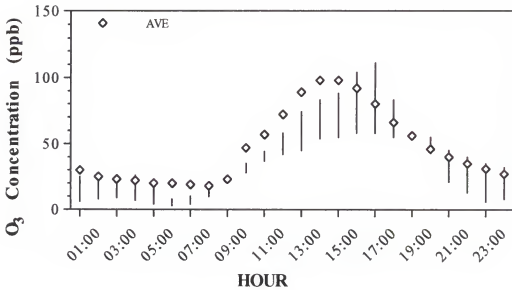
Figure 5.21. Range of observed and mean of predicted hourly averaged ozone levels at monitoring sites on July 23, 1987.
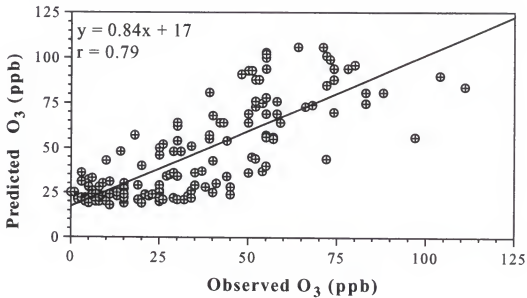

Figure 5.22. Linear regression analysis of predicted and observed ozone levels on July 23, 1987.

128
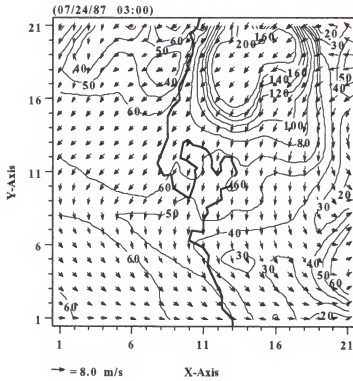
(a)
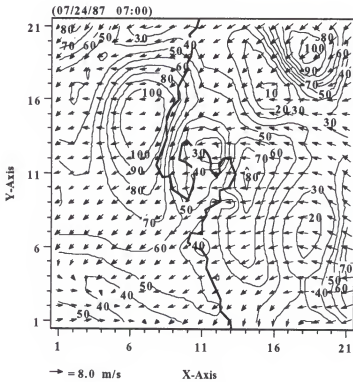
(b)

Figure 5.23. Surface flow fields and isopleths of ozone concentrations at (a) 03:00 hr, and (b) 07:00 hr, on July 24, 1987.
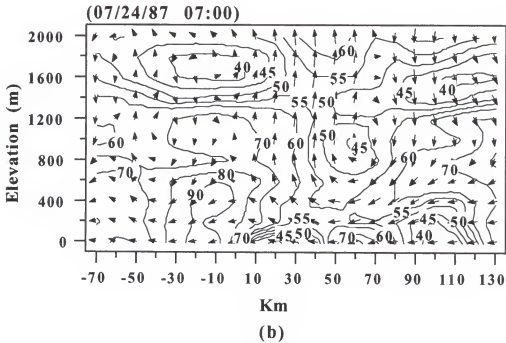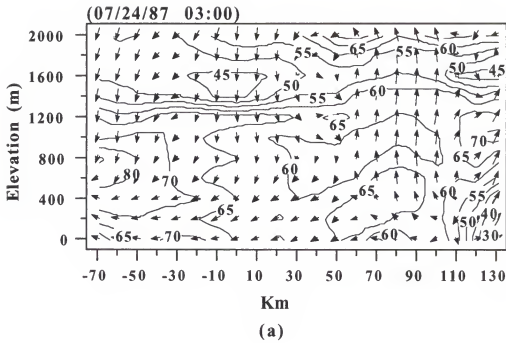
Figure 5.24. X-Z cross section flow fields and isopleths of ozone concentrations at (a) 03:00 hr, and (b) 07:00 hr, on July 24, 1987.

At 07:00 hr on July 24, 1987, the air flows shifted to the east and northeast in a major portion of the domain (Figure 5.23 (b)). There was a 45 to 60 degree discrepancy when the predicted wind direction was compared to that observed (north-northeast) at Tampa International airport. The high ozone center, which originated at the northern boundary of the domain was transported from inland regions to the Gulf. Another high ozone center (> 100 ppb) moved into the domain from the northeast boundary. The east shore of Tampa bay experienced relatively high ozone levels, which was a result of a split air mass from the high ozone center predicted at 03:00 hr. Turbulence above 200 m elevation was projected to move toward the coastal area. The highest ozone isopleth shown by the X-Z cross sections (Figure 24 (b)) was greater than 90 ppb above the Gulf surface waters at about 10 km off the shore line.

Two high ozone centers were predicted to exist in the Gulf (Figure 25 (a)). One was apparently produced by a highly polluted air mass from the Tampa Bay area. The other could be due to unreal meteorological predictions. The questionable high ozone center disappeared in the next hour, and it did not seem to have an influence on the later predictions. Ozone did not reach a peak at this time in the Tampa Bay area. A counterclockwise circular flow was predicted to the south of Tampa Bay. Over the land surface, the northerly winds led to a convergent area at the east boundary of the domain, and a divergent area at the east shore of Tampa bay, therefore, uplifting flows and down flows were predicted (Figure 5.26 (a)) at the corresponding areas.

At 15:00 hr, the sea breeze started to form (Figure 5.25 (b)) along the Gulf coast from Tampa Bay to the north boundary of the domain. A high ozone center originating from west of Pinellas County (> 180 ppb) was intensified due to continuous ozone generation. A second high ozone center (> 140 ppb) was predicted in the Tampa Bay. It was formed by the pollutant rich air mass that was transported from the Tampa region by a northeasterly wind, and low NO_x emissions in the bay area. A third high ozone center was transported from the north boundary of the domain. Uplifting flows at the sea
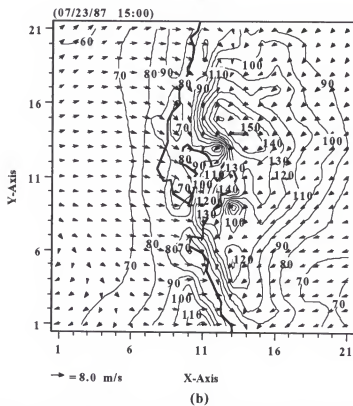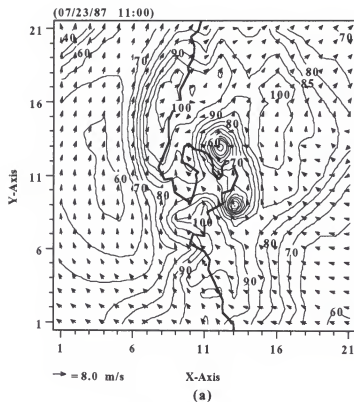
(a)

(b)
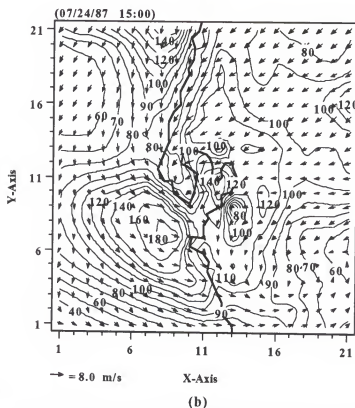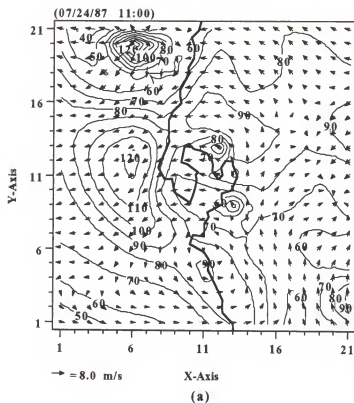
Figure 5.25. Surface flow fields and isopleths of ozone concentrations at (a) 11:00 hr, and (b) 15:00 hr, on July 24, 1987.
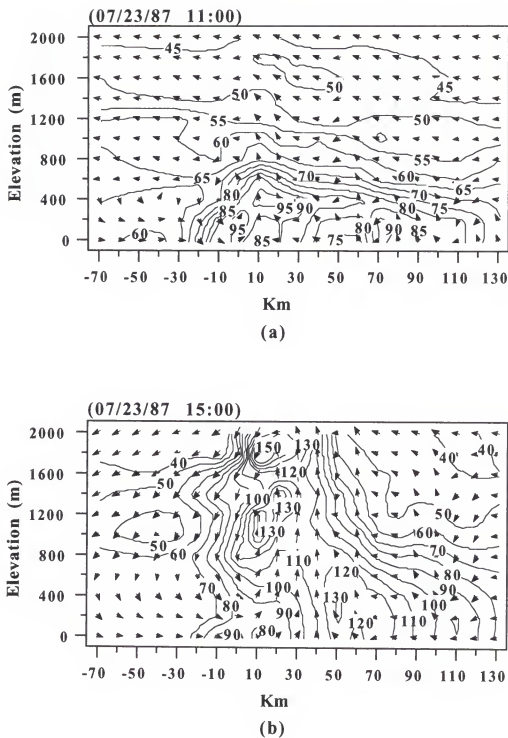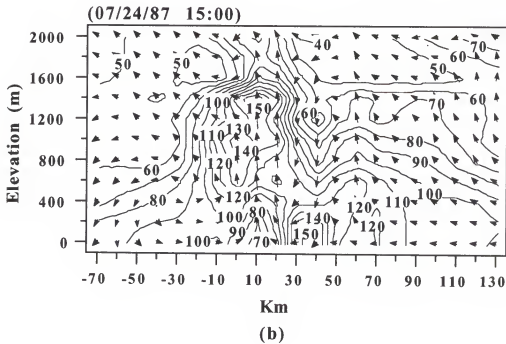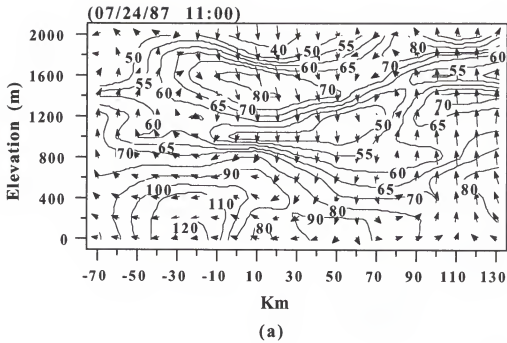
Figure 5.26. X-Z cross section flow fields and isopleths of ozone concentrations
at (a) 11:00 hr, and (b) 15:00 hr, on July 24, 1987.

breeze front caused two high ozone centers (> 140 ppb) to be predicted at elevations of 800 and 1200 m (Figure 5.26 (b)). A zone with downflows was predicted in front of the sea breeze uplifting zone. The downflow zone was similar to that for the previous day, but was stronger.

The surface wind field at 19:00 was similar to that at 15:00 hr, but the convergent zone described above was weakened. One high ozone center (> 150 ppb) was transported south in the Gulf from the north boundary of the domain (Figure 27 (a)). High ozone centers, which originated to the south of Pinellas County and in Tampa Bay were merged and decreased in intensity to form a high ozone center (> 130 ppb) to the south of Tampa Bay. The latter center caused a slight ozone increase to be predicted at site 1 in Hillsborough County. Another high ozone center (> 120 ppb) to the north of Tampa was transported from the east boundary of the domain. The predicted wind did not match the observed wind at the Tampa International airport, but the south boundary had a wind field similar to that observed. The strength of uplifting flows decreased as the convergent zone disappeared. There was still a zone of uplifting flows at the interface of the land and the Gulf waters (Figure 28 (a)). The maximum ozone center was at an elevation of 1000 m. The low ozone center at the surface was due to titration of strong NO_x emissions from Pinellas County before being transported to the Gulf of Mexico.

At 23:00 hr, easterly winds predominated over the domain. All the high ozone centers with concentrations greater than 100 ppb were either titrated or transported out of the domain (Figure 5.27 (b)). The Tampa Bay area was dominated by the ozone levels in the range from 30 to 70 ppb. No uplifting flows were predicted below an elevation of 1200 m at this hour (Figure 28 (b)). The high ozone center (> 100 ppb) at high elevation was transported toward the west boundary of the domain.

Figure 5.29 shows the predicted and observed ozone concentrations at each of the monitoring sites. The model predicted the O_3 peak concentrations from 0 to 3 hours later than those observed. Two thirds of the monitoring sites had peak prediction accuracies
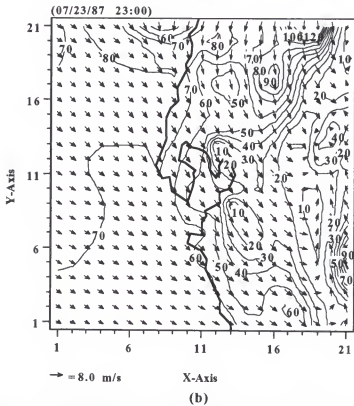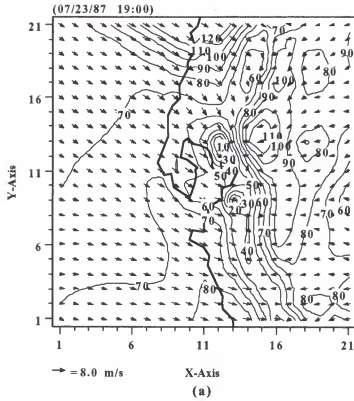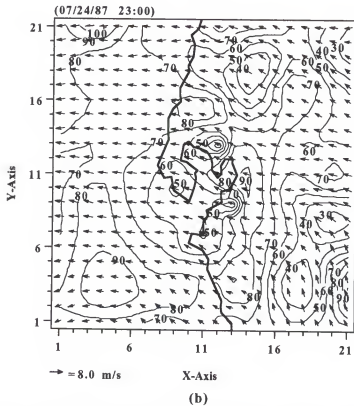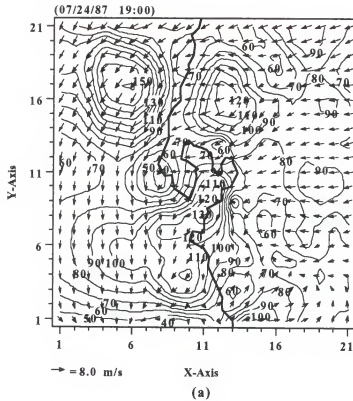
Figure 5.27. Surface flow fields and isopleths of ozone concentrations at (a) 19:00 hr, and (b) 23:00 hr, on July 24, 1987.
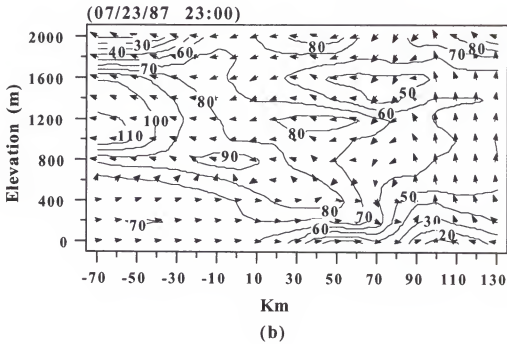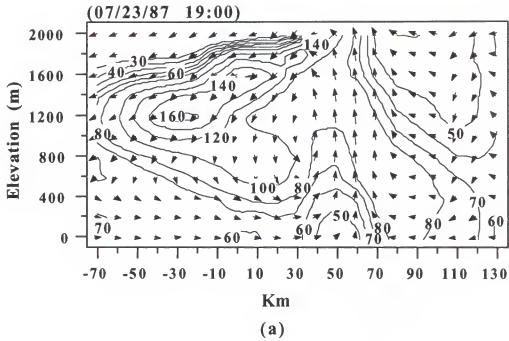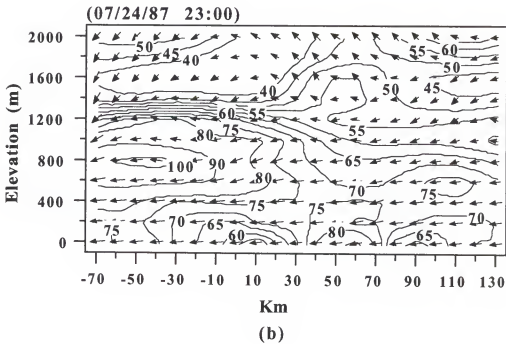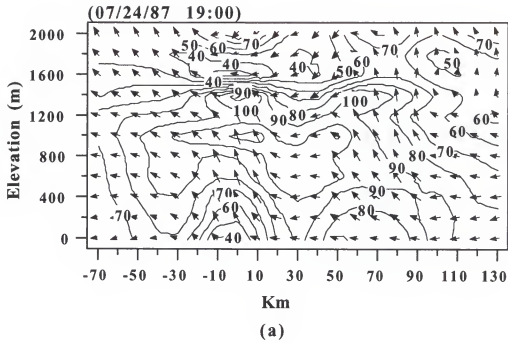
Figure 5.28. X-Z cross section flow fields and isopleths of ozone concentrations at (a) 19:00 hr, and (b) 23:00 hr, on July 24, 1987.
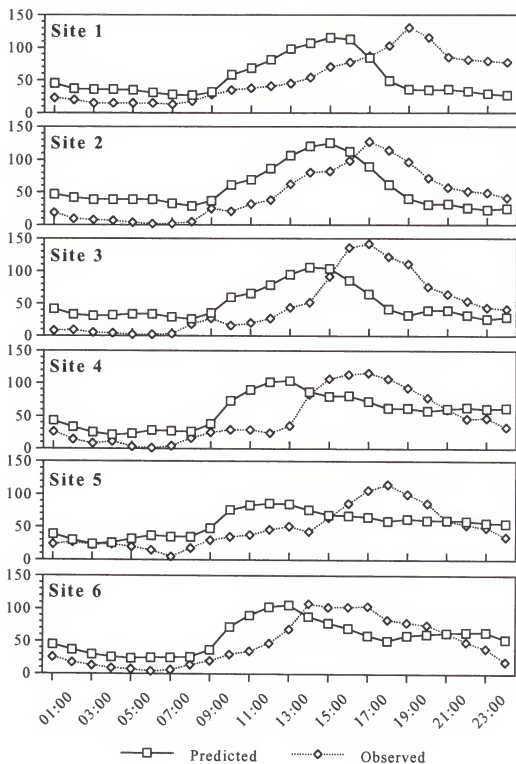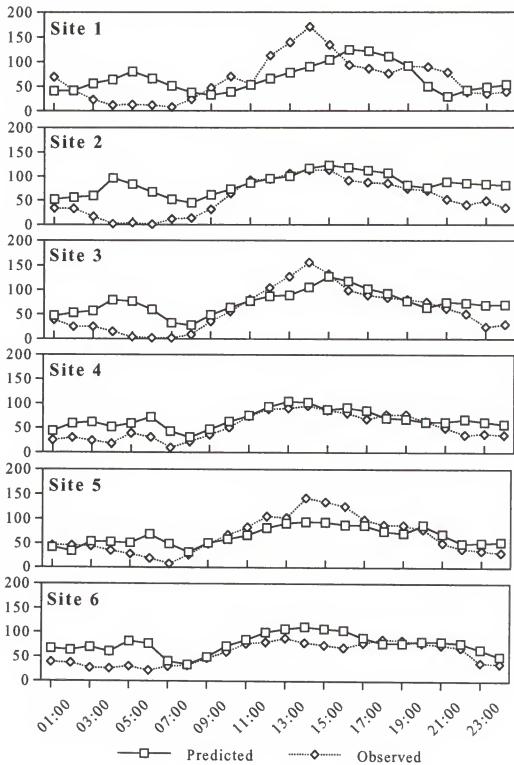
Figure 5.29. Comparisons of predicted and observed hourly ozone concentrations at each of the monitoring site in the Tampa Bay area on July 24, 1987.

of -8.8%, -1.6%, -18.6 and 9.5% with data unpaired in time and paired by sites. The peak prediction accuracy with data unpaired in time and sites was only -25.7% which is 5.7% less than the recommended range for a typical ozone model performance. The peak prediction accuracy with data unpaired in time and space was 9.9% for the Tampa Bay area, which fulfilled the recommended range requirement.

Table 5.3 shows results of statistical calculations which were used to evaluate model performance. The smallest (21 ppb) root of mean square difference (RMS) values was obtained at site 4. It indicated that the predicted ozone levels were closest to those observed at site 4. On the average, the model overestimated the ozone concentrations at all sites, but site 5 had a positive ME value. All the sites in Pinellas County had average fractional differences less than 0.33 which indicates a factor of two difference between predicted and observed ozone levels. The higher AFD values (> 0.36) at sites 1, 2, and 3 were due to unexpected ozone peaks predicted in the early morning. AFD values were much lower (< 0.21) during the daytime than the nighttime at sites 1, 2 and 3. Except for

Table 5.3. Statistical evaluation of model performance on the O_3 predictions on July 24, 1987.

Statistics*	Site 1	Site 2	Site 3	Site 4	Site 5	Site 6
RMS (ppb)	39	38	33	21	24	26
ME (ppb)	-1	-28	-15	-15	1	-20
AFD (24 hrs)	0.36	0.43	0.41	0.25	0.23	0.23
AFD (day)	0.21	0.11	0.10	0.07	0.12	0.11
AFD (night)	0.42	0.54	0.52	0.52	0.28	0.28
Correlation	0.47	0.74	0.78	0.87	0.85	0.70

site 1, the correlation coefficients for the monitoring sites were greater than 0.70, which was much better than the values for the previous day.

Figure 5.30 shows that the model more frequently overpredicted than under-predicted ozone concentrations for the July 24, 1987 case. The distributions of residual ozone were mainly in the range from -3 to -9 ppb, which showed a better model prediction capability than in the case of the previous day. The model tended to over-predict (Figure 5.31) when the observed concentrations were lower than 80 ppb, and underestimate when observed values were higher than 80 ppb. The average predicted ozone levels at the sites were in the range of observed ozone (Figure 5.32) values for daytime, but were much higher than the maximum of the hourly observed ozone range in the early morning. The correlation coefficient between predicted and observed ozone concentrations (Figure 5.33) for all sites was 0.64. A slope of 0.41 and an intercept of 47 ppb was deduced from linear regression analysis.

5.3 Evaluation of Regional Ozone Predictions

The Tampa Bay region can be naturally divided into the Pinellas County region and the Tampa region. Average concentrations of observed and predicted ozone levels for sites in each region were evaluated. The California ARB has suggested that the performance goals for simulating ozone concentrations are ±30% for normalized bias and ≤40% for normalized error. These are the most frequently used parameters for evaluating model performance in ozone prediction, which are defined in Chapter 3.

The model performed well in terms of O_3 peak predictions, and in daytime ozone predictions (Table 5.4). Only the peak prediction accuracies with data unpaired time and by sites for both Tampa and Pinellas County region on July 24, 1987 were larger than the recommended value (±20%). The daily normalized bias and errors indicated that the performance of the model did not reach the recommended goals. The poor performances in these categories generally were due to poor nighttime ozone predictions. During the
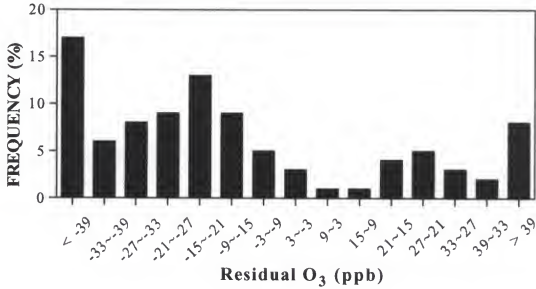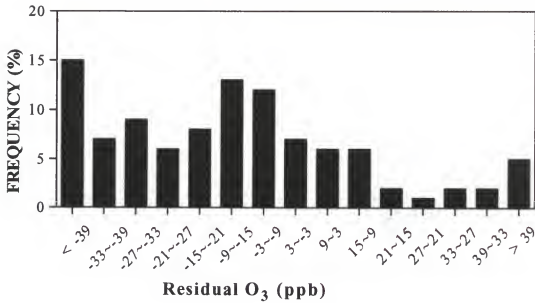
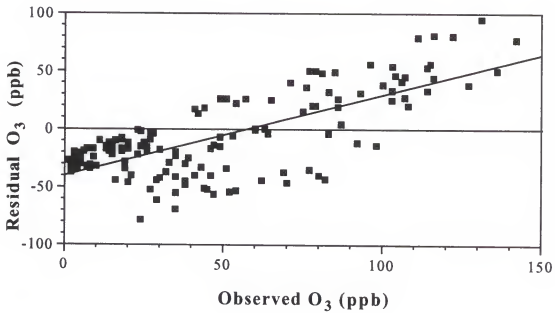Figure 5.30. Frequency (%) of residual ozone values on July 24, 1987.
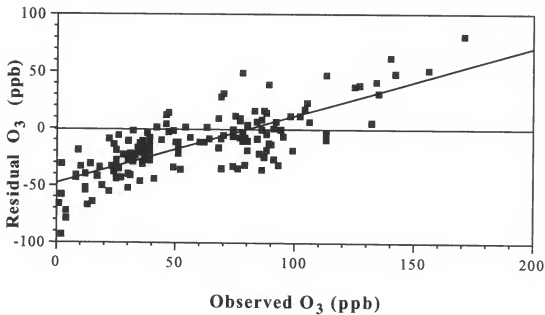
Figure 5.31. Distribution of residual ozone concentrations as a function of observed ozone concentrations on July 24, 1987.
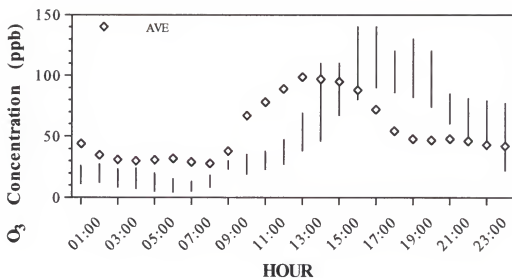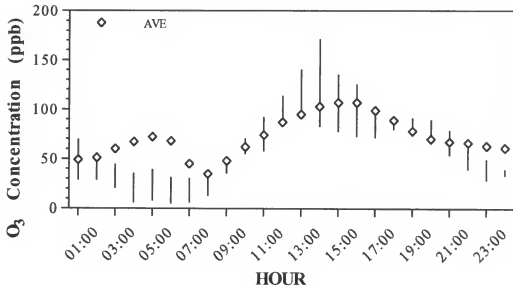
Figure 5.32. Range of observed and mean of predicted hourly averaged ozone levels at monitoring sites on July 24, 1987.
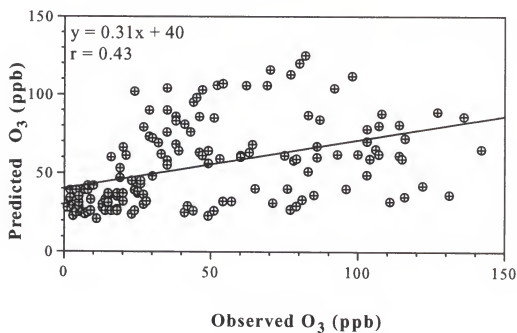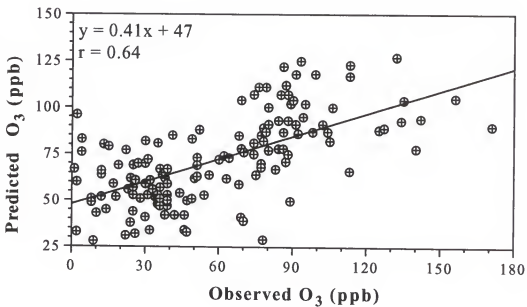

Figure 5.33. Linear regression analysis of predicted and observed ozone levels on July 24, 1987.

Table 5.4. Statistical evaluation of model performance for O_3 predictions in the Pinellas County, and Tampa regions.

Date	07/22/87		07/23/87		07/24/87	
Term	Tampa	Pinel	Tampa	Pinel	Tampa	Pinel
PPA* %	-2	6	-12	-9	-26	-22
Bias %	-239	-143	-106	-89	-169	-106
Bias day %	-24	-24	-36	-42	0.48	-0.84
ERR %	240	155	141	104	178	109
ERR day %	25	30	73	71	19	6
AFD	0.39	0.31	0.46	0.35	0.40	0.24
AFD day	0.18	0.20	0.35	0.29	0.15	0.10
Correlation	0.96	0.87	0.38	0.57	0.70	0.88

daytime, only the simulations on July 23, 1987 had high normalized bias and error values. The model performance for July 24, 1987 was extremely good. The normalized biases were less than ±1% for both Tampa and Pinellas County regions.

Daily AFD values (Table 5.4) show that only predicted ozone concentrations in Pinellas County on July 22, and 24, 1987, were within a factor of two when compared with observed ozone concentrations. AFD values for the daytime hours suggest that the daytime ozone predicted concentrations and observed values were generally within a factor of two in both regions during the ozone episode, except in the Tampa region on July 23, 1987.

The model had trouble in predicting the diurnal variations in ozone concentrations for both regions on July 23, 1987, so the correlation coefficients were low. On July 23, 1987, the correlation coefficient for the Tampa region was lower than that for Pinellas

County. A relative low correlation coefficient (0.70) was obtained for the Tampa region on July 24, 1987.

On July 22, 1987, the predicted sea breeze front could only penetrate about 10 km inland in Pinellas County. The Tampa region was dominated by uniform easterly to northeasterly winds. Relatively complex flows on the approach of the sea breeze front caused the worst evaluation results in Pinellas County during the daytime when compared to those for the Tampa region. The passage of the sea breeze front on July 23, 1987 created complex meteorological conditions. Evaluations of the simulation results for Pinellas County were a little better than those for the Tampa region. The latter differences could be due to the relatively complicated geography of the Tampa Bay shore line in Hillsborough County . On July 24, 1987, the model performed better in Pinellas County than in the Tampa region. A bay breeze observed at the east side of Tampa Bay at 13:00 hr on July 24, 1987, created a complicated meteorological condition, as a result, the model did not perform well for ozone predictions in the Tampa region.

5.5 Trajectory Analyses

A trajectory analysis algorithm is incorporated into the MM4 model system as an appropriate tool for tracing sources. Back trajectory analyses were used to identify the possible sources of ozone and its precursors, which might have contributed to the ozone episode in the Tampa Bay area. Forward trajectory analyses were used to identify the areas that would be affected by the high ozone levels in the Tampa bay area during the episode. The trajectories presented are the projections of three dimensional trails of the air masses. All trajectory calculations are started from four grid positions that are close to the Tampa Bay area. Grid points (8,9), (8,10), (9,9) and (9,10) are used to represent the individual trajectories.

The first set of back trajectory analyses (Figure 5.34 (a)) were initiated at 17:00 hr on July 23, 1987, when the maximum ozone concentration (142 ppb) was observed.
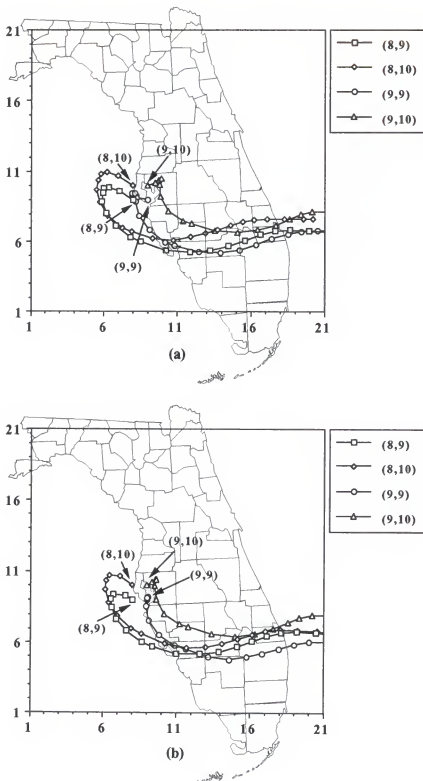
Figure 5.34. Horizontal back trajectories started at (a) 17:00 hr, on 07/23/87; and (b) 15:00 hr, on 07/23/87.

Three out of four back trajectories ((8,9), (8,10), and (9,9)) showed that the air masses passed over the east coast of Florida (St. Lucie and Martin counties), and mixed with the pollutants emitted during the early morning traffic hours on July 22, 1987. These air masses continued to travel from the Gulf coast (Lee and Charlotte counties) into the Gulf in the early morning of July 23, 1987. The air masses were, then transported clockwise due to the sea breeze, and returned to the Tampa Bay area in the afternoon on the same day. Trajectory (9,9) suggested that the air mass remained stationary around the Tampa Bay area for 4 hours. The fourth air mass collected pollutants emitted on the east coast (Martin County) close to the afternoon traffic hours (17:00 hr) on July 22, 1987. This air mass was then transported through south central Florida, and eventually became relatively stationary in the Tampa Bay region for 12 hours on July 23, 1987.

The second set of back trajectories (Figure 5.34 (b)) were initiated at 15:00 hr on July 23, 1987 when the maximum ozone concentration (127 ppb) was predicted at one of the Tampa sites. The two hour time lag changed the back trajectory patterns only slightly. One of the major discrepancies between the two sets of trajectories was that two trajectories ((8,10) and (9,10)) of the second set moved inland from the Atlantic coast two hours earlier than the corresponding trajectories from the first set. Another difference was that air mass (9,9) of the second set traveled along the west coast, and arrived at Tampa bay directly, without making a clockwise circle as shown for the former case in Figure 5.34 (a), and remained in the Tampa Bay area for more than 6 hours prior to 15:00 hr on July 23, 1987. All air masses were limited to elevations below about 250 m, where it was possible that significant exchange of surface emissions could occur.

For the July 24, 1987 case, the first set of back trajectories (Figure 5.35 (a)) started at 13:00 hr when the maximum ozone concentration (171 ppb) was observed. Trajectory (9,9) suggested that the air mass was transported onshore from Palm Beach County in the afternoon (14:00 hr) on July 22, 1987. After crossing south central Florida, it continued flowing offshore from the west coast of Florida, and was transported inland
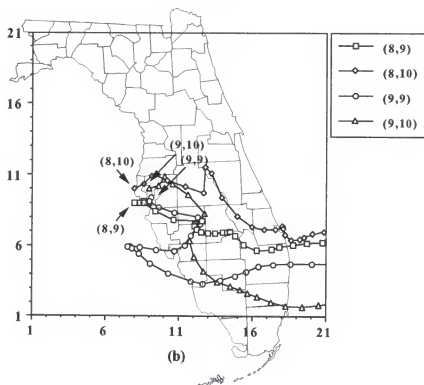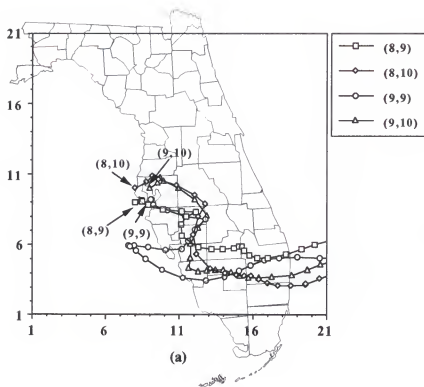
Figure 5.35. Horizontal back trajectories started at (a) 14:00 hr, on 07/24/87; and (b) 15:00 hr, on 07/24/87.

again from Lee County at 18:00 hr on July 23, 1987. Subsequently, it circulated counterclockwise to the Tampa Bay area at 08:00 hr on July 24, 1987, and stayed nearly stationary for 4 hours. The other trajectory (9,10) indicated that the air mass was conveyed across the coast of Palm Beach County at 20:00 hr on July 22, 1987. It traveled through south Florida to the west coast, and then moved north and turned counterclockwise into the Tampa Bay area. The latter air mass stayed near the bay area for more than 6 hours prior to 14:00 hr on July 24, 1987. Trajectory (8,9) also indicated that the air mass stayed in the bay area for about four hours.

The second set of back trajectories (Figure 5.35 (b)) began at 15:00 hr, on July 24, 1987, when the maximum ozone concentration (127 ppb) was predicted at a site in Hillsborough County. Two trajectories ((8,10) and (9,10)) were significantly different from those started at 14:00 hr. Trajectory (8,10) moved inland at the border of St. Lucie and Martin counties instead of Palm Beach County, and collected pollutants emitted from 7:00 to 11:00 hr on the east coast. It was then transported to central Florida before arriving in the Tampa Bay area. Trajectory (9,10) suggested that the air mass passed the Miami urban area around 05:00 hr on July 22, 1987. It moved northwest to southwest Florida, and then turned counterclockwise to the Tampa Bay area. The latter air mass remained nearly stationary in the bay area for about four hours. Trajectory (9,9) passed through Palm Beach County at about 11:00 hr on July 22, 1987. The air mass followed the same route as shown in Figure 5.35 (a), but arrived at Tampa Bay two hours earlier and remained near the bay for two hours more than the (9,9) trajectory, based on the observed O_3 maximum..

Forward trajectories based on the observed O_3 maximum, which were initiated at 17:00 hr on July 23, 1987 (Figure 5.36 (a)), indicated that the air masses, rich in pollutants and with high ozone concentrations proceeded to the Gulf. One of the four forward trajectories showed a back and forth path around the Tampa Bay area. About 4 hours after initiation, the latter air mass was caught up in the uplifting flow of the sea

147
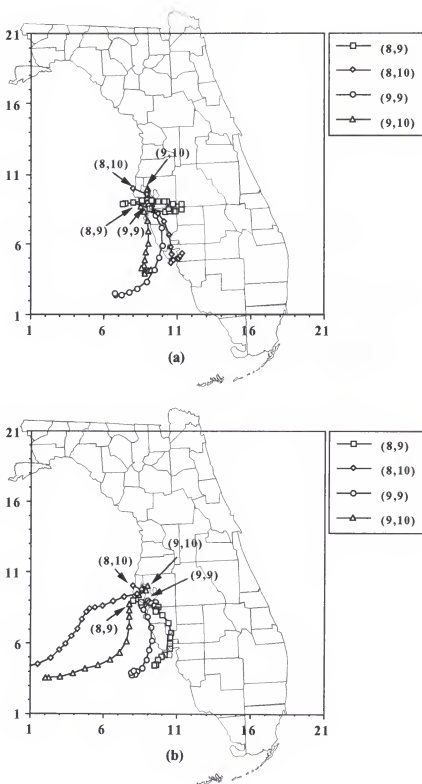
Figure 5.36. Horizontal forward trajectories started at (a) 17:00 hr, on 07/23/87; and (b) 15:00 hr, on 07/23/87.

breeze, and was transported from 100 m to 500 m height within two hours. The rest of the trajectories showed that the air masses had been transported to the south and into the Gulf after about 33 hours. These air masses were transported away from the surface by the sea breeze front earlier than in the case of the first air mass. Consequently, all the air masses reached an elevation above 1300 m at the end of their trajectories.

Forward trajectories based on the predicted O_3 maximum, (Figure 5.36 (b)) which were initiated two hours earlier from those in Figure 5.36 (a) on July 23, 1987, showed a different pattern. Two of the second set of trajectories suggested that the polluted air masses were moving southward, and away from the coast near Lee and Sarasota counties. One of the latter air masses passed through Pinellas County, and then moved south into the Gulf of Mexico. The last of the four forward trajectories in the second set showed that the air mass was transported inland during the first two hours due to the sea breeze, and was then turned back into the Gulf by the upper return air flow. Since this second set of trajectories were initiated earlier in the day, the air masses were estimated to be raised by the stronger uplifting force at the sea breeze front than those based on the observed O_3 maximum. At the end of their trajectories, these air masses arrived at elevations in the range from 1500 to 2200 m.

On July 24, 1987, the highly contaminated air masses (Figure 5.37) were transported out of Tampa Bay after the occurrence of the ozone episode. Similar patterns were predicted for the two sets of forward trajectories which were initiated at 14:00 hr (Figure 5.37 (a)) and at 15:00 hr (Figure 5.37 (b)). Emissions from Hillsborough County must have had a major impact on the levels of ozone in Pinellas County, when air mass (9,10) was transported to the Gulf.

5.6 Episode Predictions for the Year 2000

Emissions in the year 2000 were estimated in order to predict expected ozone levels as influenced by population growth and using current control strategies. The projected
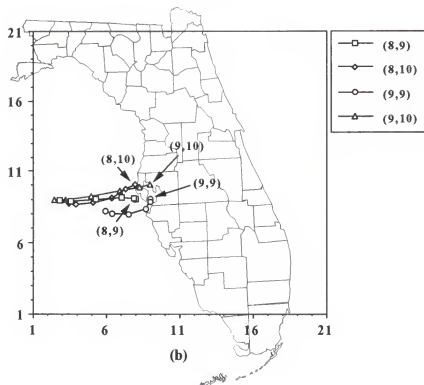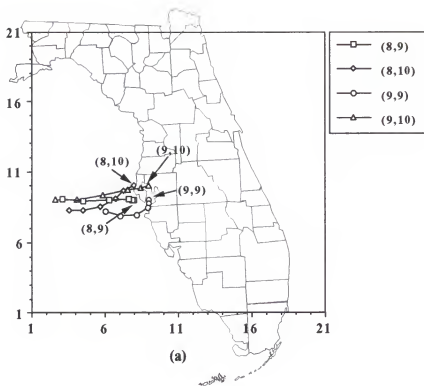
Figure 5.37. Horizontal forward trajectories started at (a) 14:00 hr, on 07/24/87; and (b) 15:00 hr, on 07/24/87.

population growth was based on the Florida Statistical Abstract 1988. Point sources, biogenic emissions, and area sources based on urban expansion were not taken into account for these predictions, because no information was available to be able to predict such changes. The growth factors for population were calculated first on a county basis, and then those results were applied to estimate the urban growth in each county. The same procedures as described previously in Chapter 4, were used to calculate emissions. Comparisons between estimated peak ozone concentrations in 1987 and 2000 during a similar three-day episode, are described in this section.

Since 1994, a total of 6 Florida counties have been subjected to regulation of air quality under the vehicle emission inspection program. The Florida Department of Highway Safety and Motor Vehicles estimated (Cloutier, 1993) that inspections have reduced VOC emissions by about 8% in Dade, Pinellas, and Duval counties, and 8.1% in Palm Beach, 7.9% in Broward, and 7.8% in Hillsborough counties. These VOCs reductions reported for these counties were used also to estimate emissions in the year 2000.

The predicted concentrations of ozone in 2000 at the observation sites are shown in Figure 5.38. Maximum ozone concentrations were estimated to increase at every monitoring site in the Tampa Bay area on July 22 for the year 2000 episode case. Increases in peak ozone concentrations ranged from 0 to 12 ppb when compared to the base case (1987) predictions. East Lake Tarpon (a rural site) in Pinellas County had the highest increase (12 ppb) in peak ozone concentrations. Suburban sites in Pinellas County were projected to show nearly no increases in maximum O_3 levels in the year 2000. Three sites in Hillsborough County, including two suburban sites and one unidentified site, would experience nearly identical increases (7, 6 and 6 ppb) in peak ozone concentrations.

For the July 23 case, decreases in peak ozone concentrations were predicted at every site in the Tampa Bay area in 2000. The East Lake Tarpon and the Clearwater J.C.
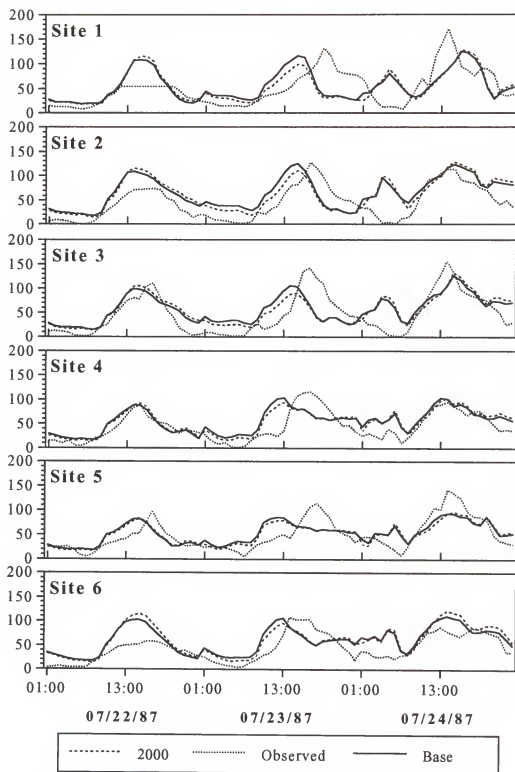
Figure 5.38. Comparisons of ozone concentrations for base case prediction , and observations (1987), and prediction for the year 2000 case at each monitoring site. (Unit:ppb)

campus sites in Pinellas County had the same decrease (10 ppb) in peak ozone concentrations, and the Azalea Park site was projected to experience a 7 ppb O_3 decrease in the maximum value. Three sites in Hillsborough County would also experience nearly identical decreases (17, 15 and 16 ppb) in peak ozone concentrations.

Increases in ozone concentrations were predicted at all monitoring sites for the ozone episode situation on July 24 for year 2000, except for the Clearwater J.C. campus site (-1 ppb) in Pinellas County. The East Lake Tarpon site in Pinellas County would experience the largest increase (11 ppb) in peak ozone concentration as it did for the July 22, 2000 case. The other site in Pinellas County would be expected to show only a 3 ppb increase in peak ozone. Relative largely increases in maximum ozone concentrations were predicted at the suburban sites in Hillsborough County (5 and 6 ppb), but the Simmons County Park site (1) would experience a small increase (3 ppb) in peak ozone.

The ratios of VOC/NO_x for mobile source emissions in the Tampa area are generally relatively low (≤ 2), so an increase in the total mobile source emissions, and control of VOC emissions alone would have an overall effect of reducing the VOC/NO_x ratios in the ambient air. A larger increase in mobile source emissions (32%) was predicted for Hillsborough County when compared to Pinellas County (15%), which tended to create lower VOC/NO_x ratios in Hillsborough County, therefore, the "VOC-only" control strategy should be more effective in Hillsborough County than in Pinellas County. This factor could be one of the reasons why sites in Hillsborough County should experience larger decreases in peak ozone concentrations than corresponding sites in Pinellas County for the July 23, 2000 case.

Passage of the sea breeze front for the July 23 case could also contribute to a decrease in peak ozone concentrations. The sea breeze front was beyond the Pinellas County border at 15:00 hr on July 23. Strong uplifting flow would pump up the generated high concentrations of O_3 from the surface to higher elevations, meanwhile the increase in NO emissions would titrate out more of the O_3 remaining over the surface. In

addition to the latter factor, reduction of VOCs in the Tampa Bay area could contribute to predicted decreases in peak ozone concentrations under the passage of sea breeze front.

For the case of July 22, the sea breeze front only reached the shore along the Gulf coast. The uplifting flow only had a slight influence on the suburban sites in Pinellas County, therefore, there was nearly no increase in peak O_3 concentrations. The rural site (East Lake Tarpon) in Pinellas County is relatively further away from the sea breeze front, and was influenced more by an increase in emissions in the surrounding suburban area, therefore, it would be expected to experience the highest increase in peak ozone concentrations. The increase in ozone peak concentrations predicted at East Lake Tarpon could also be explained on the basis of a change in emission inventory. Since the site is located in a rural area, a high ambient VOC/NO_x ratio would be expected, and the increase in mobile source emissions is expected to be less than those in a suburban area. The decrease in VOC/NO_x ratio is expected to be smaller, as a result, the control in VOCs emissions would be less effective, and the increase in peak ozone concentrations would be the highest. Since the sea breeze front did not extend to Hillsborough County, the higher emissions projected in 2000 would lead to an increase in ozone peak concentrations.

A similar change in ozone peak concentrations on July 24, was predicted at the Tampa Bay area sites as compared to the case two days previously (July 22). The surface air flows along the northern coast of the Tampa Bay area were similar to those on July 22. To the south of the Tampa Bay area, the sea breeze front moved further into the shore line of the bay as compared to the front on July 22. This difference in penetration would lead to a lower increase in peak ozone concentrations at Simmons County Park in Hillsborough County. The justifications used for the July 22 case could be used also to explain the change in peak ozone concentrations at the other sites in the Tampa Bay area.

Figures 5.39 and 5.40 show contour plots of ozone concentration differences ($\Delta O_3 = O_3^{2000} - O_3^{1987}$) between the July 22 case in 2000 and that in 1987. The relative increase

154
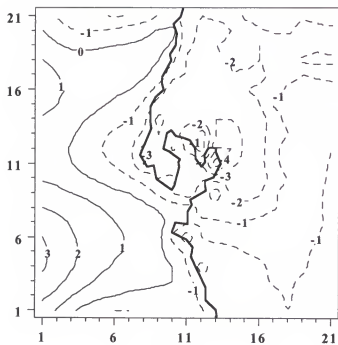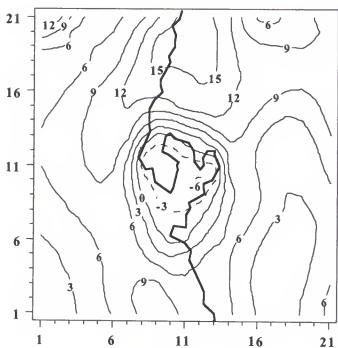
(a) 07:00 hr

(b) 13:00 hr

Figure 5.39. Isopleths of differences in predicted ozone concentrations for July 22, 1987, and July 22, 2000. (a) 07:00 hr, and (b) 13:00 hr.
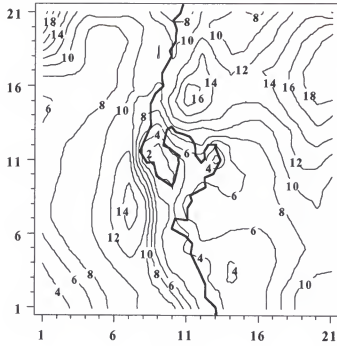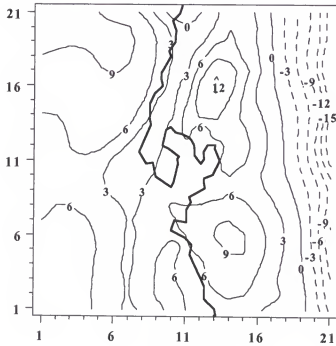
(a) 17:00 hr

(b) 23:00 hr

Figure 5.40. Isopleths of differences in predicted ozone concentrations for July 22, 1987, and July 22, 2000. (a) 17:00 hr, and (b) 23:00 hr.

in NO_x emissions in 2000 would reduce ozone concentrations over land areas within the domain at 07:00 hr (Figure 5.39 (a)). Except for half of Pinellas County and Tampa Bay, O_3 concentrations would increase at 13:00 hr (Figure 5.39 (b)), as a result of the larger NO_x emissions in 2000. Four hours later (17:00 hr), an increase in ozone concentrations (Figure 5.40 (a)) would be recorded all over the domain. At 23:00 hr (Figure 5.40 (b)), the area with a relatively large increase in O_3 originally in the northeast of the domain, would move to the west and be titrated at the same time by the increased emissions of NO_x. The NO_x emissions in late evening would not be strong enough to titrate all of the ozone increase, therefore, most of the land surface within the domain would experience an increase in ozone over year 1987 level. There would be a decrease in ozone concentrations observed close to the eastern boundary of the domain. This effect could be due to the decline in O_3 beyond the eastern boundary of the domain, which could result from titration by larger fractional increases in NO_x emissions for the counties in central Florida before being transported into the east boundary of the domain.

Passage of the sea breeze front through the Tampa Bay area on July 23 created different ozone isopleth plots (Figures 5.41, and 5.42) from those predicted for the July 22 case. In the morning (07:00 hr), nearly the entire domain showed a decline in O_3, since NO_x emissions would have increased in 2000. The decline in O_3 would be limited only to the Tampa Bay area, and the east and southeast part of the domain at 13:00 hr. As mentioned earlier, passage of the sea breeze front and VOC controls would cause a decrease in peak ozone levels in the Tampa Bay area. An increase in generated O_3 could not compensate for the decline in O_3 in the morning in the southeast, which is a relatively low emissions area. In the northern part of the land surface, larger fractional increase in emissions by the year 2000, due to higher population growth and no emissions control enforcement, could cause an increase in O_3 for that area.

As the sea breeze front moved further inland, the area of declining O_3 also shifted inland. At 17:00 hr, the center of the predicted O_3 decline (Figure 5.42(a)) would move
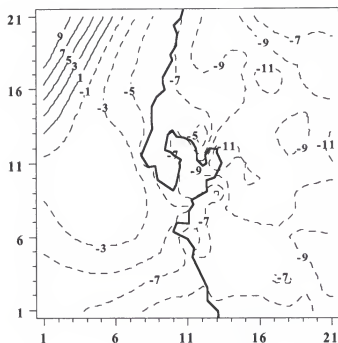
(a) 07:00 hr
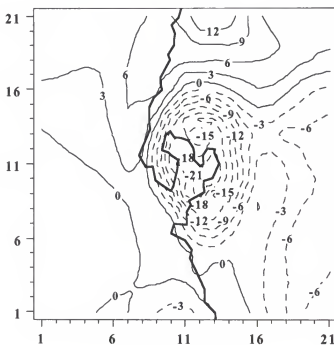
(b) 13:00 hr

Figure 5.41. Isopleths of differences in predicted ozone concentrations for July 23, 1987, and July 23, 2000. (a) 07:00 hr, and (b) 13:00 hr.
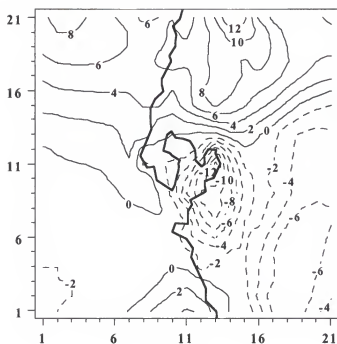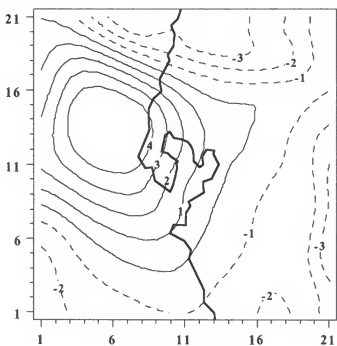
Figure 5.42. Isopleths of differences in predicted ozone concentrations for July 23, 1987, and July 23, 2000. (a) 17:00 hr, and (b) 23:00 hr.

about 20 km within 4 hours, which is about the same speed as the estimated sea breeze front (1.4 m/s) as it passed the Tampa Bay area. After 6 hours (Figure 5.42 (b)), the continued sea breeze brought to the area an increase in O_3 from the Gulf to the Tampa Bay area. Since a relatively larger fractional increase in emissions would be expected to the north of the Tampa Bay area (Pasco, Hernando and Citrus counties), associated stronger emissions of NO_x would quickly titrate out the O_3. Thus, an O_3 decline was observed at the northern boundary in the late evening.

Figures 5.43 and 5.44 show the differences in O_3 concentrations between the estimates for July 24, 1987, and projections for July 24, 2000. The O_3 increase zone would move to the Tampa Bay area from an region that was originally an extension of the O_3 increase zone at the northeast boundary of the domain in the early morning. Since an increase in O_3 would be titrated out by the greater morning emissions of NO_x in the Tampa Bay area in the year 2000, an area of negative O_3 change at 07:00 was projected to the east of the Tampa Bay area. The only predicted "O_3 decline" areas at 13:00 hr would be those surrounding Tampa Bay. Four hours later (Figure 5.44 (a)), the predictions indicated that the O_3 concentrations would be increased by the year 2000. Under the same meteorological conditions as on July 24, 1987, however, the increase would be small in the Tampa Bay area when compared to urban growth areas in the vicinity. In the late evening (Figure 5.44 (b)), the areas with the larger O_3 increases would allow for transport from Pasco County to the north of the Tampa Bay area, and could cause a higher O_3 increase than at 17:00 hr. At the same time, increased NO_x emissions in 2000 could titrate out some of this O_3 increase.

5.7 A Case Study of the Spring 1987 Ozone Episode

The ozone episode which occurred on April 23, 1987 had very different meteorological characteristics when compared to the episodic situation occurring from July 22 to July 24, 1987. An intensive cold front system, which extended from the south
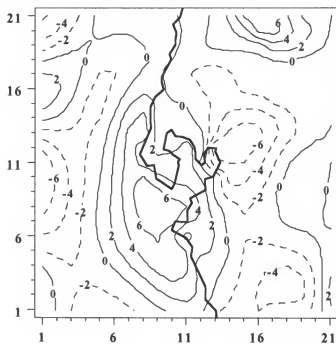
(a) 07:00 hr
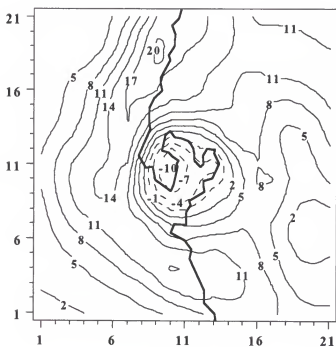
(b) 13:00 hr

Figure 5.43. Isopleths of differences in predicted ozone concentrations for July 24, 1987, and July 24, 2000. (a) 07:00 hr, and (b) 13:00 hr.
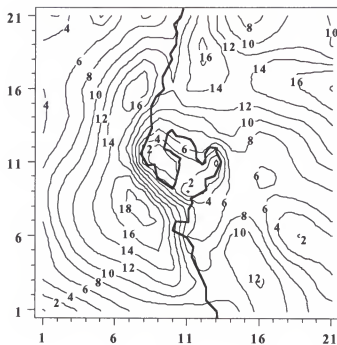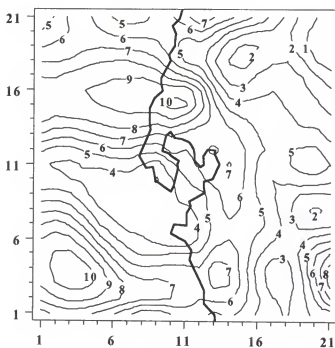
(a) 17:00 hr

(b) 23:00 hr

Figure 5.44. Isopleths of differences in predicted ozone concentrations for July 24, 1987, and July 24, 2000. (a) 17:00 hr, and (b) 23:00 hr.

of Greenland to Texas was observed at 07:00 hr on April 21, 1987. This cold front system moved eastward, and formed another low pressure center in Ohio at 19:00 hr on April 22, 1987. At this time, the cold front approached the Florida panhandle area. At 07:00 hr on April 23, 1987, a third low pressure center formed over Georgia, and the frontal system moved further eastward. The air flow along the west coast of Florida varied from north to northwest at this time. Twelve hours later, the cold front had passed the Florida panhandle area, and moved south across the rest of Florida. The low pressure system associated with the cold front covered the entire central and north Florida region, therefore, a westerly wind was observed along the west coast. The cold front arrived in the Tampa Bay area at 07:00 hr on April 24, 1987.

The maximum ozone concentration (129 ppb) was observed at 13:00 hr on April 23, 1987. All the monitoring sites detected ozone concentrations (Figure 5.45) which were higher than 60 ppb even after sunset. Three sites in Pinellas County recorded relatively constant ozone levels after 09:00 hr, 11:00 hr and 12:00 hr, and slight increases in O_3 during the evening on April 23, 1987. One of the sites in Hillsborough County also recorded a significant increase in ozone in the evening. The occurrence of relatively constant ozone concentrations continued for more than one day. Predicted ozone levels using the STEM-II model only reached a typical average peak O_3 level (40-50 ppb) in the Tampa Bay area. The existing model has difficulty in predicting this type of event.

On the basis of back trajectory analyses (Figure 5.46), the air masses flowed directly from the Gulf to the Tampa Bay area. Since the air masses originated from outside the simulation domain, prior assumptions of the boundary conditions were not valid. Real measurements are required to provide the boundary conditions to predict the ozone concentrations in the Tampa Bay area for this case. Forward trajectory analyses (Figure 5.47) suggested that the polluted air masses would continuously move across central Florida.
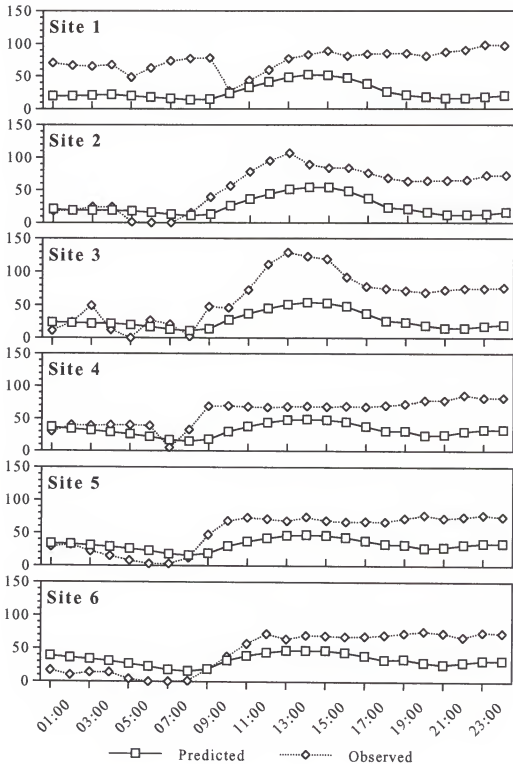
Figure 5.45. Comparisons of predicted and observed hourly ozone concentrations at each of the monitoring sites in the Tampa Bay area on April 23, 1987.
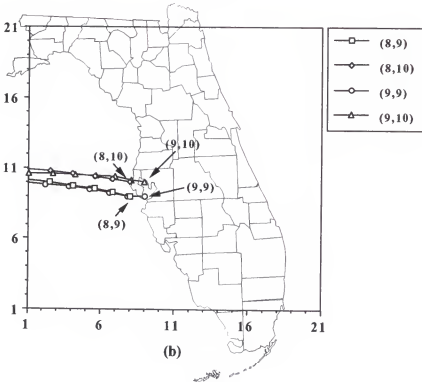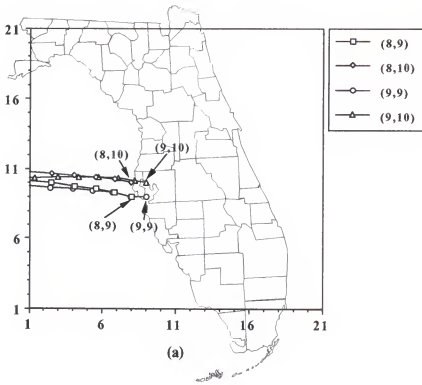
Figure 5.46. Horizontal back trajectories started at (a) 13:00 hr, on 04/23/87; and (b) 14:00 hr, on 04/23/87.
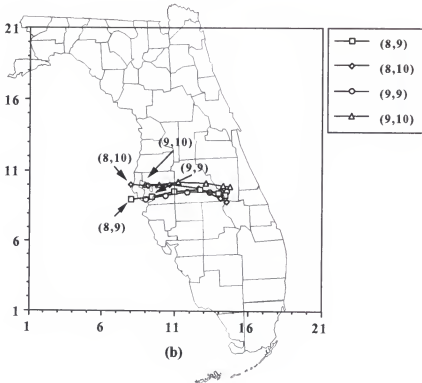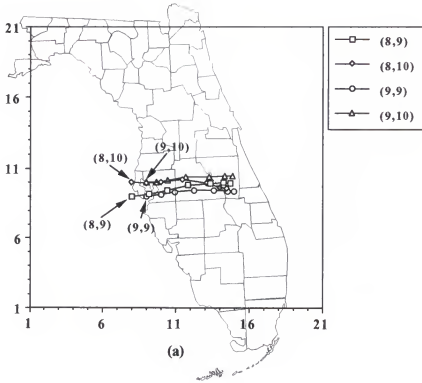
Figure 5.47. Horizontal forward trajectories started at (a) 13:00 hr, on 04/23/87; and (b) 14:00 hr, on 04/23/87.

There were two possible long term sources of ozone and/or its precursors which could contribute to the exceedance of the ozone NAAQS, and to relatively high O_3 concentrations during the evening of April 23, 1987. The first source was intrusion of stratospheric ozone. Since the strongest intrusion of stratospheric ozone occurs normally in spring (Danielsen and Mohnen, 1977), this could be the critical source of ozone. The other possible source was long term transport from another part of the continent, such as Houston, TX., or Mexico City, Mexico.

On the basis of a stratospheric ozone study by Viezee et al. (1983), intrusion of stratospheric ozone could explain the occurrences of the ozone exceedance and the high background ozone levels after sunset. Viezee et al. suggested that the intrusion of stratospheric ozone is associated with the presence and location of a 500 mb trough. They also suggested that the intrusion area could be located at either the front or rear part of a trough at the 500 mb surface, and cover an area up to 500 km diameter over or behind a cold front system at the surface. On April 23, 1987, a 500 mb trough moved into the eastern part of the U.S. at 07:00 hr, and the line of the cold front was about 400 km from the Tampa Bay area over the Gulf. Day time mixing could convey the intruded ozone in front of the cold front to the surface. The ozone received later in the day might contribute to the flattening of the ozone concentration levels in Pinellas County in the afternoon. Also, the latter could have raised the background level of ozone in Hillsborough County. In addition to intrusion of stratospheric ozone, ozone generated due to local emissions could have contributed to the exceedance of the O_3 NAAQS for at least one of the sites in Hillsborough County.

Theoretically, the downdraft of air at the cold front can also bring ozone-rich air to the ground (Johnson and Viezee, 1981). The ozone being carried down to the surface by the cold front over the Gulf could be transported into the Tampa Bay area. In the evening, the cold front moved closer to the Tampa bay area, resulting in the intrusion center being closer to the Tampa Bay area. The higher ozone levels in the intrusion

center may compensate for increasing NO emissions during heavy traffic hours in the evening of April 23, 1987. Also, this condition may have caused the slight increases in ozone concentrations that were observed in the evening in Pinellas County. Ozone rich air masses were transported from Pinellas County to the Tampa area and mixed with the emissions from the area, therefore, the ozone concentrations could exceed the NAAQS at the Hillsborough County site. The ozone concentrations did decrease after the early afternoon peak at two of the Hillsborough County sites, but they maintained relatively high values (≥ 60 ppb) in the late afternoon and increased slightly in the evening. The ozone levels were relatively constant throughout the next day (April 24, 1987), while the cold front passed the Tampa Bay area.

Long term transport of ozone and its precursors from other urban areas might be the alternate cause of the ozone episode on April 23, 1987. Since there were no ozone measurements over the Gulf, it is impossible to demonstrate the influence of emissions from other urban centers outside the state of Florida. As polluted air masses were transported across the Gulf, the main removal mechanism for pollutants would be dry deposition. Dry deposition of ozone over water surfaces normally is much lower than that over land surfaces. Thus, air masses could maintain high ozone concentrations during transport processes across the Gulf, and then, could have a significant impact on the background ozone levels in the Tampa Bay area.

Since there were no ozone measurements over the Gulf or at high altitudes, it is difficult to determine the sources of excess ozone. Both potential sources could have contributed to the ozone episode. For example, stratospheric ozone could have contributed to ozone levels in other urban areas where the cold front had passed before it reached the Tampa Bay area. Subsequently, the mixed urban-stratospheric ozone air masses could have been transported to Tampa Bay. In order to understand this type of ozone episode, however, vertical and horizontal profiles of ozone over the Gulf of Mexico should be measured.

5.8 O$_3$ Control Strategies

Good control efforts should be able to ensure that the maximum ozone concentrations in urban areas are below the ozone NAAQS in the future. Currently, the design of O$_3$ control strategies are based on applying the local VOC/NO$_x$ ratio (ppbC/ppb or ppmC/ppm) to the EPA-recommended EKMA model. U.S. EPA has also recommended specifically that ambient VOC/NO$_x$ ratios in the range for the time period between 06:00 hr and 09:00 hr should be used. If the ratio of VOC/NO$_x$ is greater than 10, then reduction of NO$_x$ is more effective than controlling the VOCs in lowering the maximum ozone level. For a low VOC/NO$_x$ ratio, only VOCs should be reduced to be effective in controlling peak O$_3$ levels.

The ratios of VOC (ppmC) to NO$_x$ (ppm) from 6 a.m. to 9 a.m. were calculated for the two episodic days July 23 and July 24, 1987, and also for the case of the year 2000. Information from VOC/ NO$_x$ ratios during the ozone episode could be used to evaluate the current control strategies for the Tampa Bay area. Those ratios projected for the year 2000, could be used as a basis for adjusting control strategies in the future.

Isopleths of VOC/NO$_x$ ratios on July 23, 1987, are shown in Figure 5.48 (a). Pinellas County was in the region where the VOC/NO$_x$ ratio was between 5 to 10. Two-thirds of Hillsborough County was within an area where the VOC/NO$_x$ ratio was less than 10. There were two small regions in Hillsborough County that had ratios smaller than 5. The lowest ratio of 2 was due to the strong emissions of NO$_x$ from two electrical utility companies. A ratio of 7 was observed at more grid points than any other value in the Tampa Bay area. Other parts of the domain over the land surface normally had a ratio greater than 20. The north part of the domain over the land (Pasco, Sumter, and Hernando counties) showed lower ratios of VOC/NO$_x$ when compared to the southeast part of the domain (Hardee and De Soto counties), because there were higher population densities to the north of the Tampa Bay area. One third of Pasco County was in the area

(a) Year 1987 Case

(b) Year 2000 Case

Figure 5.48. Isopleths of VOC/NOx ratios (ppmC/ppm) for the years (a) 1987, and (b) 2000 cases, on July 23.

having a ratio less than 10. To the south of the Tampa Bay area, only a small region, around Sarasota, had a ratio less than 10. High VOC/NO_x ratios were obtained over the water surface, which could be due to the higher dry deposition velocities for NO_x as compared to VOCs.

For the case of the year 2000 (Figure 5.48(b)), the areas with VOC/NO_x ratios from 5 to 10, and below 5 are expanded to about twice their original (1987) size. In addition to Pinellas County, nearly the whole of Hillsborough, and three fourths of Pasco counties were in an area where the ratio was less than 10. Projected ratios between 5 and 10 were observed also along the Gulf coast from Bradenton to Sarasota. This change probably was due to an 8% reduction of VOCs in vehicle emissions and an increase in the density of mobile source emissions. The ratio 5 occurred more frequently within the domain than any other ratio. The distributions of VOC/NO_x ratios for 2000 were similar to the 1987 case, except that the ratios were generally lower.

Suggested control strategies for VOCs, NO_x, and VOCs and NO_x on July 23, 1987 and for the year 2000, are listed in Table 5.5. Generally, the Tampa Bay area showed VOC/NO_x ratios from 4 to 10. If the ratio was 10, a 36.8% reduction of VOCs was required to reduce ozone from 142 ppb to 120 ppb, alternatively a 43.8% reduction of NO_x was necessary to lower the ozone to 120 ppb. In those areas where the ratio was 4, only a 6.8% reduction in VOCs would diminish the ozone levels to the NAAQS, but an 80.8% reduction of NO_x was needed to achieve the desired end point. A major region of Tampa bay had a VOC/NO_x ratio equal to 7 for the 1987 case, and 5 for the 2000 case. A VOC control strategy would be proper, but at least 34% and 27.5% reduction of VOC would be required for these areas with ratios of 7 and 5, respectively. If VOCs and NO_x were controlled at the same time by following the constant VOC/NO_x ratio, the sum of required VOCs and NO_x reduction factors would normally be greater than 50%, except for those areas with VOC/ NO_x ratios less than 4.

Table 5.5. Suggested ambient NO_x and VOC reductions ratios (%) that should meet the ozone NAAQS for the observed and simulated ozone episodes on July 23, 1987, and year 2000, respectively.

ITEM		VOC(ppmC)/NO_x(ppm) Ratio						
		10/1		7/1		5/1		4/1
A. VOCs Reduction Only								
142 ppb (Peak Ozone)		0.400*		0.347		0.313		0.336
120 ppb (NAAQS)		0.240		0.229		0.227		0.313
% Reduction		36.8		34.0		27.5		6.8
B. NO_x Reduction Only								
142 ppb (Peak Ozone)		0.040†		0.049		0.068		0.130
120 ppb		0.023		0.026		0.029		0.030
% Reduction		43.8		46.9		57.4		80.8
		10/1		7/1		5/1		4/1
C. VOCs & NO_x	VOC	NO_x	VOC	NO_x	VOC	NO_x	VOC	NO_x
Reduction	0.400	0.040	0.347	0.049	0.313	0.068	0.336	0.130
142 ppb	0.307	0.029	0.263	0.036	0.233	0.048	0.277	0.106
120 ppb	23.3	28.0	24.2	26.5	25.6	29.4	17.6	18.5
% Reduction								

* The VOC values for the corresponding ozone concentrations from the EKMA model.
† The NO_x values for the corresponding ozone concentrations from the EKMA model.

The VOC/NO_x ratios for the whole domain (Figure 5.49 (a)) on July 24, 1987, showed some differences from those for July 23, 1987. The land area having VOC/NO_x ratios of 10 or less was smaller than that for the previous day. A major part of Pinellas County was still in the range, with ratios from 5 to 10, but only the region around Tampa Bay in Hillsborough County was in this range with ratios from 5 to 10, and less than 5. A ratio of 6 was observed more frequently within the Tampa Bay area.

For the case of year 2000 (Figure 5.49(b)), the areas with the ratios from 5 to 10 extended tremendously northward and southward. The ratio 5 occurred more frequently within the domain than others. Almost all of Pinellas, and two thirds of Hillsborough counties were covered by the area with VOC/NO_x ratios less than 10. An area with ratios
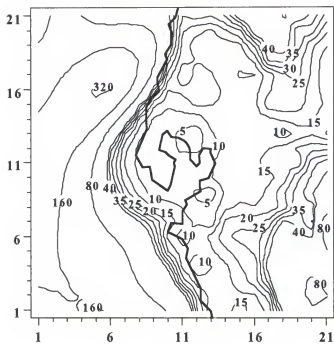
(a) Year 1987 Case
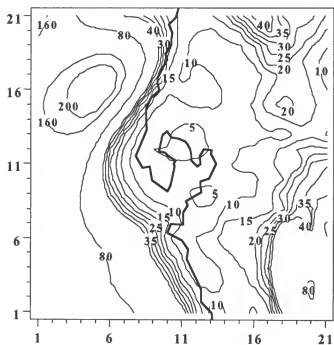
(b) Year 2000 Case

Figure 5.49. Isopleths of VOC/NOx ratios (ppmC/ppm) for the years (a) 1987, and (b) 2000 cases, on July 24.

from 5 to 10, was observed also in some parts of Pasco and Hernando counties, and along the Gulf coast from Bradenton to Sarasota. The distributions in the VOC/NO_x ratios were similar to the 1987 case.

Greater reductions in VOCs, NO_x, and combinations of VOCs and NO_x were required for the ozone episode on July 24 in both year 1987 and 2000. The suggested control strategies for VOCs, NO_x, and VOCs and NO_x on July 24, 1987 and for the year 2000, are listed in Table 5.6. A lesser reduction in NO_x (42.3%) than for VOC (55.8%) was required for areas with VOC/ NO_x ratios of 10. The majority of the region in the Tampa bay area had a VOC/NO_x ratio of 6 for the 1987 case, and 5 for the 2000 case. A VOC control strategy would be proper in both cases, but at least 42% and 37.5% in

Table 5.6. Suggested ambient NO_x and VOC reductions ratios (%) that should meet the ozone NAAQS for the observed and simulated ozone episodes on July 24, 1987, and year 2000, respectively.

ITEM		VOC(ppmC)/NO_x(ppm) Ratio						
		10/1		6/1		5/1		4/1
A. VOC Reduction Only								
171 ppb (Peak Ozone)		0.520*		0.413		0.400		0.480
120 ppb (NAAQS)		0.230		0.240		0.250		0.400
% Reduction		55.8		41.9		37.5		16.7
B. NO_x Reduction Only								
171 ppb (Peak Ozone)		0.052†		0.068		0.080		0.186
120 ppb		0.030		0.030		0.030		0.030
% Reduction		42.3		55.9		62.5		83.9

		10/1		6/1		5/1		4/1	
C. VOC & NO_x									
Reduction	VOC	NO_x	VOC	NO_x	VOC	NO_x	VOC	NO_x
171 ppb	0.520	0.051	0.400	0.080	0.500	0.187	0.413	0.068
120 ppb	0.306	0.028	0.240	0.045	0.280	0.107	0.240	0.040
% Reduction	41.2	44.7	40.0	43.8	44.0	42.8	41.9	35.0

* The VOC values for the corresponding ozone concentrations from the EKMA model.
† The NO_x values for the corresponding ozone concentrations from the EKMA model.

VOCs reduction were required for these areas with VOC/NO$_x$ ratios of 6 and 5, respectively. The combined VOCs and NO$_x$ reduction ratios would normally be greater than 77% for nearly all of the Tampa Bay area.

VOC/NO$_x$ ratios predicted in the Tampa Bay area were similar to those observed in other urban areas of the U.S. The VOC/NO$_x$ ratios observed in some urban areas (Wolff and Korson, 1992), such as Philadelphia, Atlanta, St. Louis, and New York were found to be in the range from 5 to 11.4. The ratios increased during a high ozone day in those areas, but most of the time the ratio fell in the range from 7 to 10.

The control strategies discussed in this subsection were developed on the basis of predicted ambient level of VOCs and NO$_x$. The reduction rates indicate that the ratios of ambient VOCs and/or NO$_x$ were required to decrease   Wolff and Korson (1992) suggested that the correlation coefficients between the 06:00 hr to 09:00 hr VOC/NO$_x$ ratio and the 1-hr maximum ozone were very low ($\leq$ 0.20). Thus, this approach in reducing photochemical oxidants could be controversial, but the method definitely provides a general guideline for planning ozone control strategies.

It is not surprising that ambient levels of VOCs and NO$_x$ do not always have strong correlations with emissions of VOCs and NO$_x$, since they are the result of different processes in the atmosphere, such as mixing, deposition, emission, and generation. Suggestions for control strategies based on emission reductions could be different from those based on ambient levels of VOCs and NOx. Control strategies suggested by simulations of VOCs and/or NOx emission reductions are discussed in the following subsection.

5.9 Projected Control Strategies for VOC and NO$_x$ Emissions

In order to predict the effects of VOCs and NO$_x$ emissions control, model simulations were performed for six case studies with; 1) 75% of existing VOCs, 2) 50% of existing VOCs, 3) 75% of existing NO$_x$, 4) 50% of existing NO$_x$, 5) 75% of existing

VOCs and NO_x, and 6) 50% of existing VOCs and NO_x, where the existing emissions of pollutants refer to those estimated for 1987. The lowering of VOCs emissions did not include biogenic emissions, since they cannot be controlled. The reductions in VOCs and/or NOx emissions were assumed to be consistent over the entire domain. Differences in O_3 peak concentrations discussed in this section, are from comparisons between those for the various study cases and for the base case prediction described in the previous subsection.

Expected decreases or increases in peak ozone concentrations are listed in Table 5.7. Generally, the reduction of VOCs emissions could induce a decrease in peak ozone concentrations for the July 22 case. The site with the smallest decrease in peak ozone concentrations was the rural site 6 (East Lake Tarpon) in Pinellas County, when only

Table 5.7. Differences in peak ozone concentrations for various VOCs and NO_x reduction cases as compared to the base case.

Item	Site 1	Site 2	Site 3	Site 4	Site 5	Site 6
07/22/87						
VOC 75%	-6	-6	-7	-13	-19	-5
VOC 50%	-8	-9	-10	-16	-24	-7
NOx 75%	+4	-5	-2	+0	+1	-7
NOx 50%	+14	-7	-1	+13	+18	-13
VOC, NOx 75%	-11	-8	-5	-6	-6	-12
VOC, NOx 50%	+6	-12	-8	+1	+6	-16
07/23/87						
VOC 75%	-37	-36	-38	-30	-17	-31
VOC 50%	-41	-42	-44	-37	-21	-37
NOx 75%	-10	-15	-11	-11	-9	-12
NOx 50%	+10	-8	+6	-4	-8	-6
VOC, NOx 75%	-16	-21	-19	-17	-12	-18
VOC, NOx 50%	+1	-18	-5	-15	-13	-16
07/24/87						
VOC 75%	-29	-14	-17	-21	-19	-7
VOC 50%	-39	-20	-24	-28	-25	-10
NOx 75%	+5	-6	-4	-5	-5	-9
NOx 50%	+19	-12	-5	+0	+6	-20
VOC, NOx 75%	-5	-11	-10	-12	-12	-12
VOC, NOx 50%	+5	-18	-13	-11	-9	-23

VOCs were controlled. This site could be in an area with high VOC/NO$_x$ ratios, therefore, reduction of NO$_x$ emissions could reduce ozone more effectively than reduction of VOC emissions. The site (5) with the largest decrease in peak ozone concentrations was Azalea Park site for VOCs reductions, but reduction of NO$_x$ at this location would lead to an increase in peak ozone concentrations. The maximum ozone concentration (111 ppb) was observed at Tampa pump station site on July 22, 1987, in this case any reduction of VOCs and NOx would not cause an exceedance of the ozone NAAQS.

On the basis of the episodic day July 23, 1987, reduction of VOCs could induce a decrease in ozone peak levels more effectively than on the previous day, July 22, 1987. A 25% reduction of VOCs (75% VOC emissions) could reduce ozone more than 30 ppb, except for the Azalea Park site (5). The exceedances of ozone NAAQS observed on July 23, 1987 were 131, 127, and 142 ppb at Simmon County Park (site 1), Davis Island (site 2), and Tampa Pump Station (site 3) sites, respectively. Less than 25% VOCs reduction were required to decrease ozone concentrations to meet the ozone NAAQS at all sites in the Tampa Bay area.

It would be very difficult to reduce the ozone concentrations to meet the ozone NAAQS for the case on July 24, 1987. The excess (above NAAQS) ozone concentrations which were required to be eliminated on July 24, 1987 were 51, 36, and 22 ppb at Simmons County Park (site 1), Tampa Pump Station (site 3), and Azalea Park sites, respectively. The ozone NAAQS could not be achieved at both Simmon County Park and Tampa Pump Station sites, even with a 50% reduction in VOCs. Azalea Park site would require nearly 50% VOCs reduction to meet the ozone NAAQS.

Since only 6 studies were attempted, employment of the Kriging algorithm and one additional assumption were used to construct relationships between variations in peak ozone concentrations and corresponding VOCs and NO$_x$ emission ratios. The background level (remote rural site) in peak ozone concentrations was assumed to be 30

background level (remote rural site) in peak ozone concentrations was assumed to be 30 ppb without any influence from anthropogenic emissions. The Kriging algorithm is a weighted fill method (Fortner, 1992) that automatically calculates the 'best' weighting function and cut-off radius at every missing data point. On the basis of the designed analyses, more precise control strategies could be obtained.

Data plotted in Figure 5.50 indicate that about an 8% VOC reduction alone could relieve the non-attainment status in the Simmons County Park area. It would be impossible, however, to fulfill the ozone NAAQS with NO_x emission control. For the Davis Island site, only 5% VOC reduction alone, or 10% NOx reduction alone (Figure 5.51) could reduce the peak ozone concentrations to meet the ozone NAAQS. Roughly, 18% VOC only reduction (Figure 5.52) would be required to reduce the peak ozone level to lower than 120 ppb at Tampa Pump Station site. The ozone NAAQS could not be met, however, with only NO_x emissions control.

Since a reduction of 51 ppb ozone was required at the Simmons County Park area, either VOCs only or NOx only control strategy would not be effective in lowering the peak ozone concentrations to the ozone NAAQS. At least a 76% reduction (Figure 5.53) for both VOCs and NOx emissions would be needed to reach the ozone NAAQS. For the Tampa Pump Station site, 90% VOC reduction alone (Figure 5.54) would enable resulting ozone concentrations to meet the ozone NAAQS, but it is impossible to achieve such a reduction efficiency. At least a 60% reduction in both VOCs and NOx emissions would be the another approach to reach the ozone NAAQS. Approximately, 40% VOC only reduction (Figure 5.55) would be required to lower the peak ozone level below 120 ppb at Azalea Park site. The ozone NAAQS could not be met, however with NO_x only emissions control.

From a practical viewpoint, a VOC control strategy could be the best approach in reducing peak ozone levels for some meteorological conditions. Unfortunately, such an effort could not be successful in achieving the 120 ppb goal when meteorological
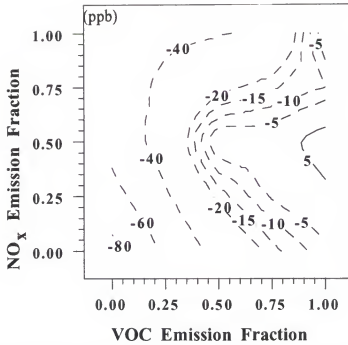
Figure 5.50. Isopleths of peak ozone concentration changes (ppb) for corresponding VOCs and NOx emissions fractions at site 1 on July 23, 1987.
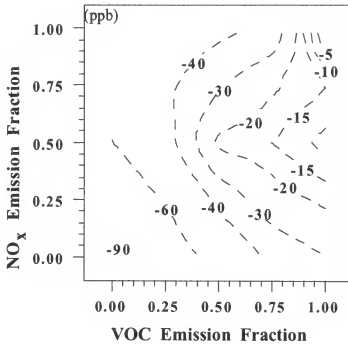
Figure 5.51. Isopleths of peak ozone concentration changes (ppb) for corresponding VOCs and NOx emissions fractions at site 2 on July 23, 1987.
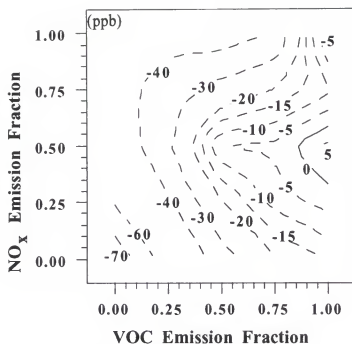
Figure 5.52. Isopleths of peak ozone concentration changes (ppb) for corresponding VOCs and NOx emissions fractions at site 3 on July 23, 1987.
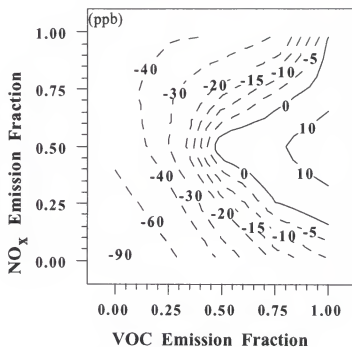
Figure 5.53. Isopleths of peak ozone concentration changes (ppb) for corresponding VOCs and NOx emissions fractions at site 1 on July 24, 1987.
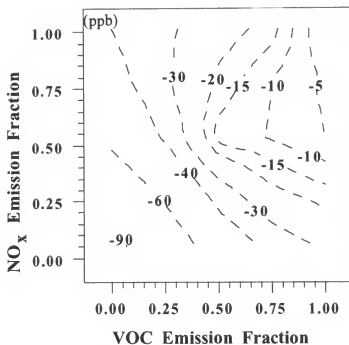
Figure 5.54. Isopleths of peak ozone concentration changes (ppb) for corresponding VOCs and NOx emissions fractions at site 3 on July 24, 1987.
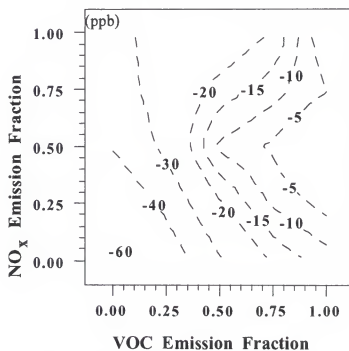
Figure 5.55. Isopleths of peak ozone concentration changes (ppb) for corresponding VOCs and NOx emissions fractions at site 5 on July 24, 1987.

conditions occur similar to the ozone episode of interest. Meteorological conditions, alone, however, were not the only important factors in causing ozone non-attainment problems, nor for limiting the selection of control strategies.

CHAPTER 6
SUMMARY AND CONCLUSIONS

The main purpose of this research was to simulate the worst recorded ozone episode in Tampa Bay using a combination of meteorological (MM4) and air quality (STEM-II) models, in order to evaluate the effects of the coastal meteorology on ozone air quality, and the effectiveness of current control strategies in the Tampa Bay area. To achieve this purpose, meteorological conditions were simulated and evaluated during the first phase of research. Transport and chemical simulations were conducted and evaluated in the second phase of the study. Evaluations of current and possible future control strategies were accomplished during the third phase of work.

On the basis of the research that was conducted, the following conclusions may be drawn:

1. Separate dry deposition velocities for pollutants over land and water surfaces should be used for the corresponding types of surfaces in the domain during the simulations. If only land-based dry deposition velocities are used in maritime areas, the simulations could underpredict the average ozone peak concentrations by as much as 25 ppb. Comparisons of simulation results show that changes in dry deposition velocities could significantly affect the predicted maximum ozone concentrations. Dry deposition is a complicated process, which depends on the characteristics of chemical species, types and conditions of deposition surfaces and meteorological conditions. Dry deposition velocities, therefore, can vary over a wide range of values even for the same type of surface and the same time period. Also, dry deposition velocities for most of the chemical species included by the model are not well known or are unknown. The STEM-II model can incorporate a

182

dry deposition algorithm to describe dry deposition velocities more accurately, but this facility would cost much more in terms of computer resources than pre-determined data sets.

2. Concentrations of chemical species under moderate pollution conditions are appropriate initial boundary conditions for land-water body boundaries in air quality simulations of coastal airsheds, if similar meteorological conditions exist over land and water surfaces. It was more realistic in this work that concentration of pollutants at the boundary could be used as new boundary conditions for the following time step, when compared to incorporation of constant boundary conditions.

3. Better overall model performances were obtained for the episodic case of July 22, 1987 than for July 23 and 24, 1987. This result could be due to less complex meteorological conditions, especially wind fields occurring on July 22, 1987. On July 22, 1987, relatively uniform wind fields were predicted over the land surfaces for the entire day. The accuracy of estimated pollutant emissions could be the main factor affecting the performance of model simulations when compared to the influences of meteorological predictions for simplistic wind fields.

4. Performance of the STEM-II model on July 23, 1987 was the worst when compared to the adjacent episodic days. The best correlation coefficient obtained was only 0.63 at East Lake Tarpon in Pinellas County, which is a rural monitoring site. The passage of a sea breeze front led to complicated 3-D meteorological wind fields, which could be difficult to predict accurately by the MM4 model with insufficient observational data and relatively low spatial resolution. Performance of the STEM-II model could have been controlled primarily by the accuracy of meteorological predictions instead of emission distributions under these meteorological conditions.

5. Predicted ozone concentrations were closer to the observed ozone levels for July 24, 1987 than for corresponding comparisons on July 23, 1987. The predicted

meteorological conditions along the coast showed some similarity to those predicted during the daytime of July 22, 1987. The sea breeze was limited along the coast in the north of Tampa Bay, therefore, a better model performance was expected.

6. The model performed reasonably well in terms of predicting peak ozone concentrations and day time ozone levels. The peak prediction accuracy for unpaired time and sites on July 24, 1987 was the only relation that was slightly outside the recommended criteria (±20%). Daytime normalized bias and errors between predicted and observed ozone levels at monitoring sites in Tampa and Pinellas County regions on July 22, and 24, 1987, achieved the model performance goals (± 30% bias and ≤40% errors) recommended by the California Air Resources Board. The complex meteorological conditions existing at the passage of the sea breeze front could be the reason why performance of the model was not able to fulfill the goals even for daytime ozone prediction on July 23, 1987. These qualities of model performances ensured reasonable evaluations of control strategies.

7. The resolution of the simulations could not accurately predict the complex meteorological conditions influenced by the complicated shore line along Tampa Bay in Hillsborough County, therefore, model performances were worse in the Tampa region than in Pinellas County on July 23, and July 24, 1987. Higher spatial resolutions, which could provide a more realistic shore line for Tampa Bay, are required for better meteorological model performances in simulating the passage of sea breezes.

8. Trajectory analyses suggested that there could be three major contributors to ozone and its precursors for the ozone episodes on both July 23 and 24, 1987. The first contribution could be local emissions on July 22, 1987 from the southeast coast of Florida. Emissions from urban areas of the Gulf coast in southwestern Florida comprised the second set of contributions. Stagnant conditions in the Tampa Bay

area would also accumulate both transported and local pollutants and contribute to induction of the ozone exceedance during the ozone episode.

9. Meteorological conditions do not only dominate the distributions of ozone, but also strongly affect the efficiency of emission control strategies. The passage of a sea breeze front could lead to a greater reduction in ozone peak concentrations if the emissions of VOCs were reduced. Increase in mobile source emissions in the year 2000 might also partially contribute to ozone peak reductions under these meteorological conditions, because stronger NO emissions could titrate out generated ozone. Another factor that would affect the effectiveness of emission control strategies in the future would be a change in VOC/NO_x ratios in the local ambient air due to an increase in certain source emissions.

10. With the exception of horizontal and vertical profiles for the available detailed boundary conditions, the model cannot predict ozone air quality which is associated with passage of a cold front system. Approach of a cold front generally indicates long term transport of O_3 and its precursors, and/or stratospheric ozone intrusions. Intrusion of stratospheric ozone, which can be brought down to the surface by daytime mixing or by frontal downdraft, could raise the background ozone levels. Additional locally generated O_3 could easily cause the observed exceedance of the O_3 NAAQS.

11. On the basis of VOC/NO_x ratios from 06:00 hr to 09:00 hr in the Tampa Bay area, a "VOC only" control strategy is the best approach to reducing peak ozone concentrations, currently and in the future. However, stricter control policies should be employed in order to reduce the episodic O_3 peak concentrations to the required O_3 NAAQS. Reduction of VOCs would be more effective for those areas with higher population growth, if mobile sources are the only sources of emissions that will increase with population growth. Although the predictions for the year 2000 did not include changes in point source, industrial area source, or biogenic

source emissions, the simulations did provide valuable information on the characteristics of ozone air quality in the future.

12. In order to reduce O_3 levels, a statewide emission control program should be employed, but this strategy does not guarantee that practical emission control can reduce the ozone levels to below the ozone NAAQS during the onset of certain meteorological conditions. On the basis of emission reduction studies, a reduction of 18% in VOC emissions would be required to reduce the peak ozone level at each site in the Tampa Bay area to meet the ozone NAAQS for meteorological conditions existing on July 23, 1987. It would be impractical to reduce the peak ozone (171 ppb) level by either "VOC- only" or "NO_x-only" control strategies. Even with simultaneous VOCs and NOx emissions control at least a 76% reduction would be needed to achieve the ozone standard. Such a reduction in O_3 levels could not reasonably be achieved from a practical viewpoint.

Insufficient data and limited computer resources were the two primary restrictions preventing better model performances. To overcome these restrictions, several assumptions and simplifying methods were incorporated in the model. It was difficult to evaluate these assumptions and simplifying methods, except for the simulation results. These procedures were limited by the available computer resources. Although the transport and chemical calculations did not have accurate or complete emission inventory input, sufficient resolution of meteorological fields, and accurate dry deposition velocities, the results of these simulations can be applied with reasonable certainty to meeting the proposed objectives.

CHAPTER 7
RECOMMENDATIONS

This work could be improved with additional financial and monitoring data resources, which were not available during the research. Improving the spatial resolution and completion of a detailed emissions inventory are essential. The spatial resolution and accuracy of meteorological simulations are also essential for generating better simulation results. The following improvements in modeling O_3 exceedances are suggested:

1. Mobile source emissions should be distributed and allocated on the basis of each grid size. This would require more detailed information about lengths of accessible highways, regular roads, water ways and railroads. In addition to the distances, the temporal amounts of traffic flows are required for estimating highway and non-highway mobile source emissions.

2. A detailed map of land-use data is needed to estimate residential and biogenic emissions .

3. Locations of each of the area sources should be identified, to enable area emissions to be located on the exact grids.

4. Diurnal variations of each emission source should be included in inventories.

5. To improve the resolution for meteorological conditions could involve modification of the MM4 algorithm. A few research groups have tried trying to reduce the 10 km resolution limit (grid scale) to 5 km. Provision of additional meteorological data could help improve the accuracy of predicted meteorological conditions in this type of complex geographic area . Since some of the locally operated monitoring stations normally have records of meteorological information, collection of these databases

187

could provide a better first guess for the simulations. As a result, better and more realistic meteorological conditions could be obtained.

Preparation of a detailed emission inventory is an enormous task, which involves manipulating large amounts of information. It may take more than a year just to prepare a detailed inventory for a county. A statewide inventory would need the combined efforts of every county. The state of Florida should try to establish a detailed emission inventory which should be updated every 5 years because of the rate of growth in population. This emission inventory database would benefit all who need to understand the air quality problems in the state, and could be used as a basis for planning control strategies.

A few other modification could also improve the performance of model simulations.

1. The gas-phase chemical mechanisms used did not include the reactions of biogenic species. Although the contributions of biogenic emissions to ozone levels might be small in the Tampa Bay area, including those reactions may improve the simulation results. Also such reactions would be necessary , if an understanding of rural area air quality was needed.

2. The contributions from biogenic emissions should be examined for each day of the ozone episode, because they could be different every day.

3. Increasing the time resolution for the meteorological input data could also improve the simulations, but data files could grow too large to be handled.

4. Real boundary conditions could help to eliminate the error due to the selection of unrealistic values. Unfortunately, measurements done over large water bodies, such as the Gulf of Mexico are seldom available or conducted. It is important to have air quality measurements over the Gulf, because it is surrounded by several major metropolitan areas, such as Mexico City in Mexico, Houston, New Orleans, and the Tampa Bay area. Some air quality measurements in the Gulf could help us to understand the interchange and interaction of polluted air masses in this maritime

region, which are presently unknown. These maritime studies could also provide valuable boundary information on pollutant concentrations for these types of model studies.

A detailed investigation of historical weather patterns existing during ozone episodes in Florida should be pursued. Establishing a statewide vehicle emission inspection program may require considerable effort and expense. It is important to investigate this approach in more detail before planning any specific control strategies. On the basis of this research, an estimate is provided of the control effort needed. A major uncertainty is the frequency of occurrence of the type of ozone episode examined in this work. Such information would be important for the policy maker to consider before making decisions on appropriate control strategies.

GAS PHASE CHEMICAL MECHANISMS

Reaction			Rate constant ($ppm^{-1}\ min^{-1}$ unit)
1.	$NO_2 + h\upsilon$	---> $NO + O_3$	radiation dependent *
2.	$NO + O_3$	---> $NO_2 + O_2$	$1.0 \times 10^6 x T^{-1} e^{-1450/T}$
3.	$O_3 + h\upsilon$	---> $2\ OH$	radiation dependent *
4.	$OH + NO$	---> $HONO$	$8.7 \times 10^8 x T^{-2}$
5.	$OH + NO_2$	---> HNO_3	$1.5 \times 10^9 x T^{-2}$
6.	$HONO + h\upsilon$	---> $OH + NO$	radiation dependent *
7.	$HO_2 + NO$	---> $OH + NO_2$	$3.7 \times 10^6 x T^{-1}$
8.	$HO_2 + NO_2$	---> HO_2NO_2	$1.5 \times 10^8 x T^{-2}$
9.	HO_2NO_2	---> $HO_2 + NO_2$	$7.8 \times 10^{15} e^{-10420/T}$
10.	$HO_2 + HO_2$	---> $H_2O_2 + O_2$	special function **
11.	$H_2O_2 + h\upsilon$	---> $2\ OH$	radiation dependent *
12.	$OH + CO$	---> $HO_2 + CO_2$	$1.3 \times 10^5 x T^{-1}$
13.	$NO_2 + O_3$	---> NO_3	$5.3 \times 10^4 x T^{-1} e^{-2450/T}$
14.	$NO + NO_3$	---> $2\ NO_2$	$8.4 \times 10^6 x T^{-1}$
15.	$NO_2 + NO_3$	---> N_2O_5	$3.1 \times 10^7 x T^{-1} e^{-1100/T}$
16.	$N_2O_5 + H_2O$	---> $NO_2 + NO_3$	$3.5 \times 10^{18} x T^{-1} e^{-12280/T}$
17.	$N_2O_5 + H_2O$	---> $2\ HNO_3$	$1.33 \times 10^{-3} x T^{-1}$
18.	$NO_3 + h\upsilon$	---> $0.3\ NO + 0.7\ NO_2 + 0.7\ O_3$	radiation dependent *
19.	$OH + O_3$	---> $HO_2 + O_2$	$7.0 \times 10^5 x T^{-1} e^{-940/T}$
20.	$HO_2 + O_3$	---> $OH + 2\ O_2$	$4.8 \times 10^3 x T^{-1} e^{-580/T}$
21.	$HCHO + h\upsilon$	---> $2\ HO_2 + CO$	radiation dependent *
22.	$HCHO + h\upsilon$	---> $CO + H_2$	radiation dependent *
23.	$OH + HCHO$	---> $HO_2 + CO$	$1.9 \times 10^{-2} x T^2 e^{648/T}$ #
24.	$CH_3CHO + h\upsilon$	---> $CH_3O_2 + HO_2 + CO$	radiation dependent *
25.	$OH + CH_3CHO$	---> CH_3CO_3	$8.4 \times 10^3 e^{311/T}$ #
26.	$CH_3CO_3 + NO_2$	---> PAN	1.2×10^4 #

continued

27. PAN	--->	$CH_3CO_3 + NO_2$	$4.7 \times 10^{31} e^{-13592/T}$ #
28. $CH_3CO_3 + NO$	--->	$NO_2 + CH_3O_2 + CO$	$7.7 \times 10^3 e^{200/T}$ #
29. $CH_3O_2 + NO$	--->	$HCHO + HO_2 + NO_2$	$6.4 \times 10^3 e^{180/T}$ #
30. $OH + Propane$	--->	PO_2	$2.3 \times 10^{-2} \times T^2 e^{-44/T}$
31. $PO_2 + NO$	--->	$HO_2 + NO_2 + CH_3COCH_3$	$6.4 \times 10^3 e^{180/T}$
32. $OH + Alkane$	--->	AO_2	$6.6 \times 10^6 \times T^{-1} e^{-400/T}$
33. $AO_2 + NO$	--->	$1.7\ NO_2 - 0.8\ NO + 0.9\ HO_2$	
		$+ 0.15\ HCHO + 0.3\ CH_3CHO$	
		$+ 0.1\ RCHO + 0.45\ MEK$	
		$+ 0.3\ CH_3COCH_3$	$6.4 \times 10^3 e^{180/T}$
34. $OH + RCHO$	--->	RCO_2	$1.3 \times 10^7 \times T^{-1}$
35. $RCO_3 + NO_2$	--->	PPN	1.2×10^4 #
36. PPN	--->	$RCO_3 + NO_2$	$2.4 \times 10^{32} \times T^{-1} e^{-14073/T}$ #
37. $RCO_3 + NO$	--->	$C_2H_5O2 + NO$	$7.7 \times 10^3 e^{200/T}$
38. $C_2H_5O_2 + NO$	--->	$CH_3CHO + HO_2 + NO_2$	$6.4 \times 10^3 e^{180/T}$
39. $RCHO + h\upsilon$	--->	$C_2H_5O_2 + CO + HO_2$	radiation dependent *
40. $OH + MEK$	--->	XO_2	$4.4 \times 10^6 \times T^{-1} e^{-330/T}$
41. $XO_2 + NO$	--->	$NO_2 + CH_3CHO + CH_3CO_3$	$3.1 \times 10^6 \times T^{-1}$
42. $MEK + h\upsilon$	--->	$CH3CO3 + C_2H_5O_2$	radiation dependent *
43. $CH_3COCH_3 + h\upsilon$	--->	$CH_3CO_3 + CH_3O_2$	radiation dependent *
44. $OH + Ethene$	--->	$2\ HCHO + NO_2 - NO + HO_2$	$3.0 \times 10^3 e^{438/T}$ #
45. $OH + Propene$	--->	$HCHO + CH_3CHO + HO_2$	
		$+ NO_2 - NO$	$7.4 \times 10^3 e^{504/T}$ #
46. $OH + Butene$	--->	$1.8\ CH_3CHO + 0.9\ NO_2$	
		$+ 0.9\ HO_2 - NO$	$9.9 \times 10^3 e^{467/T}$ #
47. $O_3 + Ethene$	--->	$HCHO + 0.4\ CH_2O_2 + 0.4\ CO$	
		$+ 0.12\ HO_2$	$1.8 \times 10^1 e^{-2630/T}$ #
48. $O_3 + Propene$	--->	$0.5\ HCHO + 0.5\ CH_3CHO$	
		$+ 0.2\ CH_2O_2 + 0.2\ CH_3CHOO$	
		$+ 0.3\ CO + 0.2\ HO_2$	
		$+ 0.1\ OH + 0.2\ CH_3O_2$	$2.0 \times 10^1 e^{-2105/T}$ #
49. $O_3 + Butene$	--->	$CH_3CHO + 0.4\ CH_3CHOO$	
		$+ 0.3\ HO_2 + 0.2\ OH$	
		$+ 0.45\ CH_3O_2 + 0.2\ CO$	$5.3 \times 10^0 e^{-1713/T}$ #
50. $CH_2O_2 + NO$	--->	$HCHO + NO_2$	$3.1 \times 10^6 \times T^{-1}$

continued

51. $CH_3O_2 + NO_2$	--->	$HCHO + NO_3$	$3.1 \times 10^5 xT^{-1}$
52. $CH_2O_2 + SO_2$	--->	$HCHO + Sulfate$	$3.0 \times 10^4 xT^{-1}$
53. $CH_2O_2 + H_2O$	--->	product	$1.5 xT^{-1}$
54. $CH_3CHOO + NO$	--->	$CH_3CHO + NO_2$	$3.1 \times 10^6 xT^{-1}$
55. $CH_3CHOO + NO_2$	--->	$CH_3CHO + NO_3$	$3.1 \times 10^5 xT^{-1}$
56. $CH_3CHOO + SO_2$	--->	$CH_3CHO + Sulfate$	$3.1 \times 10^4 xT^{-1}$
57. $CH_3CHOO + H_2O$	--->	Product	$1.5 xT^{-1}$
58. $OH + Benzene$	--->	0.25 Cresol	
		$+ 0.25 HO_2 + 0.75 ADD$	$3.8 \times 10^3 e^{-207/T}$ #
59. $OH + Toluene$	--->	$0.15 ARO_2 + 0.2$ Cresol	
		$+ 0.2 HO_2 + 0.65 ADD$	$2.8 \times 10^3 e^{355/T}$ #
60. $OH + Xylene$	--->	0.25 Cresol $+ 0.25 HO_2$	
		0.75 ADD	$7.8 \times 10^6 xT^{-1}$ #
61. $ADD + NO$	--->	$0.75 NO_2 + 0.75 HO_2$	
		$+ 0.75$ DIAL $+ \alpha1$ CHOCHO	
		$+ \alpha2$ CH_3COCHO	$3.1 \times 10^6 xT^{-1}$
62. $OH + DIAL$	--->	El	$1.3 \times 10^7 xT^{-1}$
63. $El + NO_2$	--->	$El2NO_2$	$2.1 \times 10^6 xT^{-1}$
64. $ElNO_2$	--->	$El + NO_2$	$1.2 \times 10^{18} e^{-13543/T}$
65. $El + NO$	--->	$3 NO_2 - 2 NO + \alpha3 HO_2$	
		$+ \alpha3$ CHOCHO $+ \alpha4$ CH_3CO_3	
		$+ \alpha4$ $CH_3COCHO + \alpha3$ CO	$3.1 \times 10^6 xT^{-1}$
66. $OH + (CHO)_2$	--->	$HO_2 + CO$	$8.8 \times 10^6 xT^{-1}$
67. $(CHO)_2 + h\upsilon$	--->	$HCHO + CO$	radiation dependent *
68. $OH + CH_3COCHO$	--->	$CH_3CO_3 + CO$	$6.6 \times 10^6 xT^{-1}$
69. $CH_3COCHO + h\upsilon$	--->	$CH_3CO_3 + HO_2 + CO$	radiation dependent *
70. $OH + Cresol$	--->	ADD_2	$1.9 \times 10^7 xT^{-1}$
71. $ADD_2 + NO$	--->	$0.75 NO_2 + 0.75 HO_2$	
		0.75 DIAL	$3.1 \times 10^6 xT^{-1}$
72. $NO_3 + Cresol$	--->	$HNO_3 + Phenoxy$	$6.6 \times 10^6 xT^{-1}$
73. $Phenoxy + NO_2$	--->	Products	$6.6 \times 10^6 xT^{-1}$
74. $ARO_2 + NO$	--->	$0.75 NO_2 + 0.75 HO_2$	
		$+ 0.75$ ARCHO	$3.1 \times 10^6 xT^{-1}$
75. $ARCHO + h\upsilon$	--->	Products	radiation dependent *
76. $OH + ARCHO$	--->	$ARCO_3$	$5.8 \times 10^6 xT^{-1}$

continued

77. $ARCO_3 + NO_2$	--->	PBzN	$2.1 \times 10^6 \text{x} T^{-1}$
78. PBzN	--->	$ARCO3 + NO_2$	$1.0 \times 10^{17} \text{x} T^{-1} e^{-13025/T}$
79. $ARCO_3 + NO$	--->	$PhO2 + NO_2$	$3.1 \times 10^6 \text{x} T^{-1}$
80. $PhO_2 + NO$	--->	$Phenoxy + NO_2$	$3.1 \times 10^6 \text{x} T^{-1}$
81. $OH + SO_2$	--->	$Sulfate + HO_2$	$1.5 \times 10^{13} T^{-4}$
82. $HNO_3 + NH_3$	--->	NIT	0.0286
83. $HNO_3 + OH$	--->	NO_3	117.6
84. $HNO_3 + h\upsilon$	--->	$NO2 + OH$	radiation dependent *
85. $HCHO + NO_3$	--->	$HNO_3 + CO$	$2.64 \times 10^2 \text{x} T^{-1}$ #
86. $RCHO + NO_3$	--->	$HNO_3 + RCO_3$	$6.2 \times 10^5 \text{x} T^{-1} e^{-1860/T}$ #
87. $HNO3 + H_2O$	--->	$HNO3_{(l)}$	1.2×10^{-5}

*   see Lurmann, et al.(1986) for the detailed description of the PT dependent and radiation dependent rate constants and the form of the special fucntion.

** $k_{10} = 3.4 \times 10^4 \text{x} T^{-1} e^{1100/T} + 5.8 \times 10^{-5} \text{x} T^{-2} e^{-5880/T}$ [HO]

\#   Updated chemical reaction rate constants

COORDINATION TRANSFER PROGRAM

```
ccccccccccccccccccccccccccccccccccccccccccccccccccccccccccccccccccccccc
C RDMM Program:  This program is to manipulate the output from MM4
C model, so the data can be used as inputs for STEM-II models.
C This program will:
C a) extract the required data for the STEM-II simulation domain;
C b) interpolate the data from sigma coordinate system to the elevation
C    coordinate system;
C c) interpolate the variables (U and V) from dot grid points to cross
C    grind points, and
C d) calculate the vertical velocities.
ccccccccccccccccccccccccccccccccccccccccccccccccccccccccccccccccccccccc
      PARAMETER(IX=52,JX=41,KX=15,IX2=21,IY2=21,IZ2=16,IZZ=11,MX=43)
      COMMON /BLCK3/ PSTAR(IX2,IY2),SIG(IZ2),
     *               UW(IX2,IY2,IZ2),VW(IX2,IY2,IZ2)
      COMMON /BLCK4/ PVAL(IX2,IY2),H(IZZ)
C
      DIMENSION U(IX,JX,KX),   V(IX,JX,KX),   T(IX,JX,KX),
     *          Q(IX,JX,KX),RNW(IX,JX,KX),CLW(IX,JX,KX),
     *          PS(IX,JX)  ,TGD(IX,JX)  ,RNN(IX,JX)  ,RNC(IX,JX)
      DIMENSION   TER(IX,JX), XMFC(IX,JX), XMFD(IX,JX),
     *          F(IX,JX)   ,TRES(IX,JX) ,XLATC(IX,JX),
     *          XLONC(IX,JX),XLAND(IX,JX),SNOW(IX,JX)
      DIMENSION TEM(IX,JX,KX), QEM(IX,JX,KX), RNWEM(IX,JX,KX),
     *          CLWEM(IX,JX,KX), PSDOT(IX,JX),VELEM(IX,JX,KX),
     *          UEM(IX,JX,KX),VEM(IX,JX,KX),UELEM(IX,JX,KX),
     *          DSIGMA(KX),DH(JX,IX,KX)
      DIMENSION KKH(IX,KX),KKV(IX,KX),SIG1(IZ2),
     *          KHEM(MX,IX,KX),KVEM(MX,IX,KX),
     *          W(IX2,IY2,IZ2),DIV(IX,JX,KX),OMG(IX,JX,KX)
C
      INTEGER MIF(30),IVCOORD(100),JYR(18),JMO(18),JDY(18),JHR(18)
      INTEGER OLD2,STEP,TSTEP,HOUR,DAY,SAVEFRE,SKIP,INDEX,ST
C
      REAL    MRF(10),VCOORD(100),NEW(IX2,IY2,IZ2),
     *        OLD(IX2,IY2,IZ2),TEMP(IX2,IY2,IZ2),PRE(IX2,IY2,IZ2),
     *        Z(IX2,IY2,IZ2),TT5(IX2,IY2),TT4(IX2,IY2),DELT(IX2,IY2),
     *        PSTAR,UW,VW,NEW2,DENS(IX2,IY2,IZ2),RC,DIV,
     *        GRAV,RCP,KKV,KHEM,KVEM,DSIGMA,DH,KKH,DX,OMG,PVAL
      LOGICAL MLF(10)
C
      DATA SIG/1.,0.995,0.985,0.97,0.945,0.91,0.87,0.825,0.75,
     * 0.65,0.55,0.45,0.35,0.25,0.15,0.05/
      DATA SIG1/0.05,0.15,0.25,0.35,0.45,0.55,0.65,0.75,0.825,
     * 0.91,0.945,0.97,0.985,0.995,1./
      DATA DSIGMA/0.1,0.1,0.1,0.1,0.1,0.1,0.1,0.1,0.05,
     * 0.04,0.04,0.03,0.02,0.01,0.01/
```

```
      DATA H/10.,300.,600.,900.,1200.,1500.,1800.,2100.,2400.,
     * 2700.,3000./
      DATA RC/287.0/
      DATA RCP/2.87/
      DATA GRAV/9.8/
      DATA DX/30000./
C++++++++++++++++++++++++++++++++++++++++++++++++++++++++++++++++++++++C
C This segment of code reads the variables from the binary output files
C of MM4.
C++++++++++++++++++++++++++++++++++++++++++++++++++++++++++++++++++++++C
      READ(1) MDATE,IPROG,ICOORD,NLV,(VCOORD(L),L=1,NLV),
     *         MIF,MRF,MLF,JYR,JMO,JDY,JHR,IOLDPROG,IOLDCORD,
     *         IOLDNLV,(IVCOORD(L),L=1,IOLDNLV),
     *         IBLTYP,ISFFLX,ITGFLG,ICDCON,ISFPAR,IVMIXM,
     *         IDRY, IMOIST,ICLOUD,IBOUDY,IMOIAV,IFSNOW,
     *         ICUSTB,ITQPBL,IFRAD
C
      READ(1) TER
C
      READ(1) XMFC
      READ(1) XMFD
      READ(1) F
      IF (ITGFLG.NE.3) READ(1) TRES
C
      READ(1) XLATC
      WRITE(21,102) ((XLATC(I,J), J=10,30), I=9,29)
C
      READ(1) XLONC
      WRITE(21,102) ((XLONC(I,J), J=10,30), I=9,29)
C
      READ(1) XLAND
      READ(1) SNOW
C
      READ(1,END=400) THEEND
      PRINT *,'EOF MARK EXPECTED, NOT FOUND'
  400 CONTINUE
C
      TSTEP=24
      SKIP=5
      SAVEFRE=1
      TOPP=650.
      PRINT *,'SKIP 5 HOURS!'
      IF (SKIP .LT. 1) GOTO 499
      DO 33 ST=1,SKIP
      READ(1) XTIME,IDRY,IMOIST,IBLTYP,ISFPAR,ITGFLG
      PRINT *,'XTIME= ',XTIME
      READ(1) U
      READ(1) V
      READ(1) T
      IF(IDRY.NE.1) READ(1) Q
      IF((IMOIST.EQ.2).OR.(IMOIST.EQ.4)) READ(1) CLW
      IF((IMOIST.EQ.2).OR.(IMOIST.EQ.4)) READ(1) RNW
      READ(1) PS
      IF(ITGFLG.NE.3) READ(1) TGD
      IF(IDRY.NE.1) READ(1) RNC
      IF(IDRY.NE.1) READ(1) RNN
      READ(1,END=401) THEEND
      PRINT *,'EOF MARK EXPECTED, NOT FONDUND'
```

```
  401     CONTINUE
C
        DO 34 I=2,JX-1
        READ(2) XTIME,KKH
   34   CONTINUE
        DO 35 I=1,JX-1
        READ(3) XTIME,KKV
   35   CONTINUE
   33   CONTINUE
C
  499   PRINT *,'START TO TRANSFER VALUE!'
        DO 40 ST=1,TSTEP
          STEP=ST-1
          INDEX=1
          READ(1) XTIME,IDRY,IMOIST,IBLTYP,ISFPAR,ITGFLG
          PRINT *,'XTIME= ',XTIME
          READ(1) U         !UxPs
          READ(1) V
          READ(1) T
          IF(IDRY.NE.1) READ(1) Q
          IF((IMOIST.EQ.2).OR.(IMOIST.EQ.4)) READ(1) CLW
          IF((IMOIST.EQ.2).OR.(IMOIST.EQ.4)) READ(1) RNW
          READ(1) PS
          IF (ITGFLG.NE.3) READ(1) TGD
          IF (IDRY.NE.1) READ(1) RNC
          IF (IDRY.NE.1) READ(1) RNN
          READ(1,END=408) THEEND
          PRINT *,'EOF MARK EXPECTED, NOT FOUND'
  408   CONTINUE
C
        DO 42 J=10,30
          L=J-9
          DO 42 I=9,29
            M=I-8
            PSTAR(L,M)=PS(I,J)
   42   CONTINUE
C
        CALL INIT1(NEW,OLD)
C
        PRINT *,'STEP, SAVE= ', STEP, SAVEFRE
        DAY=1
        HOUR=MOD(ST,24)
C++++++++++++++++++++++++++++++++++++++++++++++++++++++++++++++++++++++C
C This segment of code calculates the P* at dot points from cross point
C P* values.
C++++++++++++++++++++++++++++++++++++++++++++++++++++++++++++++++++++++C
        DO 402 J=2,JX-1
          DO 402 I=2,IX-1
            PSDOT(I,J)=(PS(I,J)+PS(I-1,J)+PS(I,J-1)+PS(I-1,J-1))
     *                  *0.25
  402   CONTINUE
C
        DO 403 J=2,JX-1
          PSDOT(1,J)=((PS(1,J)+PS(1,J-1))*1.5-
     *                (PS(2,J)+PS(2,J-1))*0.5)*0.5
  403   CONTINUE
C
        DO 404 J=2,JX-1
```

```
             PSDOT(IX,J)=((PS(IX-1,J)+PS(IX-1,J-1))*1.5-
     *                   (PS(IX-2,J)+PS(IX-2,J-1))*0.5)*0.5
  404    CONTINUE
C
         DO 405 I=2,IX-1
            PSDOT(I,1)=((PS(I,1)+PS(I-1,1))*1.5-
     *                 (PS(I,2)+PS(I-1,2))*0.5)*0.5
  405    CONTINUE
C
         DO 406 I=2,IX-1
            PSDOT(I,JX)=((PS(I,JX-1)+PS(I-1,JX-1))*1.5-
     *                  (PS(I,JX-2)+PS(I-1,JX-2))*0.5)*0.5
  406    CONTINUE
C
         PSDOT(1,1)=4.*PS(1,1)-(PSDOT(1,2)+PSDOT(2,1)+PSDOT(2,2))
         PSDOT(IX,1)=4.*PS(IX-1,1)-(PSDOT(IX-1,1)+
     *                PSDOT(IX-1,2)+PSDOT(IX,2))
         PSDOT(1,JX)=4.*PS(1,JX-1)-(PSDOT(1,JX-1)+
     *                PSDOT(2,JX)+PSDOT(2,JX-1))
         PSDOT(IX,JX)=4.*PS(IX-1,JX-1)-(PSDOT(IX,JX-1)+
     *                PSDOT(IX-1,JX-1)+PSDOT(IX-1,JX))
C++++++++++++++++++++++++++++++++++++++++++++++++++++++++++++++++++++++++++C
C This segment of code assigns the temperature and pressure to each
C grid.
C++++++++++++++++++++++++++++++++++++++++++++++++++++++++++++++++++++++++++C
C Assign the surface temperature to TEMP
         DO 43 J=10,30
            L=J-9
            DO 43 I=9,29
              M=I-8
              TEMP(L,M,1)=TGD(I,J)
  43     CONTINUE
C Calculate the pressure at each sigma elevation
         DO 45 K=1,IZ2
            DO 45 J=1,IY2
               DO 45 I=1,IX2
                 PRE(I,J,K)=100.+SIG(K)*PSTAR(I,J)*10.
  45     CONTINUE
C Assign the temperature at each grid point
         DO 46 K=KX,1,-1
            N=KX+2-K
            DO 46 J=10,30
              L=J-9
              DO 46 I=9,29
                M=I-8
                TEMP(L,M,N)=T(I,J,K)/PS(I,J)
  46     CONTINUE
C++++++++++++++++++++++++++++++++++++++++++++++++++++++++++++++++++++++++++C
C The segment of code calculates elevation at each sigma elevation
C and thickness at each layer
C++++++++++++++++++++++++++++++++++++++++++++++++++++++++++++++++++++++++++C
C Initialize the Z
         DO 49 J=1,IY2
            DO 49 I=1,IX2
               Z(I,J,1)=0.0
  49     CONTINUE
C
         DO 301 J=1,JX-1
```

```
       DO 301 I=1,IX-1
          DH(J,I,1)=RC/(GRAV*2.)*(T(I,J,KX)+TGD(I,J))/PS(I,J)
     1                *ALOG((100.+SIG(1)*PS(I,J)*10.)/
     2                (100.+SIG(2)*PS(I,J)*10.))
          DO 301 K=KX,2,-1
             M=KX-K+2
             L=M+1
             DH(J,I,M)=RC/(GRAV*2.)*(T(I,J,K)+T(I,J,K-1))/PS(I,J)
     1                *ALOG((100.+SIG(M)*PS(I,J)*10.)/
     2                (100.+SIG(L)*PS(I,J)*10.))
 301   CONTINUE
C
       DO 50 K=2,IZ2
          DO 50 J=1,IY2
             DO 50 I=1,IX2
                M=K-1
                Z(I,J,K)=Z(I,J,M)+RC/(GRAV*2.0)*(TEMP(I,J,K)+
     1                TEMP(I,J,M))*ALOG(PRE(I,J,M)/
     2                PRE(I,J,K))
 50    CONTINUE
C Start temperature interpolations
       IF (MOD(STEP,SAVEFRE) .EQ. 0) THEN
          DO 47 K=1,IZ2
             DO 47 J=1,IY2
                DO 47 I=1,IX2
                   OLD(I,J,K)=TEMP(I,J,K)
 47       CONTINUE
C
          DO 48 J=1,IY2
             DO 48 I=1,IX2
                CALL VERT(I,J,NEW,OLD,INDEX,Z)
 48       CONTINUE
C
          WRITE(13,103) DAY,HOUR
          DO 90 K=1,IZZ
             WRITE(13,100) ((NEW(I,J,K), I=1,IX2),J=1,IY2)
 90       CONTINUE
C++++++++++++++++++++++++++++++++++++++++++++++++++++++++++++++++++++++C
C This segment of code alculateS the temperature difference between 400
C and 5 ft, and assignS a p constant for power law.
C++++++++++++++++++++++++++++++++++++++++++++++++++++++++++++++++++++++C
          DO 901 J=1,IY2
          DO 901 I=1,IX2
          TT4(I,J)=NEW(I,J,1)+(NEW(I,J,2)-NEW(I,J,1))/(300.-10.)*
     1             (121.92-10.)
          TT5(I,J)=OLD(I,J,1)+(NEW(I,J,1)-OLD(I,J,1))/(10.-0.)*
     1             (1.524-0.)
          DELT(I,J)=(TT4(I,J)-TT5(I,J))*9./5.
          IF (DELT(I,J).LE.-2.25) PVAL(I,J)=0.145
          IF ((DELT(I,J).LE.-1.75).AND.(DELT(I,J).GT.-2.25))
     1       PVAL(I,J)=0.17
          IF ((DELT(I,J).LE.-0.5).AND.(DELT(I,J).GT.-1.75))
     1       PVAL(I,J)=0.25
          IF ((DELT(I,J).LE.1.).AND.(DELT(I,J).GT.-0.5)) PVAL(I,J)=0.29
          IF ((DELT(I,J).LE.2.).AND.(DELT(I,J).GT.1.)) PVAL(I,J)=0.32
          IF ((DELT(I,J).LE.4.).AND.(DELT(I,J).GT.2.)) PVAL(I,J)=0.44
          IF ((DELT(I,J).LE.6.).AND.(DELT(I,J).GT.4.)) PVAL(I,J)=0.53
          IF ((DELT(I,J).LE.8.).AND.(DELT(I,J).GT.6.)) PVAL(I,J)=0.63
```

```
        IF ((DELT(I,J).LE.10.).AND.(DELT(I,J).GT.8.)) PVAL(I,J)=0.72
        IF (DELT(I,J).GT.10.) PVAL(I,J)=0.77
901    CONTINUE
C
        WRITE(13,103) DAY,HOUR
        DO 90 K=1,IZZ
          WRITE(13,100) ((NEW(I,J,K), I=1,IX2),J=1,IY2)
90     CONTINUE
C
        ENDIF
        CALL INIT1(NEW,OLD)
C++++++++++++++++++++++++++++++++++++++++++++++++++++++++++++++++++++++C
C This segment of code calculates horizontal velocities (U,V) at the dot
C points in the sigma coordinate system, and then transfers them to the
C cross points in elevation system.
C++++++++++++++++++++++++++++++++++++++++++++++++++++++++++++++++++++++C
        DO 51 K=1,KX
          N=KX-K+1
          DO 51 J=1,JX
            DO 51 I=1,IX
              UEM(I,J,N)=U(I,J,K)/PSDOT(I,J)
              VEM(I,J,N)=V(I,J,K)/PSDOT(I,J)
51     CONTINUE
C
        CALL DOTCRO(UEM,UELEM,IX,JX,KX)
C
        IF (MOD(STEP,SAVEFRE) .EQ. 0) THEN
          DO 52 K=1,KX
            N=K+1
            DO 52 J=10,30
              L=J-9
              DO 52 I=9,29
                M=I-8
                OLD(L,M,N)=UELEM(I,J,K)
C               UW(L,M,N)=UELEM(I,J,K)
52       CONTINUE
C
          DO 53 J=1,IY2
            DO 53 I=1,IX2
              INDEX=3
              CALL VERT(I,J,NEW,OLD,INDEX,Z)
53       CONTINUE
C
          WRITE(11,103) DAY,HOUR
          DO 91 K=1,IZZ
            WRITE(11,100) ((NEW(I,J,K), I=1,IX2),J=1,IY2)
91       CONTINUE
C
        ENDIF
        CALL INIT1(NEW,OLD)
C
        CALL DOTCRO(VEM,VELEM,IX,JX,KX)
C
        IF (MOD(STEP,SAVEFRE) .EQ. 0) THEN
          DO 54 K=1,KX
            N=K+1
            DO 54 J=10,30
              L=J-9
```

```
          DO 54 I=9,29
          M=I-8
          OLD(L,M,N)=VELEM(I,J,K)
C         VW(L,M,N)=VELEM(I,J,K)
 54    CONTINUE
C
       DO 55 J=1,IY2
         DO 55 I=1,IX2
           INDEX=3
           CALL VERT(I,J,NEW,OLD,INDEX,Z)
 55    CONTINUE
C
       WRITE(12,103) DAY,HOUR
       DO 92 K=1,IZZ
         WRITE(12,100) ((NEW(I,J,K), I=1,IX2),J=1,IY2)
 92    CONTINUE
C
       ENDIF
       CALL INIT1(NEW,OLD)
C+++++++++++++++++++++++++++++++++++++++++++++++++++++++++++++++++C
C This segment of code transfers liquid water contents at the cross
C points in the sigma coordinate system to the elevation system.
C+++++++++++++++++++++++++++++++++++++++++++++++++++++++++++++++++C
       INDEX=2
       DO 56 K=1,KX
         N=KX-K+1
         DO 56 J=1,JX-1
           DO 56 I=1,IX-1
             QEM(I,J,N)=Q(I,J,K)/PS(I,J)
             CLWEM(I,J,N)=CLW(I,J,K)/PS(I,J)
 56    CONTINUE
C
       IF (MOD(STEP,SAVEFRE) .EQ. 0) THEN
         DO 57 K=1,KX
           N=K+1
           DO 57 J=10,30
             L=J-9
             DO 57 I=9,29
               M=I-8
               OLD(L,M,N)=QEM(I,J,K)
 57    CONTINUE
C
       DO 58 J=1,IY2
         DO 58 I=1,IX2
           CALL VERT(I,J,NEW,OLD,INDEX,Z)
 58    CONTINUE
C
       WRITE(14,103) DAY,HOUR
       DO 93 K=1,IZZ
         WRITE(14,104) ((NEW(I,J,K), I=1,IX2),J=1,IY2)
 93    CONTINUE
C
       ENDIF
       CALL INIT1(NEW,OLD)
C+++++++++++++++++++++++++++++++++++++++++++++++++++++++++++++++++C
C This segment of code transfers cloud water contents at the cross
C points in the sigma coordinate system to the elevation coordination
C+++++++++++++++++++++++++++++++++++++++++++++++++++++++++++++++++C
```

```
          IF (MOD(STEP,SAVEFRE) .EQ. 0) THEN
            DO 59 K=1,KX
              N=K+1
              DO 59 J=10,30
                L=J-9
                DO 59 I=9,29
                  M=I-8
                  OLD(L,M,N)=CLWEM(I,J,K)
 59       CONTINUE
C
            DO 60 J=1,IY2
              DO 60 I=1,IX2
                CALL VERT(I,J,NEW,OLD,INDEX,Z)
 60       CONTINUE
C
            WRITE(17,103) DAY,HOUR
            DO 94 K=1,IZZ
              WRITE(17,104) ((NEW(I,J,K), I=1,IX2),J=1,IY2)
 94       CONTINUE
C
        ENDIF
C
        CALL INIT1(NEW,OLD)
C++++++++++++++++++++++++++++++++++++++++++++++++++++++++++++++++++++++C
C This segment of code transfers horizontal and vertical eddies at the
C cross points in the sigma coordinate system to the elevation
C coordinatation.
C++++++++++++++++++++++++++++++++++++++++++++++++++++++++++++++++++++++C
        INDEX=2
        DO 84 K=1,KX
          DO 84 J=1,IX
            DO 84 I=1,MX
              KHEM(I,J,K)=0.
 84     CONTINUE
C
        PRINT *,'READ HORIZONTAL EDDY DIFFUSIVITIES!'
        WRITE(18,103) DAY,HOUR
        DO 74 I=2,JX-1
          READ(2) XTIME,KKH
          WRITE(18,*) 'X= ',I
          DO 907 K=KX,1
 907      WRITE(18,104) (KKH(J,K),J=1,IX)
C
          DO 61 J=2,IX-1
            DO 61 K=KX,1,-1
              N=KX-K+1
              KHEM(I,J,N)=KKH(J,K)
 61       CONTINUE
 74     CONTINUE
C
        DO 86 K=1,KX
          DO 88 J=2,JX-1
            KHEM(J,1,K)=0.8*KHEM(J,2,K)+0.2*KHEM(J,3,K)
 88       CONTINUE
          DO 76 J=2,IX-1
            KHEM(1,J,K)=0.8*KHEM(2,J,K)+0.2*KHEM(3,J,K)
 76       CONTINUE
 86     CONTINUE
```

```
C
        DO 89 K=1,KX
          KHEM(1,1,K)=0.4*(KHEM(1,2,K)+KHEM(2,1,K))+0.2*KHEM(2,2,K)
  89      CONTINUE
C
C

        IF (MOD(STEP,SAVEFRE) .EQ. 0) THEN
          DO 62 K=1,KX
            N=K+1
            DO 62 J=9,29
              M=J-8
              DO 62 I=10,30
                L=I-9
                OLD(L,M,N)=KHEM(I,J,K)
  62      CONTINUE
C
          DO 63 J=1,IY2
            DO 63 I=1,IX2
              CALL VERT(I,J,NEW,OLD,INDEX,Z)
  63      CONTINUE

          WRITE(18,103) DAY,HOUR
          DO 95 K=1,IZZ
            WRITE(18,104) ((NEW(I,J,K), I=1,IX2),J=1,IY2)
  95      CONTINUE
C         PRINT *,'HORIZONTAL EDDY DIFFUSIVITIES!'
C         PRINT *,NEW
C
        ENDIF
        CALL INIT1(NEW,OLD)
C
        PRINT *,'READ VERTICAL EDDY DIFFUSIVITIES!'
        DO 85 K=1,KX
          DO 85 J=1,IX
            DO 85 I=1,MX
              KVEM(I,J,K)=0.
  85    CONTINUE
C
        WRITE(19,103) DAY,HOUR
        DO 75 I=1,JX-1
          READ(3) XTIME,KKV
          DO 908 K=KX,1,-1
 908        WRITE(19,104) (KKV(J,K),J=1,IX)
C
          DO 64 J=1,IX-1
            DO 64 K=KX,2,-1
              N=KX-K+1
              KVEM(I,J,N)=KKV(J,K)
  64      CONTINUE
  75    CONTINUE
C
        DO 87 J=1,IX-1
          DO 87 I=1,JX-1
            KVEM(I,J,15)=1./(1./(DH(I,J,15)**2.)+1./((DH(I,J,15)+
     1      DH(I,J,14))**2.))*(1./((DH(I,J,15)**2.)*KVEM(I,J,14)+
     2      1./((DH(I,J,15)+DH(I,J,14))**2.)*KVEM(I,J,13)))
  87    CONTINUE
C
```

```
        IF (MOD(STEP,SAVEFRE) .EQ. 0) THEN
          DO 65 K=1,KX
            N=K+1
            DO 65 J=9,29
              M=J-8
              DO 65 I=10,30
                L=I-9
                OLD(L,M,N)=KVEM(I,J,K)
 65     CONTINUE
C
          PRINT *,'PASS 2!'
          DO 66 J=1,IY2
            DO 66 I=1,IX2
              CALL VERT(I,J,NEW,OLD,INDEX,Z)
 66     CONTINUE
C
          WRITE(19,103) DAY,HOUR
          DO 96 K=1,IZZ
            WRITE(19,104) ((NEW(I,J,K),I=1,IX2),J=1,IY2)
 96     CONTINUE
C
        ENDIF
        CALL INIT1(NEW,OLD)
C++++++++++++++++++++++++++++++++++++++++++++++++++++++++++++++++++++++C
C This segment of code transfers air densities at the cross points in
C the sigma coordinate system to the elevation coordination
C++++++++++++++++++++++++++++++++++++++++++++++++++++++++++++++++++++++C
        IF (MOD(STEP,SAVEFRE) .EQ. 0) THEN
          DO 67 K=1,IZ2
            DO 67 J=1,IY2
              DO 67 I=1,IX2
                DENS(I,J,K)=PRE(I,J,K)/(RCP*TEMP(I,J,K))
                OLD(I,J,K)=DENS(I,J,K)
 67     CONTINUE
C
          DO 68 J=1,IY2
            DO 68 I=1,IX2
              CALL VERT(I,J,NEW,OLD,INDEX,Z)
 68     CONTINUE
C
          WRITE(16,103) DAY,HOUR
          DO 97 K=1,IZZ
            WRITE(16,104) ((NEW(I,J,K), I=1,IX2),J=1,IY2)
 97     CONTINUE
C
        ENDIF
        CALL INIT1(NEW,OLD)
C++++++++++++++++++++++++++++++++++++++++++++++++++++++++++++++++++++++C
C This segment of codecalculates vertical velocities at the cross points
C in the sigma coordinate system, and transfers the data to the
C elevation coordination
C++++++++++++++++++++++++++++++++++++++++++++++++++++++++++++++++++++++C
       DO 69 K=1,IZ2
         DO 69 J=1,IY2
           DO 69 I=1,IX2
             W(I,J,K)=0.
 69    CONTINUE
C
```

```
      PRINT *,'CALCULATE VERTICAL VELOCITIES!'
C
      CALL
OMEGA(U,V,XMFC,XMFD,PS,PSDOT,DSIGMA,SIG1,IX,JX,DX,DIV,OMG)
C
C
      DO 71 K=KX,1,-1
        N=KX-K+2
         DO 71 J=10,30
           L=J-9
           DO 71 I=9,29
             M=I-8
             W(L,M,N)=OMG(I,J,K)
 71   CONTINUE
C
      DO 304 K=2,IZ2
        DO 304 J=1,IY2
          DO 304 I=1,IX2
            OLD(I,J,K)=-W(I,J,K)*RC*TEMP(I,J,K)*10./PRE(I,J,K)/GRAV
 304  CONTINUE
C
C
C
      INDEX=2
      DO 81 J=1,IY2
          DO 81 I=1,IX2
            CALL VERT(I,J,NEW,OLD,INDEX,Z)
 81   CONTINUE
C
      IF (MOD(STEP,SAVEFRE) .EQ. 0) THEN
        WRITE(20,103) DAY,HOUR
        DO 98 K=1,IZZ
          WRITE(20,110) ((NEW(I,J,K),I=1,IX2),J=1,IY2)
 98   CONTINUE
C
      ENDIF
      CALL INIT1(NEW,OLD)
C
C
C
C
 100  FORMAT(10F7.2 )
 102  FORMAT(8F9.4)
 103  FORMAT('DAY= ',I2,'HOUR= ',I2)
 104  FORMAT(1X,5E11.4)
 105  FORMAT(1X,5E12.4)
 110  FORMAT(1X,5E11.3)
C
 40   CONTINUE
C
      CLOSE(1)
      CLOSE(2)
      CLOSE(3)
      CLOSE(11)
      CLOSE(12)
      CLOSE(13)
      CLOSE(14)
      CLOSE(15)
```

```
      CLOSE(16)
      CLOSE(17)
      CLOSE(18)
      CLOSE(19)
      CLOSE(20)
      CLOSE(21)
C
      STOP
      END
C*********************************************************************C
C VERT subroutine is used to adjust the data to the elevations of
C vertical grids in STEM-II
C*********************************************************************C
      SUBROUTINE VERT(I,J,NEW,OLD,INDEX,Z)
C
      PARAMETER (IX2=21,IY2=21,IZ2=16,IZZ=11)
      COMMON /BLCK4/ PVAL(IX2,IY2),H(IZZ)
C
      DIMENSION DEL(16)
C
      REAL NEW(IX2,IY2,IZ2),OLD(IX2,IY2,IZ2),Z(IX2,IY2,IZ2),PVAL
      REAL*8 DEL,TOT
C
      INTEGER I,J,N,M,L,K,A,INDEX,M2
C+++++++++++++++++++++++++++++++++++++++++++++++++++++++++++++++++++++C
C The following code is a loop adjust the output values based on
C pressure level to the values based on elevation
C (10,300,600,---,3000) for coarse domain and (10,200,400,---,2000) for
C fine domain.
C
C The values at each elevation are calculated by weighting the data
C values of pressure levels which are within 600 m vertical range of
C the assigned elevation.
C All the values within 600 m distance are found and assigned the
C weights of 1/d^2 (d=the distance between the elevation and its
C adjacent elevation of a pressure surface.)  For U and V,
C surface values are interpolated from the power law U=U1*(Z/Z1)^p.
C+++++++++++++++++++++++++++++++++++++++++++++++++++++++++++++++++++++C
      DO 40 K=1,IZZ
        N=0
        IF ((K .EQ. 1) .AND. (INDEX .EQ. 3)) THEN
          NEW(I,J,1)= OLD(I,J,2)*(H(1)/Z(I,J,2))**PVAL(I,J)
          INDEX=2
          GOTO 40
        ENDIF
        DO 30 L=INDEX,IZ2
          IF ((H(K)-Z(I,J,L)) .EQ. 0) THEN
            NEW(I,J,K)=OLD(I,J,L)
            GOTO 40
          ELSE
            IF(((H(K)-Z(I,J,L)) .LT. 600.0) .AND. ((H(K)-Z(I,J,L))
     *         .GT. -600.0)) THEN
              N=N+1
              DEL(N)=1.0/((H(K)-Z(I,J,L))**2.0)
            ELSE
              IF (Z(I,J,L) .GT. H(K)) THEN
                TOT=0.0
                IF (N .GT. 1) THEN
```

```
                  DO 10 M=1,N
                    TOT=TOT+DEL(M)
 10               CONTINUE
                  DO 20 M=1,N
                    A=L-(N+1)+M
                    NEW(I,J,K)=DEL(M)/TOT*OLD(I,J,A)+NEW(I,J,K)
 20               CONTINUE
                  GOTO 40
                ELSE
                  M=L-1
                  M2=L
                  IF(Z(I,J,M).GT.H(K))THEN
                    M=M-1
                    M2=L-1
                  ENDIF
                  NEW(I,J,K)=OLD(I,J,M2)-((OLD(I,J,M2)-OLD(I,J,M))/
     *            (Z(I,J,M2)-Z(I,J,M)))*ABS(Z(I,J,M2)-H(K))
                  GOTO 40
                ENDIF
              ELSE
                GOTO 30
              ENDIF
            ENDIF
          ENDIF
 30     CONTINUE
 40     CONTINUE
C
      RETURN
      END
C+++++++++++++++++++++++++++++++++++++++++++++++++++++++++++++++++++++++C
C The subprogram interpolates the velocity at dot point to that at cross
C point.
C+++++++++++++++++++++++++++++++++++++++++++++++++++++++++++++++++++++++C
      SUBROUTINE DOTCRO(VEL,VELE,IIX,JJX,KKX)
C
      DIMENSION VEL(IIX,JJX,KKX),VELE(IIX,JJX,KKX)
C
      REAL VEL,VELE
      INTEGER IIX,JJX,KKX
C
      DO 161 K=1,KKX
        DO 161 J=2,JJX
          DO 161 I=2,IIX
            VELE(I-1,J-1,K)=(VEL(I-1,J-1,K)+VEL(I-1,J,K)+VEL(I,J-1,K)+
     *                       VEL(I,J,K))*0.25
 161  CONTINUE
C
      RETURN
      END
C+++++++++++++++++++++++++++++++++++++++++++++++++++++++++++++++++++++++C
C This subroutine calculates the vertical velocity omega.
C+++++++++++++++++++++++++++++++++++++++++++++++++++++++++++++++++++++++C
      SUBROUTINE
     *OMEGA(USD,VSD,XM,DM,PSC,PSD,DSG,SIGH,IMX,JMX,DS,DIV,OMG)
C
      PARAMETER (KXS=15,IM=52,JM=41,KZ=16)
C
      DIMENSION USD(IM,JM,KXS),VSD(IM,JM,KXS),DM(IM,JM),
```

```
      *          XM(IM,JM)      ,PSC(IM,JM)     ,PSD(IM,JM),
      *          DSG(KXS)       ,SIGH(KZ)       ,DIV(IM,JM,KXS)
      DIMENSION PUM(IM,JM)      ,PVM(IM,JM)     ,DPDT(IM,JM),
      *          SDOT(IM,JM,KZ) ,DUDX(IM,JM)    ,DVDY(IM,JM),
      *          DPDX(IM,JM)    ,DPDY(IM,JM)    ,UX(IM,JM),
      *          VX(IM,JM)      ,XMSQ(IM,JM)
C
      DIMENSION OMG(IM,JM,KXS)
      REAL DS,XMSQ,ONEOV2DS,DS8,CON,USD,VSD,DM,XM,PSC,PSD,OMG,
     1     DSG,SIGH,DIV,PUM,PVM,DPDT,SDOT,DUDX,DVDY,DPDX,DPDY,UX,VX
C
      EQUIVALENCE (PUM(1,1),DPDX(1,1))
      EQUIVALENCE (PVM(1,1),DPDY(1,1))
      EQUIVALENCE (DUDX(1,1),UX(1,1))
      EQUIVALENCE (DVDY(1,1),VX(1,1))
C
      PRINT *,'XMSQ='
      DO 100 I=1,IMX-1
      DO 100 J=1,JMX-1
        DPDT(I,J)=0
        XMSQ(I,J)=XM(I,J)*XM(I,J)
 100  CONTINUE
C     COUPLE U AND MAP FACTORS
      PRINT *,'ONEOV2DS='
      ONEOV2DS=1./(2.*DS)
      PRINT *,'PUM=    ,PVM=    ,DUDX=    ,DVDY=    '
      DO 150 K=1,KXS
        DO 120 J=1,JMX
        DO 120 I=1,IMX
          PUM(I,J)=USD(I,J,K)/DM(I,J)
          PVM(I,J)=VSD(I,J,K)/DM(I,J)
 120    CONTINUE
C
        PRINT *,'DUDX, DVDY'
        DO 130 J=1,JMX-1
        DO 130 I=1,IMX-1
          DUDX(I,J)=PUM(I+1,J+1)+PUM(I,J+1)-PUM(I+1,J)-PUM(I,J)
          DVDY(I,J)=PVM(I+1,J+1)+PVM(I+1,J)-PVM(I,J+1)-PVM(I,J)
 130    CONTINUE
C
        PRINT *,'DIV=    ,DPDT=    '
        DO 140 J=1,JMX-1
        DO 140 I=1,IMX-1
          DIV(I,J,K)=(DUDX(I,J)*ONEOV2DS+DVDY(I,J)*ONEOV2DS)*XMSQ(I,J)
          DPDT(I,J)=DPDT(I,J)-DIV(I,J,K)*DSG(K)
 140    CONTINUE
 150  CONTINUE
C     SIGMA DOT ON FULL SIGMA LEVELS, SDOT AT MODEL LID SET TO 0
      DO 170 I=1,IMX-1
      DO 170 J=1,JMX-1
        SDOT(I,J,1)=0.
 170  CONTINUE
C
      PRINT *,'SDOT=    '
      DO 260 K=1,KXS
      DO 260 J=1,JMX-1
      DO 260 I=1,IMX-1
        SDOT(I,J,K+1)=SDOT(I,J,K)-(DSG(K)/PSC(I,J))*
```

```
     *   (DPDT(I,J)+DIV(I,J,K))
 260  CONTINUE
C
C     COMPUTE OMEGA ON HALF SIGMA LEVELS
C
      PRINT *,'DPDX=    ,DPDY=    ,DPDT='
      DS8=DS*8.
      DO 280 J=1,JMX-1
      DO 280 I=1,IMX-1
        DPDX(I,J)=(PSD(I+1,J+1)+PSD(I,J+1)-PSD(I+1,J)-PSD(I,J))*XM(I,J)
        DPDY(I,J)=(PSD(I+1,J+1)+PSD(I+1,J)-PSD(I,J+1)-PSD(I,J))*XM(I,J)
        DPDT(I,J)=DPDT(I,J)*DS8
 280  CONTINUE
C
      PRINT *,'UX=    ,VX=    ,OMG=   '
      DO 350 K=1,KXS
        DO 290 J=1,JMX-1
        DO 290 I=1,IMX-1
          UX(I,J)=USD(I+1,J+1,K)/PSD(I+1,J+1)+USD(I,J+1,K)/PSD(I,J+1)+
     1            USD(I+1,J,K)/PSD(I+1,J)+USD(I,J,K)/PSD(I,J)
          VX(I,J)=VSD(I+1,J+1,K)/PSD(I+1,J+1)+VSD(I,J+1,K)/PSD(I,J+1)+
     2            VSD(I+1,J,K)/PSD(I+1,J)+VSD(I,J,K)/PSD(I,J)
 290    CONTINUE
C
        PRINT *,'CON=   '
        CON=SIGH(K)/(8.*DS)
        DO 300 J=1,JMX-1
        DO 300 I=1,IMX-1
          OMG(I,J,K)=PSC(I,J)*(SDOT(I,J,K)+SDOT(I,J,K+1))*0.5+
     *    CON*(DPDT(I,J)+UX(I,J)*DPDX(I,J)+VX(I,J)*DPDY(I,J))
 300    CONTINUE
 350  CONTINUE
      RETURN
      END
C+++++++++++++++++++++++++++++++++++++++++++++++++++++++++++++++++C
C Initialize the NEW and read the OLD record
C+++++++++++++++++++++++++++++++++++++++++++++++++++++++++++++++++C
      SUBROUTINE INIT1(NEW,OLD)
C
      PARAMETER (IX2=21,IY2=21,IZ2=16)
      REAL NEW(IX2,IY2,IZ2),OLD(IX2,IY2,IZ2)
C
      DO 41 K=1,IZ2
        DO 41 J=1,IY2
          DO 41 I=1,IX2
            NEW(I,J,K) = 0.0
            OLD(I,J,K) = 0.0
 41   CONTINUE
C
      RETURN
      END
```

LIST OF REFERENCES

Anthes R.A. , E.-Y. Hsie and Y.-H Kuo. (1987). Description of the Penn State/NCAR Meso scale Model Version 4 (MM4). NCAR Technical Note-282+STR.

Anthes R.A. and T.T.Warner (1978). Development of Hydrodynamic models suitable for air pollution and other meso-meteorological studies. Mon. Wea. Rev., 106, 1045-1078.

Atkinson B.W. (1981). Meso-scale Atmospheric Circulations. Academic Press, New York.

Atkinson R. (1990). Gas-phase tropospheric chemistry of organic compounds: A review. Atoms. Environ., 24A, 1-41.

Atkinson R., A.C. Lloyd, and L. Winges (1982), An Updated Chemical Mechanism for Hydrocarbon, NO_x/SO_2 Photooxidation Suitable for Inclusion in Atmospheric Simulation Models, Atmos. Environ., 16:1341-1362.

Bornstein R.D. and W.T. Thompson (1981). Effects of frictionally retarded sea breeze and synoptic frontal passages on Sulfur dioxide Concentrations in New York City. J Appl. Meteor., 20, 843-858.

Brost R.A., R.B. Chatfield, J.P. Greenberg, P.L. Haagenson, B.G. Heikes, S. Madronich, B.A. Ridley, and P.R. Zimmerman, (1989). Three-dimensional modeling of the ozone budget over the north Atlantic Ocean, in Ozone in the Atmosphere, R.D. Bojkov and P. Fabian, Eds. A. Peepak Publishing, Hampton, VA. 568-571.

Carmichael G.R. and L.K. Peters (1984). An Eulerian transport/transformation/removal model for SO_2 and sulfate-II. Model calculation of SO_x transport in the eastern United States. Atmos. Environ. 18, 953-967.

Carmichael G.R. L.K. Peters, and T. Kitada (1986). A second generation model for regional-scale transport/chemistry/ deposition. Atmos. Environ. 20, 173-188.

Chameides, W.L. (1984). The photochemistry of a remote marine stratiform cloud. J. Geophys. Res., 89, 4739-4755.

Chameides, W.L. (1986). The role of lighting in the chemistry of the atmosphere. Studies in Geophysics: The Earth's Electrical Environment, National Academy Press, Washington, DC, 70-77.

Chameides, W.L. and D.D. Davis (1982). The free radical chemistry of cloud droplets and its impact upon the composition of rain. J. Geophys. Res., 87, 4863-4877.

209

Chang, Y.-S., G.R. Carmichael, H. Kurta and H. Ueda (1989). The transport and formation of photochemical oxidants in central Japan. Atmos. Environ., 23, 363-393.

Chang, Y.-S., G.R. Carmichael, H. Kurita, T. Kitada and H. Ueda (1990). Diagnostic evaluation of the transport and gas chemistry components of the STEM-II model. Atmos. Environ., 24A, 2715-2737.

Cloutier, M.M. (1993). Emissions testing reduces ozone threat in six counties. The Florida Specifier, 15, 1&7.

Chu, S.-H. (1986). Coupling high pressure systems and outbreaks of high surface ozone concentrations. Air Pollut. Cont. Assoc., Florida sec., 1986 annual conference, Clearwater, FL Sep. 28-30.

Danielsen E.F. and V.A. Mohnen (1977). Project dust storm report: ozone transport in situ measurements and meteorological analyses of tropopause folding. J. Geophys. Res., 82, 5867-5877.

Demerjian K.L. (1985). Atmospheric modeling: model and accuracy. Evaluation of the Scientific Basis for Ozone/Oxidants Standards. Editor, S.D. Lee, Air Pollution Control Association, Houston, TX. 10-16.

Edinger J.G. (1973) Vertical distribution of photochemical smog in Los Angeles Basin. Environ. Sci. & Tech., 7, 247-252.

Estoque, M.A. (1961). A theoretical investigation of the sea breeze. Quart. J. R. Meteor. Soc., 87, 136-146.

Estoque M.A. (1962). The sea breeze as a function of the prevailing synoptic situation. J. Atmos. Sci., 19, 244-250.

Gill D.O., (1992). A User's Guide to the Penn State/NCAR Mesoscale Modeling System, NCAR/TN-381+1A, National Center of Atmospheric Research, Boulder, CO..

Goodin, W.R., G.J. McRae & J.H. Seinfeld (1980). An objective analysis technique for constructing three-dimensional urban-scale wind fields. J. Appl. Meteor., 19, 98-108.

Fisher,E.L. (1959). The sea breeze project, Quart. Progress Rep., 2, Contract No. DA-36-039-SC-78091, NYU, New York.

Finlayson-Pitts B.J. and J.N. Pitts, Jr. (1993). Atmospheric chemistry of tropospheric ozone formation: scientific and regulatory implications. J. Air Waste Manage. Assoc., 43, 1091-1100.

Fortner B. (1992). The data handbook: A guide to understanding the organization and visualization of technical data. Spyglass, Champaign, IL.

Hong M.S. and G.R. Carmichael (1986). Examination of a subgrid-scale parameterization for the transport of pollutants in a nonprecipitating cumulus cloud ensemble. Atmos. Environ., 20, 2205-2217.

Jacob, D.J. (1986). Chemistry of OH in remote clouds and its role in the production of formic acid and peroxymonosulfate. J. Geophys. Res., 91, 9807-9826.

Johnson W.B. and W. Viezee (1981). Stratospheric ozone in the lower troposphere-I. Presentation and interpresentation of aircraft measurements. Atmos. Environ., 15, 1309-1323.

Kaiser, J.A. & R.H. Hill (1976). Irradiance at sea. J. Geophys. Res., 81, 395-398.

Kardono (1990). Investigation of soil nitric oxide emission, fluxes at Austin Cary Forest, Master's thesis, Univeristy of Florida, Gainesville.

Kauper E.K. (1960). The zone of discontinuity between the land and sea breezes and its importance to southern California air-pollution studies. Bull. Amer. Meteor. Soci., 41, 410-422.

Kitada T., K. Igarashi and M. Owada (1986a). Numerical analysis of air pollution in a combined field of land/sea breeze and mountain/valley wind. Amer. Meteo. Soc., 25, 767-784

Kitada T., G.R. Carmichael and L.K. Peter (1986b). Effects of dry deposition on the concentration-distributions of atmospheric pollutants within land- and sea-breeze circulations. Atmos. Environ., 20, 1999-2010.

Lamb B., A. Guenther, D.Gay and H. Westberg (1987). A national inventory of biogenic hydrocarbon emissions. Atmos. Environ., 21, 1695-1705.

Lonneman W.A., R.L. Sella and S.A. Meeks (1986). Non-Methane Organic Composition in the Lincoln Tunnel. Envirion. Sci. Technol., 20, 790-796.

Lurmann, F.W., Nitta B., Ganesan K. and A.C. Lloyd (1984). Modeling potential ozone impacts from natural sources-III Ozone modeling in Tampa/St. Petersburg, Florida. Atmos. Environ., 18, 1133-1143.

Lurmann, F.W., A.C. Lloyd and R.Atkinson (1986). A chemical mechanism for use in long-range transport/acid deposition computer modeling. J. Geophys. Res., 91, 10, 905-10,936.

Lyons, W.A. and L.E. Olsson (1972). Mesoscale air pollution transport in the Chicago lake breeze. J. Air Pollut. Cont. Assoc., 22, 876-881.

Meagher J.F., N.T. Lee, R.J. Valente and W.J. Parkhurst (1987). Rural ozone in the southeastern United States. Atmos. Environ., 21, 605-615.

Milford J.B., A.G. Russell, and G.J. McRae (1989). A new approach to photochemical pollution control: implications of spatial patterns in pollutant responses to reduction in nitrogen oxides and reactive organic gas emissions, Environ. Scie. Technol., 23, 1290-1301.

Molton J.P. (1979). An Introduction to Dynamic Meteorology. Academic Press, New York.

Odman M.T., N. Kurmar and A.G. Russell (1992). A comparison of fast chemical kinetic solvers for air quality modeling. Atmos. Environ. 26A, 1783-1789.

Payne, W.J. (1973). Reduction of nitrogenous oxides by microorganisms. Bacterial Rev, 37, 409-442.

Pearce, R.P. (1955). The calculation of a sea-breeze circulation in terms of the differential heating across the coastline. Quart. J. R. Met.Soc., 81, p351-381

Pielke, R.A. (1974). A three-dimensional numerical model of the sea breezes over south Florida. Mon. Wea. Rev., 102, 115-139.

Pielke, R.A., NcNider R.T., Segal M. and Mahrer Y. (1983). The use of a mesoscale numerical model for evaluations of pollutant transport and diffusion in coastal regions and over irregular terrain. Amer. Met. Soc., 64, 243-249.

Preussner, P.R. and K.P. Brand (1981). Application of a semi-implicit Euler method to mass action kinetics. Chem. Eng. Sci., 10, 1633-1641.

Ryan R.T., H.H. Blau, P.C. Thuna, and M.L. Cohen (1972). Cloud Microstructure as Determined by an Optical Cloud Particle Spectrometer. J. Appl. Meteor., 11, 149-156.

Seinfeld J.H. (1986). Atmospheric Chemistry and Physics of Air Pollution. Wiley, New York, 1986.

Shim S.-G. and G.R. Carmichael (1991). The STEM-II acid deposition and photochemical oxidant model-II. A diagnostic analysis of mesoscale acid deposition. Atmospheric Environment, 25B, 25-45.

Simpson J.E., D.A. Mansfield, and J.R. MilFord (1977). Inland penetration of sea-breeze fronts. Quart. J. Royal Met. Soc., 103, 47-76.

Stump F.D., K.T. Knapp and W.D. Ray (1990). Seasonal impact of blending oxygenated organics with gasoline on motor vehicle tailpipe and evaporatative emission. J. Air Waste Manage. Assoc., 40, 872-880.

Sutton O.G. (1953). Micrometeorology: A Study of Physical Processes in the Lowest Layers of the Earth's Atmosphere. McGraw-Hill, New York.

Tesche T.W. (1988). Accuracy of ozone air quality models. J. Environ. Engin., 104, 739-752.

Viezee W., W.B. Johnson, and H.B. Singh (1983). Stratospheric ozone in the lower troposphere-II. Assessment of downward flux and ground-level impact. Atmos. Environ., 17, 1979-1993.

Yanenko N.N. (1971). The Method of Fractional Steps. Springer, Berlin.

Young G.S. and J.W. Winchester (1980). Association of non-marine sulfate aerosol with sea breeze circulation in Tampa Bay. Amer. Meteor. Soci., 19, 419-425.

Wexler, R. (1946). Theory and observations of land and sea breezes. Bull Am. met. Soc., 27, 272-287.

Wolff G.T. and P.E. Korsog (1992). Ozone control strategies based on the ratio of volatile organic compounds to nitrogen oxides. J. Air Waste Manage. Assoc., 42, 1173-1177.

Zimmerman P.R. (1979). Testing for hydrocarbon emissions from vegetation leaf litter and aquatic surfaces, and development of a methodology for compiling biogenic emission inventories. EPA-450/4-4-79-004.

BIOGRAPHICAL SKETCH

Junne-Yih Robert Yeh was born in Taina, Taiwan, on July 5, 1961. He graduated from Taipei Chung-Ching High School in 1979. Upon graduation, he took the University/College Entrance Examination and attended the Department of Atmospheric Physics at the National Central University. He received a bachelor's degree in atmospheric physics from National Central University in 1983.

After completing a two-year military service obligation, he continued his education at North Carolina State University and obtained a Master of Science degree in atmospheric sciences in 1989.

He continued his graduate studies towards a Ph.D. in the air pollution program, Department of Environmental Engineering Sciences, at the University of Florida from 1988 to 1994.
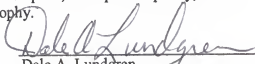
He has been treasurer and vice chairman of the UF student chapter of the Air & Waste Management Association. Also, he was the recipient of the Axel Hendrickson scholarship award from the Florida section Air & Waste Management Association in 1991.

I certify that I have read this study and that in my opinion it conforms to acceptable standards of scholarly presentation and is fully adequate, in scope and quality, as a dissertation for the degree of Doctor of Philosophy.

Eric R. Allen, Chair
Professor of Environmental Engineering
Sciences

I certify that I have read this study and that in my opinion it conforms to acceptable standards of scholarly presentation and is fully adequate, in scope and quality, as a dissertation for the degree of Doctor of Philosophy.
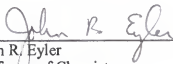
Dale A. Lundgren
Professor of Environmental Engineering
Sciences

I certify that I have read this study and that in my opinion it conforms to acceptable standards of scholarly presentation and is fully adequate, in scope and quality, as a dissertation for the degree of Doctor of Philosophy.
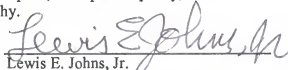
Michael D. Annable
Assistant Professor of Environmental
Engineering Sciences

I certify that I have read this study and that in my opinion it conforms to acceptable standards of scholarly presentation and is fully adequate, in scope and quality, as a dissertation for the degree of Doctor of Philosophy.

John R. Eyler
Professor of Chemistry

I certify that I have read this study and that in my opinion it conforms to acceptable standards of scholarly presentation and is fully adequate, in scope and quality, as a dissertation for the degree of Doctor of Philosophy.

Lewis E. Johns, Jr.
Professor of Chemical Engineering

This dissertation was submitted to the Graduate Faculty of the College of Engineering and to the Graduate School and was accepted as partial fulfillment of the requirements for the degree of Doctor of Philosophy.

April, 1994

Winfred M. Phillips
Dean, College of Engineering

Karen A. Holbrook
Dean, Graduate School